DENDRIMER-COATED IRON OXIDE NANOPARTICLES AS TARGETED MRI CONTRAST AGENTS

by

Kevin J. Landmark

A dissertation submitted in partial fulfillment
of the requirements for the degree of
Doctor of Philosophy
(Applied Physics)
in the University of Michigan
2008

Doctoral Committee:

Professor Mark M. Banaszak Holl, Co-Chair
Professor Bradford G. Orr, Co-Chair
Professor James R. Baker, Jr.
Professor Roy Clarke

"If my mental processes are determined wholly by the motions of atoms in my brain, I have no reason to suppose my beliefs are true…and hence I have no reason for supposing my brain to be composed of atoms."

--J. B. S. Haldane

DEDICATION

This thesis is dedicated to my grandmother, Minnie Landmark, and my grandparents who are now home with the Lord: Lydia and George Jandron and James Landmark.

ACKNOWLEDGEMENTS

I am under no illusion; completing my Ph.D. work would not have been possible without the support of others, and I am so grateful to a long list of people and the various roles they played. A comprehensive "thank you" would take another hundred pages, but a blanket statement is just not enough. The following is an attempt to succinctly execute the former.

I thank my entire committee for their scientific guidance and input. Given the multidisciplinary nature of the project, each person's contributions were essential. Brad Orr was my anchor to my physics roots and taught me how to be a professional physicist. Roy Clarke was also a physics stronghold, especially regarding magnetism. I also really enjoyed working with him in the summer program for women in science. My emergence as a "synthetic physicist" would not have been possible without the expert tutelage of Mark Banaszak Holl; he taught me how to think and work like a chemist. I am also very thankful for his pivotal suggestion to use the Advanced Photon Source (APS) for single-cell elemental analysis and his help in making it happen. James R. Baker, Jr. provided a deeper understanding of the biological aspects of my research; I am also grateful for his financial support.

I am grateful for the mentorship I received at Michigan Technological University from John Jaszczak and my advisor, Robert Weidman. Their wise counsel and encouragement ultimately led me back to and through academia.

Thank you to my classmates from Applied Physics and Physics at the University of Michigan: Damian Khan, Carolyn Kuranz, Dr. Joel McDonald, Dr. Brandon McNaughton, Porscha McRobbie, Moussa Ngom, Dr. Steve Reed, Dr. Mariano "Pete" Trigo, and John Valenzuela. We made it through classes together, including Jackson (so yah)! No more problem sets…ever!

All group members, past and present, are talented scientists with whom it was a pleasure to work, and I am grateful to all of them. Jeff Bartolin and Dr. Amy Gottfried were brave enough to enter the chemistry lab with a physicist to get me started on synthesis; they were both very good, patient teachers. As a chemist doing physics, Dr. Bonnie Ludwig allowed me to maintain balance in the universe by being a physicist doing chemistry. Thanks to Dr. Stassi DiMaggio for functionalizing the dendrimers I used to complete my thesis work. I sincerely appreciate the advice and guidance of Dr. Pascale Leroueil, especially during writing. Thank you, Chris Kelly, for your wonderful confocal microscopy work. Thanks, Dan McNerny, for your sense of humor and countless instances of sharing your own frustrations and listening to mine. Dr. Jessica Hessler, Zubair Ahsan, Kandarpa Cousineau, Blake Erickson, Song Ge, Ajdin Kavara (he's chopping broccoli), Damian Khan, Doug Mullen, Matt Remy, Ahleah Rohr, and Randon Walker: thank you all for your friendship and contributions to my personal life as well as my professional life.

Thanks to my friends from the Math Department: Jasun Gong, Daniel Hernandez, Ryan Kinser, Yogesh More, Alan Stapledon, Kevin Tucker, Diane Vavrichek, and Kacey Walker. It was a lot of fun playing basketball with all of you; without it I probably would

not have stayed sane while writing. Several of you have finished or will soon finish your degrees. Congratulations!

Several people from the Chemistry Department made important fundamental contributions to my research. I thank Eugenio Alvarado, Carol Carter, Chris Kojiro, and Jim Windak for their help with various analytical instruments and techniques. Thanks to Kim Firestone and Al Wilson from the Instrument Shop for their help with fabrication and equipment maintenance. I really appreciate the glassblowing expertise of Roy Wentz as well as his Christian fellowship. Thanks also to James Penner-Hahn and his student Jesse Ward for their help at APS and the resulting publication.

Thank you to the staff of the Applied Physics Program: Cyndi McNabb and Charles Sutton. You are both responsible for the incredible family atmosphere of the program! Thanks also to the Physics Department staff: Matt Blank, Elizabeth Branch, Chris Mackowiak, Kimberly Smith, and Dianne Ziesmer. You were all extremely helpful and kind.

The input and assistance of my colleagues in the Michigan Nanotechnology Institute for Medicine and Biological Sciences were invaluable. Thank you Anna Bielinska, Tom Dunham, Elliott Hill, István Majoros, Andrzej Myc, and Thommey Thomas. I am especially grateful to Xiangyang Shi and Alina Kotlyar. Xiangyang and I had many helpful discussions; he also provided his guidance and materials for experiments. Alina's help and work were essential to the successful completion of all biological experiments I conducted.

It was a pleasure to work with Stefan Vogt at the Advanced Photon Source. I benefited greatly from my interactions with him. Thanks, Stefan, for your patient instruction regarding beamline physics and its practical application at 2-ID-E.

Absolutely none of what I accomplished would have been possible without my family and friends. Thank you to Erin and Tom Henshaw, Amanda and Matt Altiere, and Elizabeth Kuhl for being such good friends. Thanks, David Lemmerhirt, for your friendship and Christian mentorship. A special thanks to the Ebenhoeh family—Tammi and Dick, Alexa, Alivia, and Alandon—for letting me stay with them the last couple weeks as I finished. I am so grateful to my mother and father, Sharon and Dan Landmark, for raising me in a safe, happy, loving, and joyful home; I cannot possibly thank you enough for all that you have invested in me. Thanks to my in-laws, Sally and Ron King and Andrew. Your encouragement, patience, and support helped me finish. I also thank my beautiful, extraordinary wife, Lindsay. You have shown me endless patience, love, and support and taught me a lot about faith. I learn more every day what an incredible blessing the Lord has given me in you. I thank Jesus Christ for being my Savior, Lord, Redeemer, and Friend; without You, I am nothing.

Work on this project was supported in part by the National Institutes of Health under grant #5R01EB002657 to James R. Baker, Jr. The TEM used in this study was acquired under grant #EAR-8708276 from the National Science Foundation. XRF microscopy data were acquired at beamline 2-ID-E of the Advanced Photon Source. Use of the Advanced Photon Source was supported by the United States Department of Energy, Office of Science, Office of Basic Energy Sciences, under contract #DE-AC02-06CH11357.

TABLE OF CONTENTS

LIST OF FIGURES

LIST OF TABLES

LIST OF ABBREVIATIONS

6-TAMRA, 6T	6-carboxytetramethylrhodamine
Ab	Antibody
Ac	Acetamide
acac	Acetylacetonate
AES	Atomic emission spectroscopy
ANL	Argonne National Lab
APS	Advanced Photon Source
ATCC	American Type Culture Collection
Aβ	Amyloid-β
CEA	Carcinoembryonic antigen
Cup	Cupferron (*N*-nitrosophenylhydroxylamine)
DAPI	4’,6-diamidino-2-phenylindole
DC-SPION	Dendrimer-coated superparamagnetic iron oxide nanoparticle
DI	Deionized
DIC	Differential interference contrast
DMSA	Dimercaptosuccinic acid
DMSO	Dimethyl sulfoxide
DNA	Deoxyribonucleic acid
EDC	*N*-(3-dimethylaminopropyl)-*N*′-ethylcarbodiimide hydrochloride
EDTA	Ethylenediaminetetraacetic acid
EPR	Enhanced permeation and retention
Et_3N	Triethylamine
FA	Folic acid
FAR	Folic acid receptor
Fe_3O_4	Magnetite
Fe_3S_4	Greigite
G5	Generation 5
GPC	Gel permeation chromatography
HPLC	High performance liquid chromatography

ICP-OES	Inductively coupled plasma-optical emission spectroscopy
ID	Insertion device
IgG	Immunoglobulin G
LD	Lethal dose
LH/CG	Luteinizing hormone/chorionic gonadotropin
LHRH	Luteinizing hormone releasing hormone
linac	Linear accelerator
mAb	Monoclonal antibody
MALDI-TOF	Matrix assisted laser desorption/ionization-time of flight
MeOH	Methanol
MNiMBS	Michigan Nanotechnology Institute for Medicine and Biological
MNP	Magnetic nanoparticle
MPS	Mononuclear phagocyte system
MRI	Magnetic resonance imaging
MTX	Methotrexate
NMR	Nuclear magnetic resonance
OC-SPION	Organic-coated superparamagnetic iron oxide nanoparticle
PAMAM	Poly(amidoamine)
PBS	Phosphate-buffered saline
PEG	Poly(ethylene glycol)
PMP	Poly(methylpentene)
PyO	Pyridine-*N*-oxide
RES	Reticuloendothelial system
RF	Radio frequency
RM	Reverse micelle
SD	Standard deviation
SEM	Standard error of the mean
SPION	Superparamagnetic iron oxide nanoparticle
SQUID	Superconducting quantum interference device
TEM	Transmission electron microscopy
uMUC	Underglycosylated mucin
UV–vis	Ultraviolet–visible
VCAM	Vascular cell adhesion molecule
XPS	X-ray photoelectron spectroscopy
XRF	X-ray fluorescence
γ-Fe_2O_3	Maghemite

CHAPTER 1

INTRODUCTION

1.1 Overview

The bleak prognosis for individuals with metastatic cancer along with the substantial costs of treating the disease in its advanced stages are prompting clinical medicine to adopt a predictive and preventative modality of care.[1] Targeted MRI contrast agents are anticipated to be critical tools in fully realizing the benefits of this new paradigm.[1-3] Many approaches have been documented regarding both iron oxide contrast agents and the means of targeting them to specific tissues.[4-49] The novel approach outlined in this dissertation employs functionalized poly(amidoamine) (PAMAM) dendrimers to effect specific uptake of superparamagnetic iron oxide nanoparticles (SPIONs) by cancer cells *via* the folate receptor. The folate receptor provides an attractive internalization pathway because it is overexpressed on various types of epithelial cancer cells.[50] More importantly, research has demonstrated that such cells also internalize acetamide-capped, folic acid-conjugated dendrimers *via* receptor-mediated endocytosis.[51] The accompanying recycling of the receptor allows for internalization of large numbers of SPIONs and hence the potential for significant enhancement of image contrast.[4, 52-55]

1.2 Background

Biological entities have been capable of producing endogenous uniform, crystalline magnetic nanoparticles (MNPs) for a very long time.[56] The advent of interest in and research of such biogenic MNPs is credited to Lowenstam's discovery in 1962 of magnetite (Fe_3O_4) in chitons (mollusks of the class Polyplacophora) and the verification of its biological origins.[57] This finding was shocking because it contradicted the conventional notion that magnetite could only form under geological conditions. Through biomineralization processes, chitons are able to coat their radular denticles with a ferrihydrite precursor and subsequently convert at least a portion of the deposited mineral into a layer of aggregated fine magnetite crystals.[58] The magnetite hardens the teeth of the tongue plate to enable their rasping action by which the mollusks scrape their food from rocks. In addition, the magnetic character of these denticle caps may provide some insight[57] into the navigational abilities observed in chitons.[59, 60] Such a behavioral response to a stimulus, possibly rooted in the interaction of the magnetite nanocrystals with Earth's geomagnetic field, is an example of magnetotaxis.

In addition to chitons, many other organisms display magnetotaxis, and the only means of interacting with magnetic fields currently supported by conclusive evidence is through biogenic MNPs.[61] Table 1.1 shows a sample of some of organisms in which magnetite nanocrystals have been found and their locales within the organisms. Of these, only humans do not exhibit clear magnetotaxis;[62] this does not, however, mean that the nanocrystals' presence is biologically insignificant. Since a connection has been show between neurodegenerative diseases and abnormal iron homeostasis in the brain, the

presence of magnetic iron oxide NPs may be linked to these disorders;[56] they may also be related to epilepsy.[62]

Table 1.1 - Organisms in which biogenic MNPs have been found.

Organism type	Organism name	Location of MNPs
Amphibians	Eastern red-spotted newts	throughout bodies[63]
Birds	Bobolinks	upper beaks[64-66]
	Homing pigeons	upper beaks[67-69]
Fish	Atlantic salmon	along lateral lines[70]
	Rainbow trout	olfactory lamellae[71]
	Sockeye salmon	ethmoid cartilage of skulls[72, 73]
	Yellowfin tuna	dermethmoid bone of skulls[74]
Insects	Honeybees	abdomens[75]
	Migratory ants	thoraxes and abdomens[76]
	Termites	thoraxes and abdomens[77]
Mammals	Common Pacific dolphins	dura maters[78]
	Humans	brains[62, 79-81]
		hearts, spleens, and livers[82]
Micro-organisms	Magnetotactic bacteria	magnetosomes[83-85]
	Algae	cells[86]
Mollusks	Chitons	radular denticles[57]

Among the remaining organisms in Table 1.1 that do seem to use their endogenous magnetic nanoparticles for navigation, magnetotactic bacteria have probably been the subjects of the most scientific inquiry. Magnetotactic bacteria are Gram-negative prokaryotes capable of synthesizing magnetite or greigite (Fe_3S_4) nanocrystals ~100 nm in diameter.[87] Each particle is encased in its own lipid bilayer vesicle, forming a particle-endosome composite called a magnetosome. Since the net magnetic moments of isolated magnetite and greigite NPs are thermally randomized, magnetotactic bacteria generally organize magnetosomes in chains, leveraging cooperative magnetic effects to

form internal nanomagnets capable of interacting with the geomagnetic field. This is useful to the organisms because all known magnetotactic bacteria are either microaerophiles or anaerobes: they proliferate in regions with low oxygen content.[87] The bacteria's internal nanomagnets passively torque them into alignment with Earth's magnetic field. Since the oxygen gradient is parallel to the vertical component of the geomagnetic field, the bacteria's quests for their preferred conditions are constrained to efficient one-dimensional searches; the interaction also enhances efficiency by conferring stability on the organisms in their frequently turbulent aqueous environments.[85] Similar benefits are presumably conferred to algae containing biogenic magnetic nanocrystals.[86]

Excluding humans, all the higher-order organisms listed in Table 1 also display magnetotaxis. Phillips *et al.* demonstrated magnetic homing in Eastern red-spotted newts.[88] The animals—displaced from a point of origin while deprived of meaningful sensory stimuli during the displacement that could provide cues for their journey back—were still able to return home. Chitons[57] and homing pigeons[68] display similar behavior. Other animals may also leverage a "sixth-sense" magnetoreception to facilitate migration and foraging.[64, 70, 75-77] The mechanisms of the magnetotaxis in these organisms are more complex than the passive torques magnetotactic bacteria experience but nevertheless seem to rely on interactions between endogenous MNPs and the geomagnetic field.

1.3 Routes to Synthetic Magnetic Nanoparticles

Although many organisms have long been able to produce uniform, crystalline MNPs using biochemical means, laboratory-based methods to produce comparable synthetic MNPs suitable for biological applications are relatively recent developments.[89, 90] There are both physical ("top-down") and wet-chemical ("bottom-up") routes to

magnetic nanocrystals. Examples of the top-down methods include milling bulk materials into fine powders in the presence of surfactants and electron-beam lithography.[91-93]

Wet-chemical syntheses are currently far superior to top-down approaches. Bottom-up approaches are easier and more effective ways to produce MNPs of the quality and quantity desired for biomedical applications[89, 94, 95]: particles with well-defined size, shape, and physicochemical properties.[96, 97] Wet chemical routes offer unparalleled control over these important particle characteristics[95, 98] and generally produce MNPs with more favorable magnetic properties.[94] A few important bottom-up methods are coprecipitation, reverse micelles, and thermolysis of organometallic precursors in organic media. An overview of typical particle properties as produced by the techniques is listed in Table 1.2.[95, 98-100]

1.3.1 Coprecipitation

In the context of synthesizing iron oxide nanoparticles, coprecipitation refers to the precipitation of Fe^{3+} (ferric) and Fe^{2+} (ferrous) ions in aqueous solution using a base.[101] Although many variations exist, the approaches can be classified according to the salts used as precursors.

1.3.1.1 Ferrous Salts Only

When only ferrous salts are used as sources of iron ions, ferric ions must be produced *in situ*; a mild oxidant is introduced to convert some Fe^{2+} to Fe^{3+}. The reaction, which can be described as oxidative hydrolysis,[102] is proposed to occur in three steps.[103-105] In the first step, the ferrous salt is hydrolyzed to form ferrous hydroxide:

Table 1.2 - Particle properties as produced by the listed techniques.

Technique	M_{sat} (emu/g Fe)	Size Range (nm)	Relative Size Distribution (σ/μ)	Yield (g)
Coprecipitation	20-50	10-50	~0.3	~10
Reverse Micelle	>30	4-15	0.10-0.15	~0.1
Thermal Decomposition	>50	3-50	0.05-0.10	~1

$$Fe^{2+} + 2OH^- \rightarrow Fe(OH)_2 \quad (1.1)$$

Part of the $Fe(OH)_2$ is then oxidized to form a ferric oxyhydroxide intermediate:

$$3Fe(OH)_2 + \tfrac{1}{2}O_2 \rightarrow Fe(OH)_2 + 2FeOOH + H_2O \quad (1.2)$$

Finally, magnetite is formed *via* the dehydration reaction between ferrous hydroxide and two equivalents of ferric oxyhydroxide:

$$Fe(OH)_2 + 2FeOOH \rightarrow Fe_3O_4 + 2H_2O \quad (1.3)$$

The typical procedure for such syntheses is to prepare an aqueous solution of ferrous salt and add it dropwise to alkaline media;[106-108] however, it can also be performed by titrating the base with the metal.[109]

1.3.1.2 Ferrous and Ferric Salts

Base hydrolysis of a mixture of ferric and ferrous salts is probably the most common and most successful means of producing magnetite nanocrystals. The reaction is proposed to ultimately proceed as described in Eq. (1.3) above.[101, 103] It can be written in complete form as:[110, 111]

$$Fe^{2+} + 2Fe^{3+} + 8OH^- \rightarrow Fe(OH)_2 + 2FeOOH + 2H_2O \rightarrow Fe_3O_4 + 4H_2O \quad (1.4)$$

To conduct the synthesis, a solution containing the iron salts and an alkaline solution are prepared. As with ferrous salts alone, the metal can be titrated with the base,[112-125] or the base can be titrated with the metal.[111, 126-137] Most authors report that an $[Fe^{3+}]$ to $[Fe^{2+}]$ ratio of 2:1 in the salts solution is optimal.[111-123, 127-133] This stoichiometric ratio is important since deviations adversely impact the quality of the product.[101, 136] However, both lower[124, 125] and higher[126, 134, 137] ratios have been used successfully.

1.3.1.3 Coprecipitation Advantages

Coprecipitation is a facile and convenient way to prepare colloidal MNPs,[98] and the reactions scale well to produce copious amounts of particles: ~10 g with yields around 85%.[95, 102, 124, 131]

1.3.1.4 Coprecipitation Drawbacks and Challenges

Although coprecipitation approaches yield large amounts of MNPs, the particles vary widely in size and shape.[95, 98, 99] This lack of control over the product particles seems to be because only kinetic factors, e.g. precursor concentration, can be manipulated to influence growth.[95] Lowering the concentration of the salts solution can improve product quality but reduces yields, thus undermining the high yield advantage of coprecipitation.

1.3.2 Reverse Micelles

Reverse micelles (RMs), which can occur when surfactants are dispersed in nonpolar solvents, are spherical aggregates of surfactant molecules with their hydrophilic groups at the core and their lipophilic groups facing the solvent. When water is added to a reverse micelle solution, the RMs sequester it within their hydrophilic center to form an aqueous core.[138] In addition to other factors, the core size depends on temperature and the relative concentration of water and surfactant.[139] These water cores constitute "nano-reactors" for coprecipitation reactions to occur and produce magnetite.[114, 138-151] The benefit of the nano-reactors is that they impose thermodynamic and kinetic constraints that are not present in bulk coprecipitation; these constraints promote the formation of more uniform MNPs.[95, 152]

1.3.2.1 Reverse Micelle Advantages

The ability to modulate the size of the reverse micelles by adjusting a few simple parameters facilitates and enhances size control. Reverse micelle cores also represent ideal, confined environments for coating reactions; the technique has been used to coat MNPs *in situ* with gold,[153-157] silica,[138, 147, 149], poly(ethylene glycol) (PEG)[144] among others.

1.3.2.2 Reverse Micelle Drawbacks and Challenges

Reverse micelle methods are inefficient; large ratios of organic solvent to water are required to form nanoscale reverse micelles.[98] Particles produced using the technique exhibit poor crystallinity.[140, 158] Their size distribution is not as broad as those produced using bulk coprecipitation, but they are still polydisperse, most likely because of the poor nucleation kinetics associated with the typically low reaction temperatures.[158] Also, the surfactants need to be removed following synthesis to modify the particles' surfaces, often leading to aggregation.[148] Finally, reverse micelle techniques require judicious selection of the reactants since the wrong choice might compromise the integrity of the RMs.[146]

1.3.3 Thermolysis in Organic Media

Under appropriate solvent and surfactant conditions, heat can be used to decompose organometallic precursors in organic media to form monodisperse populations of iron oxide nanoparticles. Such approaches were first applied to synthesize semiconductor quantum dots and were only recently extended to transition metal oxides.[159, 160] A sampling of these developments is listed in Table 1.3.

Table 1.3 - Thermolytic decomposition syntheses of iron oxide nanoparticles.

Precursor	Surfactant	Solvent	Other Reagents	Temperature
$Fe(acac)_3$	hexadecylamine	hexadecylamine		250°C[161]
	oleic acid, oleylamine	benzyl ether	1,2-hexadecanediol reductant	300°C[162, 163]
$Fe(CO)_5$	oleic acid	octyl ether	$(CH_3)_3NO$ oxidant	300°C[164]
	lauric acid	octyl ether	$(CH_3)_3NO$ oxidant	300°C[164]
	lauric acid	trioctylamine	PyO oxidant	296°C[165]
	lauric acid	octyl ether	PyO oxidant	296°C[165]
	lauric acid	phenyl ether	PyO oxidant	256°C[165]
	stearic acid	octyl ether	$(CH_3)_3NO$ oxidant	290°C[166]
$FeCup_3$	trioctylamine	trioctylamine		250°C[160]
$Fe(OAc)_2$	oleic acid	trioctylamine		255°C[165]
FeO(OH)	oleic acid	1-octadecene		320°C[159]
iron oleate	oleic acid	1-octadecene		300°C[167]
	oleic acid	1-octadecene		320°C[168]

In their pioneering work, Alivisatos' group demonstrated the ferric cupferron complex ($FeCup_3$, where "Cup" represents *N*-nitrosophenylhydroxylamine) to be a suitable precursor to produce uniform maghemite nanoparticles.[160] The complex was synthesized by the precipitation of ferric ions under acidic conditions using cupferron. It was then purified and dissolved in octylamine to form a stable solution. This solution was injected into a rapidly stirring solution of trioctylamine, at 300°C. Trioctylamine is a coordinating solvent: it acts as a surfactant to coat the particles *in situ* in addition to being the dispersion medium. The colorless trioctylamine solution immediately turned black upon injection, indicating the decomposition of the $FeCup_3$ complex and the formation of nanocrystals. After aging at 225°C for 30 minutes, the reaction mixture was allowed to cool. The product nanoparticles could be isolated from this reaction mixture by the addition of excess volumes of acetone or other polar solvents and could then be

resuspended in nonpolar solvents like hexanes. Size control was possible by tuning reaction temperatures and the relative proportions of solvent and precursor.

Iron oleate is another aftermarket precursor that has been synthesized and employed to prepare iron oxide nanocrystals, as Peng's group recently reported.[167] They used 1-octadecene, a noncoordinating solvent, with oleic acid as the surfactant. Very similar work was done by Hyeon and coworkers in verifying their hypothesis that iron oleate was the intermediate product acting as the precursor when they began their reaction with iron pentacarbonyl, $Fe(CO)_5$. Their first study used $Fe(CO)_5$ with oleic acid as the surfactant along with a mild oxidant in octyl ether to produce iron oxide nanocrystals.[164] In subsequent work, they obtained very favorable results by first synthesizing the iron oleate complex rather than having it form *in situ*; oleic acid and 1-octadecence were the surfactant and solvent, respectively.[168]

One final notable precursor is iron (III) acetylacetonate, $Fe(acac)_3$. Sun and colleagues were the first to report the use of $Fe(acac)_3$ as a precursor for iron oxide nanoparticles.[162, 163] Their strategy involved long-chain diols as mild reductants along with oleic acid and oleylamine as surfactants dissolved in benzyl ether. The mixture was ultimately heated to 265°C and aged at that temperature for 30 minutes to produce monodisperse magnetic nanocrystals that could be precipitated, isolated, and redissolved in nonpolar organic solvents.

1.3.3.1 Thermolysis in Organic Media Advantages

Thermal decomposition of organometallic precursors in organic solvents is arguably the best current route to iron oxide nanoparticles. It offers the highest level of control over the size, shape, and morphology of the product,[98] consistently producing

monodisperse populations of particles. The elevated reaction temperature helps eliminate crystal defects, resulting in highly crystalline structures and consequently more favorable magnetic properties.[158, 169] Yields are also high, so large quantities of high-quality particles can be produced:[98] a 40 g reaction has been reported by Park *et al*.[168]

1.3.3.2 Thermolysis in Organic Media Drawbacks and Challenges

Iron oxide nanocrystals produced by thermolytic methods exhibit superior characteristics, but they are necessarily capped by long-chain organic surfactants and are therefore not biocompatible as synthesized.[100] In addition, the synthetic procedures themselves are elaborate and can be unexpectedly difficult to execute successfully.[98]

1.4 Properties of Magnetic Nanoparticles

1.4.1 "Magnetic"

In its common use, "magnetic" refers to the more specific phenomena called ferromagnetism and ferrimagnetism.[95] Ferro- and ferrimagnetism are, however, only two of several classes of magnetic response. Strictly speaking, magnetic phenomena are purely quantum mechanical and are rooted in the spin and orbital angular momenta of electrons. It is helpful to briefly discuss at least some of the varieties of magnetism and their underlying principles.

1.4.1.1 Diamagnetism

All materials exhibit diamagnetism, but the effects are frequently negligible compared to those of the other forms of magnetism. The diamagnetic response is linked to the orbital motion of electrons about atomic nuclei and can be understood by viewing

these motions as forming small current loops. Per Lenz's law, the orbital motion of the electrons will be altered when placed in a magnetic field to produce currents and accompanying magnetic fields that oppose the magnetic flux through the loops. The action against the applied field means that diamagnetic materials have a negative magnetic susceptibility. Their associated magnetic moments are antiparallel to the applied field, and this response is very small: diamagnetic susceptibilities are only around -10^{-6}.[170] Furthermore, the effect is not permanent; the moments and the ordering among them vanish in field-free conditions.[171]

1.4.1.2 Paramagnetism

Only materials composed of atoms or molecules having unpaired electrons are paramagnetic. Paramagnetism is due to the spin and orbital angular momenta of these unpaired electrons.[95, 172] The magnetic moments of individual paramagnetic atoms in a material are only weakly coupled to each other, and room temperature thermal energy is sufficient to overcome these interactions to eliminate any net magnetic moment.[171] When placed in a magnetic field, a small fraction of the atomic moments align parallel to the field in accord with the Boltzmann distribution[95]; conducting the analysis leads to the magnetization, M, of the sample in terms of the Langevin function, L, and the saturation magnetization, M_s:

$$M(H) = M_s L(H) \tag{1.5}$$

The Langevin function is:

$$L(H) = \coth\left(\frac{\mu H}{kT}\right) - \frac{kT}{\mu H} \tag{1.6}$$

where μ is the atomic moment, H is the applied field, k is Boltzmann's constant, and T is the absolute temperature. Similar to the case of diamagnetism, the paramagnetic interaction with the field is weak and disappears in the absence of an applied field. Paramagnetic susceptibilities are also small, but they are positive: $\sim 10^{-6}$.[95] Paramagnetic atoms are further unlike diamagnetic atoms because the moments of individual paramagnetic atoms persist in field-free conditions; it is only the ordering among them that disappears due to thermal fluctuations.

1.4.1.3 Ferromagnetism and Ferrimagnetism

The constituents of ferromagnetic materials are paramagnetic species arranged in a lattice such that they strongly interact with each other to establish permanent alignment of their dipole moments even in the absence of an applied magnetic field: they have a remanent magnetization or "exhibit remanence." The parallel alignment among moments is contrary to the notions of classical electromagnetism that predict adjacent dipoles will align antiparallel to each other. Quantum mechanics, however, provides an understanding of the phenomenon through exchange interactions. Electrons, which are fermions, are responsible for the dipole moments of paramagnetic atoms. Fermionic wave functions are antisymmetric under particle exchange. This condition favors alignment of the dipoles since such a configuration places electrons in different orbitals and actually lowers the Coulombic repulsion between them, thus reducing the energy of the system; the "exchange energy" is said to be minimized.[172]

Ferrimagnetism is nearly identical to ferromagnetism with the exception that it occurs when different paramagnetic species composing a material exist in sublattices. The moments within each sublattice are cooperatively aligned due to exchange

interactions, but the net moments of the sublattices are antiparallel to each other. A net magnetic moment still exists when these moments are unequal. (The phenomenon of antiferromagnetism occurs when the moments among sublattices sum to zero.) Because of this competition between sublattices, the magnetic moments of ferrimagnetic materials are typically lower than those of ferromagnetic materials.

Despite the difference in the magnitude of the magnetic moments between ferro- and ferrimagnetic materials and the subtle distinction underlying their moments, the materials behave similarly. One very important shared property is that the long-range ordering between the constituent paramagnetic species does not extend throughout the bulk. In bulk materials it is energetically favorable to establish regions of uniform magnetization without the moments of the regions being aligned.[173] These regions are called domains, and they are separated by barriers called domain walls. Although it costs energy to form domain walls, the reduction in magnetic energy realized by their formation yields a net energetic benefit for bulk materials.

Virgin ferro- and ferrimagnetic materials actually display no net magnetization in field-free conditions due to the arrangement of domains; there is still ordering within the domains but no overall magnetic order. When ferro- and ferrimagnetic materials become magnetized by an applied field, the domains along its direction grow at the expense of the other domains to produce a net moment. As might be expected, this magnetic response is much larger than what is observed for paramagnets. Ferro- and ferrimagnetic materials are characterized by high susceptibilities $\sim 10^6$.

1.4.1.4 Superparamagnetism

When ferro- and ferrimagnetic materials become very small, establishing domains costs more energy than the reduction in magnetostatic energy they would afford.[174] In this regime, particles thus exist as single domains. The size where monodomain structure begins to occur, referred to as the critical diameter, is typically ~10-100 nm but depends on the material[98, 174]; it is about 70 nm for Fe_3O_4.[175] In monodomain particles, all the constituent paramagnetic moments are aligned.[96, 176-178] Changes in magnetization can obviously no longer occur by rearrangement of domain walls since none exist. The particle moment, which theoretically consists of the entire complement of atomic moments, changes in response to an applied magnetic field either *via* coherent rotation of the moments themselves (Néel relaxation) or *via* physical rotation of the particle (Brownian relaxation).[179-181]

After the applied field is removed, large monodomain particles retain a net moment, and this remanent magnetization lies along an easy axis. Easy axes are certain preferred directions of magnetization corresponding to energy minima; the lack of equivalence among all possible moment orientation is called magnetic anisotropy. Many easy axes can exist separated by energy barriers. There are various sources of anisotropy and the corresponding barriers, but size is among the most critical factors involved.

Once particles become much smaller than the maximum monodomain size, the energy separating easy axes becomes comparable to ambient thermal energy.[152] The magnetic moment of the particle thus undergoes spontaneous Néel relaxation and continuously cycles through the easy directions.[100, 182, 183] These thermal fluctuations occur with a frequency given by:

$$f = f_0 \, e^{-(E_b/kT)} \tag{1.7}$$

where E_b is the height of the energy barrier, k is Boltzmann's constant, T is the absolute temperature, and f_0 is an attempt frequency 10^9-10^{12} Hz[96, 180]: a quantity proposed to be linked to the gyromagnetic precession frequency of a particle's moment in the effective anisotropy field.[96, 184, 185] Due to the persistent fluctuation of their magnetic moment, particles of this size do not exhibit remanence unless the measurement can be made faster than the frequency of transitions. They therefore behave like singular paramagnetic species but with important distinctions. The magnetic moment of such a particle is the sum of thousands of paramagnetic moments. In an applied magnetic field, these "super-moments" will align just like very large individual paramagnetic moments: they are "super-paramagnets" and exhibit the phenomenon known as superparamagnetism.[177] The magnetization behavior of a collection of monodisperse superparamagnetic particles in an applied field can be conveniently described using the Langevin function:[173, 186]

$$M(H) = M_s \left(\coth\left(\frac{\mu H}{kT} \right) - \frac{kT}{\mu H} \right) \tag{1.8}$$

where M_s is the saturation magnetization, μ is now the per-particle moment, H is the applied field, k is Boltzmann's constant, and T is the absolute temperature. Collections of superparamagnetic particles exhibit saturation magnetizations that are comparable to but smaller than those of the corresponding bulk if the parent material is ferrimagnetic.[174] The saturation magnetizations of collections of particles whose bulk parent material is ferromagnetic may actually be slightly enhanced with respect to the bulk value.[174] These phenomena are due to surface effects, size effects, or, more likely the interplay between

them[98, 187]; many excellent articles have been written containing thorough discussions and debate about the topic.[96, 126, 172, 174, 175, 187-200]

1.4.2 "Nano"

The small size of SPIONs leads to their fascinating magnetic properties that allow them to be addressed and manipulated by magnetic fields, but it is also a useful and essential feature for their applications in biology. Nanoparticles can be dispersed to form stable, uniform colloids suitable for injection.[100, 128, 179] Once *in vivo* their size facilitates widespread tissular diffusion to encounter many different biological structures.[1, 54, 128] Particles smaller than around 6 nm can extravasate through the continuous capillaries of tissues like muscle, lung, and skin.[201-203] With diameters below 20 nm, particles are able to pass through blood vessel walls.[204] Larger particles up to 60 nm can still penetrate fenestrated capillaries found in different regions, *e.g.* the kidney, pancreas, and intestines, but are susceptible to rapid splenic filtration.[201-205] Because nanoparticle dimensions are similar to biological structures, the particles are able to directly interact with such entities.[94, 97, 100, 170, 206-208] Furthermore, the particles' large relative surface area presents ample space to carry multiple copies of biofunctional molecules to moderate these interactions.[128, 179, 206]

1.5 Biomedical Applications of Magnetic Nanoparticles

1.5.1 Targeting Therapeutics

The systemic distribution of therapeutics in contemporary treatment methods is problematic and represents a major flaw that can make the difference between success and failure.[209] High doses are often needed to accumulate adequate amounts of

therapeutic at the target site, but larger doses also mean higher risk of adverse side-effects and elevated toxicity to non-target sites.[210, 211] A strategy to address these issues, fostered by several researchers in the late 1970s,[212-214] is to magnetically label therapeutics so they can be targeted to a region of interest using an external magnetic field. The field confines drugs longer in the target region to boost efficacy.[90, 215-219] Therefore, more substantial therapeutic effects can be realized at lower doses while minimizing risk to healthy tissues.[170, 215, 220] Magnetic targeting of therapeutics has been examined regarding the more fundamental issues of carrier composition and biodistribution[212, 221-225] in addition to being applied in studies *in vitro* and *in vivo*.[213, 215, 217-219, 226-234] A sampling of the latter studies is listed in Table 1.4. Reviews addressing the topic have also been written.[211, 216]

Recent *in vivo* work in the field of magnetic drug targeting has been successful although many challenges remain.[209, 216, 235] The major obstacle when using an external magnet to target particles *in vivo* is the rapid decrease of field strength with increasing distance from the magnet because strong fields are required to overcome forces from blood flow and hold the particles at the target site.[209, 236] This imposes a major limitation for use in humans as locations deeper than about 2 cm within the body are poorly targeted.[210, 237] Such sites require improved magnetic technology or alternative targeting methods.

Table 1.4 - Applications of iron oxide nanoparticles in magnetically targeted therapeutics.

Animal	Therapeutic Class	Therapeutic Name
[*in vitro*]	drug	adriamycin[213, 234]
	radionuclide	rhenium-188[228]
human	drug	doxorubicin[230, 232]
	drug	epirubicin[218, 219]
mouse	gene vector	recombinant adeno-associated virus 2[231]
	radionuclide	yttrium-90[229]
rabbit	drug	methotrexate[215]
rat	drug	adriamycin[226]
	drug	doxorubicin[233]
	drug	epirubicin[217]
swine	drug	doxorubicin[227]

1.5.2 Magnetic Resonance Imaging (MRI) Contrast Agents

Magnetic resonance imaging is among the best clinical diagnostic tools currently available.[52, 54, 238] It is a noninvasive, tomographic technique, without the dangers of ionizing radiation, that offers superb spatial resolution,[1, 9, 53, 55] perhaps even down to the cellular or subcellular level.[3] The largest contributors to MRI signal for biological applications are the hydrogen nuclei (protons) in water molecules. In a simplistic sense, MRI is just the application of proton nuclear magnetic resonance (NMR) to biological systems:[56] it yields intensity maps of water proton spin relaxation in tissue. Contrast in the resulting images is the consequence of proton density and relaxation time constants that vary throughout the sample. However, MRI suffers from relatively low sensitivity that limits its utility when relying solely upon these inherent contrast mechanisms.[111] This flaw can fortunately be addressed using exogenous magnetic agents that influence

local proton spin relaxation dynamics thereby enhancing the distinguishability of structures within images.[53, 170, 238-241]

There are several different types of contrast agents, and the two main classes are based on chelated paramagnetic ions, such as gadolinium (Gd), or SPIONs. Particulate superparamagnetic contrast agents offer advantages over their paramagnetic counterparts in both efficiency and mechanism of action. Whereas chelated paramagnetic ions must be present at the mM level to generate appreciable contrast, SPIONs are detectable at the nM concentrations or lower.[242, 243] The action of SPIONs is also not as critically dependent on their surroundings. Paramagnetic chelates produce local effects that are mediated by exchange of water protons, but SPIONs produce magnetic field gradients and corresponding changes in tissue susceptibility that impact a larger region without the need for direct contact with water flux.[52, 202, 238, 244]

A plethora of studies have examined the theory and use of SPION contrast agents; some of these investigations are presented in Table 1.5. These applications leverage the passive targeting of SPIONs *in vivo* that is a function of their physicochemical characteristics; the particles' biodistribution can be tuned by adjusting parameters such as their size, surface coating, and surface charge.[176, 245] Most of the targeting involves the reticuloendothelial system (RES), also known as the mononuclear phagocyte system (MPS): an array of phagocytic cells intended to defend against foreign matter in the circulatory system.[54] Contrast arises due to the disparity in accumulation of SPIONs resulting from the reduced or eliminated RES function of pathologic versus healthy tissue.[246] Larger particles are most useful for targeting the secondary lymphoid organs of the RES, e.g. the liver and the spleen.[176, 245] Particles with longer circulation, which are

generally smaller, accumulate in the lymph nodes and bone marrow and can even be addressed to sites of inflammation by macrophage uptake.[176, 245] Small particles can also be used as blood pool agents for imaging the vasculature and have the potential to gather in non-RES tumors.[176, 245] Such passive tumor targeting is the result of the enhanced permeation and retention effect. Malignancies exhibit leaky vasculature and poor drainage.[247] Once particles reach the tumor site, they extravasate through the porous endothelium and are retained by the tumor due to its compromised clearance mechanisms.[201, 203, 248-252]

Table 1.5 - Applications of iron oxide nanoparticles as passively targeted MRI contrast agents.

Targeting Mediator	Subject	Region of Interest
[blood pool]	human	aortoiliac vessel[253]
		coronary artery[254]
	rabbit	vasculature[255]
	rat	vasculature[256]
EPR	human	breast tumor[257]
	rat	brain tumor[258, 259]
		breast tumor[260]
macrophages	mouse	joint inflammation[261]
	rabbit	atherosclerosis[262, 263]
	rat	central nervous system inflammation[264]
		kidney allograft[265]
RES	human	bone marrow[266, 267]
		liver[268-271]
		liver and spleen[272]
		lymph nodes[273-275]
	rabbit	liver and spleen[276]
	rat	bone marrow[277]
		liver[278]
		liver and spleen[246]
		lymph nodes[279-283]

1.5.3 Actively Targeted MRI Contrast Agents

Although the physical mode of targeting employed for therapeutic delivery and the passive mode of targeting used for current clinical SPION contrast agents are very useful, further enhancement of specificity is necessary to realize the agents' full diagnostic potential.[284] The vision is to construct agents that can be addressed to very specific molecular markers of pathology so diseases can be visualized and diagnosed earlier and more accurately and treated more effectively or even prevented, ultimately improving patient survival.[1, 2, 285] Such an approach, leveraging molecular interactions, is called active targeting.

Many different agents (Table 1.6) have been used to actively target SPIONs, and antibodies have been a frequent choice.[4-17]. Funovics and co-workers used coprecipitation methods to generate targeted dextran-coated particles.[7] One half of the batch was decorated with anti-her2/neu monoclonal antibodies (mAbs); the other half was functionalized with mAbs directed against the 9.2.27 tumor antigen. The researchers demonstrated *in vitro* SPION targeting *via* both these vectors in numerous cell lines using SPIONs labeled with isotype antibodies, untreated cells and antigen-negative cells as controls.

Cheon's group recently published combined *in vitro* and *in vivo* results using anti-her2/neu mAb as a targeting moiety.[9] The investigators synthesized uniform SPIONs in organic solvents and transferred them into water *via* place exchange with the small molecule dimercaptosuccinic acid (DMSA); Herceptin molecules were subsequently linked to free thiol functions on the nanoparticle surface. Targeting of the conjugates was demonstrated *in vitro* for different cell lines with varying her2/neu expression, and the

Table 1.6 - Applications of iron oxide nanoparticles as actively targeted MRI contrast agents.

Target	Targeting Agent	Agent Class	Synthetic Method
9.2.27 antigen	anti-9.2.27 mAb	antibody	coprecipitation[7]
Aβ-plaques	Aβ1-40	peptide	coprecipitation[49]
$\alpha_{IIb}\beta_3$ integrin	RGD	peptide	coprecipitation[37]
$\alpha_V\beta_3$ integrin	cRGD	peptide	organic thermolysis[46]
anti-carcinoembryonic antigen	anti-CEA mAb	antibody	coprecipitation[13]
	rch 24 mAb	antibody	organic thermolysis[8]
asialoglycoprotein	Arabinogalactan	glycoprotein	coprecipitation[34-36]
biotinylated anti-L (IgG_1)	biotin (*via* strepavidin bridge)	antibody	coprecipitation[5]
biotinylated her2/neu mAb	Strepavidin	antibody	coprecipitation[4]
bombesin receptor	bombesin peptide	peptide	coprecipitation[45]
CD4, CD8	anti-CD4, anti-CD8 Abs	antibody	coprecipitation[11]
E-selectin	fragment of mAb H18/7	antibody	coprecipitation[10]
	sialyl $lewis^x$	carbohydrate	coprecipitation[44]
folic acid receptor	folic acid	vitamin	coprecipitation[19-25]
			organic thermolysis[18]
her2/neu receptor	anti-her2/neu mAb	antibody	coprecipitation[7]
			organic thermolysis[9]
inflammation	IgG Ab	antibody	coprecipitation[16]
L6 antigen	anti-L6 mAb	antibody	coprecipitation[12]
LH/CG receptor	luteinizing hormone/chorionic gonadotropin	hormone	coprecipitation[43]

Target	Targeting Agent	Agent Class	Synthetic Method
LHRH receptor	luteinizing hormone releasing hormone	hormone	coprecipitation[43]
myosin	antimyosin fragment	antibody	coprecipitation[17]
phosphatidylserine on apoptotic cells	annexin V	protein	coprecipitation[28, 29]
	synaptotagmin I	protein	coprecipitation[26]
reduced-folate carrier	methotrexate	drug	coprecipitation[47, 48]
surface antigen on colorectal carcinoma	mAb A7	antibody	coprecipitation[14]
surface antigen on HT-29 colon carcinoma	mAb-610	antibody	coprecipitation[6]
transferrin rececptor	transferrin	glycoprotein	coprecipitation[38-42]
uMUC-1 antigen	YCAREPPTRTFAYWG peptide	peptide	coprecipitation[31]
[unclear]	isatoic anhydride, 5-chloro-isatoic anhydride	small molecule	coprecipitation[33]
VCAM-1	anti-VCAM-1 mAb	antibody	coprecipitation[15]
	linear peptide VHPKQHR	peptide	coprecipitation[32]
	cyclic peptide CVHSPNKKC	peptide	coprecipitation[27, 30]

MRI signal intensity of cell samples was observed to drop with increasing expression. SPIONs labeled with irrelevant antibody and untreated cells served as controls. The probes were also investigated in two mice, each bearing a NIH3T6.7 xenograft. One mouse was injected with the Herceptin conjugates, and the other was similarly treated with SPIONs bearing the irrelevant antibody. The former animal's tumor rapidly became hypointense on T2*-weighted images, whereas images of the tumor in the latter animal exhibited virtually no change.

In addition to antibodies, the glycoprotein transferrin has been used as a targeting moiety for SPIONs.[38-42] The transferrin receptor is a particularly interesting choice because, as the name suggests, it is used to transport iron contained by the protein into cells. Following internalization, the receptors are recycled to the cell surface for further iron accretion. This cycle is therefore useful in loading transferrin-decorated particles into cells *via* receptor-mediated endocytosis leading the potential for particle accumulation, enhanced relaxation effects and consequently higher contrast.

1.6 Dendrimer-Coated SPIONs as Actively Targeted MRI Contrast Agents

1.6.1 Why Thermolysis? – Quality and control

Thermolytic decomposition methods are challenging and produce particles that require additional processing to be made biocompatible for use in medicine, but their characteristics and the control over them are unparalleled by other contemporary products and techniques.[98] The monodispersity and high saturation magnetization achieved are both essential to their use as targeted MRI contrast agents.[100] The particles' large

magnetic response maximizes contrast effects at minimal doses. Their narrow size distribution is critical for the understanding and optimization of behavior *in vivo* as well as facilitating comparisons among batches and formulations.[94, 176, 220]

1.6.2 Why Iron Oxide? – Safe but highly effective

Many factors make iron oxides (Fe_3O_4 and maghemite, γ-Fe_2O_3) excellent materials for developing targeted MRI contrast agents. They have been shown to naturally occur in many animals and are currently the only inorganic particulate contrast agents approved for *in vivo* human applications with more formulations now in Phase-III trials.[244, 286, 287] Iron oxides are biodegradable and exhibit neither acute nor chronic toxicity.[99, 176, 284, 288] Uncoated magnetite has an LD_{50} of 300-600 mg Fe per kg body weight, and biocompatible coatings can improve this by an order of magnitude.[52, 289]

Superparamagnetic iron oxide nanoparticles have exceptional magnetic properties, so they are able to generate sufficient contrast in low doses versus their paramagnetic counterparts, like gadolinium (Gd): nM SPIONs (μM Fe) versus mM Gd.[176, 242, 243] The typical clinical contrast agent dose for SPIONs of 1 mg Fe per kg body weight is a small fraction of the LD_{50}. It is also negligible compared to the approximately 3500 mg of total iron naturally occurring in various forms in the human body, representing less iron content than is contained in a pint of blood.[290, 291] Furthermore, the body has established methods to metabolize the excess iron introduced by the particles.[202, 203, 239, 281, 284, 292]

Although contrast agents based on strong ferromagnetic parent materials like cobalt and nickel are attractive, they are toxic in pristine and oxidized forms and are not biodegradable.[94, 183, 293-295] Pure iron nanoparticles certainly represent a possible

alternative, but metallic particles are highly unstable and readily oxidize without robust protection;[153, 175, 296] they sometimes react so strongly that they spontaneously ignite in air.[152] Magnetite is also susceptible to oxidation into maghemite; however, this transition occurs without appreciable alteration of magnetic properties.[171, 297]

1.6.3 Why Dendrimers? – Uniform, proven biocompatible coating

Poly(amidoamine) (PAMAM) dendrimers are hydrophilic, biocompatible, monodisperse, cascade-branched macromolecules with highly flexible surface chemistry that facilitates functionalization.[298-300] They can be used as uniform scaffolds carrying multiple copies of biologically relevant molecules without interfering with the components' functions.[301, 302] Their well-defined, consistent structure is crucial to their successful and reproducible use as carriers;[252] it also makes them particularly well-suited for interaction with biological entities because it emulates the inherent order of natural macromolecules.[303]

Our group has demonstrated success using PAMAM dendrimers to target tumors both *in vitro* and *in vivo*.[51, 299, 304-312] The PAMAM dendrimers used for the work described in this dissertation are unique in that the surfaces were completely neutralized by capping with acetyl groups following the covalent attachment of several molecules of both folic acid and 6-TAMRA dye. Folic acid is the targeting moiety; the dye allows optical tracking of the devices, and the neutral surface minimizes nonspecific interactions with cells.[299, 300, 304, 308, 312, 313] The dendrimers imparted targeting and fluorescence to the SPION cores in addition to protecting them from aggregation. Such a thick, hydrophilic coating relying on steric hindrance to keep the cores isolated is expected to provide enhanced stability as well as longer circulation times *in vivo*.[99, 100, 252, 314]

1.6.4 Why Folic Acid? – Small, effective agent linked to fundamental processes

Folic acid (FA) is excellent as a targeting moiety for several reasons. Folic acid is a low molecular-weight B-vitamin whose receptors are overexpressed by an array of cancers,[50, 315] including lung[316], breast[316], colon[316], choroid plexus brain[316], choriocarcinoma[316], and ovarian cancers.[316-319] Folic acid receptors (FARs) tend to occur in clusters,[251] and this morphology can be leveraged for multivalent interactions leading to enhanced targeting efficacy by using multiple folic acid moieties on the nanoparticle surface.[52, 305, 320] Although normal tissues also express FARs, the level of expression is much higher in malignant tissue and seems to increase as the cancer progresses.[321] The FARs on normal cells are also expressed in a different location that is not accessible from the bloodstream.[321]

Folic acid is a stable molecule that does not induce an immune response, presumably because of its small size.[25, 50, 52, 252] Its small size also facilitates tissular diffusion and increases residence time in the blood compartment, especially versus antibodies.[52, 285] Also unlike antibodies, FA has a high affinity for its target that does not diminish following conjugation to macromolecules or nanoparticles.[50, 285] A third and very important advantage of FA over antibodies is that FARs are expected to be more stable targets, whereas antigen expression may change over time. This is because FA is a necessary ingredient in crucial biosyntheses underlying cellular proliferation.[22, 238, 244, 285] Folic acid receptors are therefore internalized and recycled to the surface for gathering the vitamin,[22, 25, 251] a process that is highly advantageous since it should enable active loading of SPIONs and lead to MRI signal enhancement.[4, 52-55]

1.6.5 Hypotheses and Specific Aims

This dissertation work focused on exploring the possibility of SPIONs as targeted MRI contrast agents. The project was driven by these hypotheses:

1.) Thermolytic decomposition is the optimal method to produce high-quality SPIONs.

2.) Appropriately functionalized dendrimers will transfer SPIONs from organic media, solubilize and protect them in biological environments, and impart targeting.

3.) The KB cell line with an overexpression of the folate receptor provides a valid test case to prove the concept of targeting SPIONss using dendrimers.

4.) Folic acid-labeled dendrimer-SPION conjugates will target KB cells *in vitro*.

The novel research that I conducted to address these hypotheses had these specific aims:

1.) Synthesize high-quality SPIONs in organic media (OC-SPIONs).

2.) Solubilize high-quality magnetic nanocrystals in biological media using dendrimers that are conjugated to folic acid to effect targeting.

3.) Characterize organic-coated SPIONs and dendrimer-coated SPIONs (DC-SPIONs).

4.) Conduct biological experiments to verify targeting of DC-SPIONs *in vitro* using the fluorescent tag on the dendrimers as well as the elemental signature from the iron oxide core.

1.7 References

1. Morawski, A. M.; Lanza, G. A.; Wickline, S. A. Targeted Contrast Agents for Magnetic Resonance Imaging and Ultrasound. *Curr. Opin. Biotechnol.* **2005,** 16, (1), 89-92.

2. Berry, C. C. Possible Exploitation of Magnetic Nanoparticle-Cell Interaction for Biomedical Applications. *J. Mater. Chem.* **2005,** 15, (5), 543-547.

3. Sosnovik, D. E.; Weissleder, R. Emerging Concepts in Molecular MRI. *Curr. Opin. Biotechnol.* **2007,** 18, (1), 4-10.

4. Artemov, D.; Mori, N.; Okollie, B.; Bhujwalla, Z. M. MR Molecular Imaging of the Her-2/*neu* Receptor in Breast Cancer Cells Using Targeted Iron Oxide Nanoparticles. *Magn. Reson. Med.* **2003,** 49, (3), 403-408.

5. Bulte, J. W. M.; Hoekstra, Y.; Kamman, R. L.; Magin, R. L.; Webb, A. G.; Briggs, R. W.; Go, K. G.; Hulstaert, C. E.; Miltenyi, S.; The, T. H.*, et al.* Specific MR Imaging of Human Lymphocytes by Monoclonal Antibody-Guided Dextran-Magnetite Particles. *Magn. Reson. Med.* **1992,** 25, (1), 148-157.

6. Cerdan, S.; Lötscher, H. R.; Künnecke, B.; Seelig, J. Monoclonal Antibody-Coated Magnetite Particles as Contrast Agents in Magnetic Resonance Imaging of Tumors. *Magn. Reson. Med.* **1989,** 12, (2), 151-163.

7. Funovics, M. A.; Kapeller, B.; Hoeller, C.; Su, H. S.; Kunstfeld, R.; Puig, S.; Macfelda, K. MR Imaging of the Her2/neu and 9.2.27 Tumor Antigens Using Immunospecific Contrast Agents. *Magn. Reson. Imaging* **2004,** 22, (6), 843-850.

8. Hu, F.; Wei, L.; Zhou, Z.; Ran, Y.; Li, Z.; Gao, M. Preparation of Biocompatible Magnetite Nanocrystals for in Vivo Magnetic Resonance Detection of Cancer. *Adv. Mater.* **2006,** 18, (19), 2553-2556.

9. Huh, Y.-M.; Jun, Y.; Song, H.-T.; Kim, S.; Choi, J. S.; Lee, J.-H.; Yoon, S.; Kim, K.-S.; Shin, J.-S.; Suh, J.-S.*, et al.* In Vivo Magnetic Resonance Detection of Cancer by Using Multifunctional Magnetic Nanocrystals. *J. Am. Chem. Soc.* **2005,** 127, (35), 12387-12391.

10. Kang, H. W.; Josephson, L.; Petrovsky, A.; Weissleder, R.; Bogdanov, A. Magnetic Resonance Imaging of Inducible E-Selectin Expression in Human Endothelial Cell Culture. *Bioconjugate Chem.* **2002,** 13, (1), 122-127.

11. Pirko, I.; Johnson, A.; Ciric, B.; Gamez, J.; Macura, S. I.; Pease, L. R.; Rodriguez, M. In Vivo Magnetic Resonance Imaging of Immune Cells in the Central Nervous System with Superparamagnetic Antibodies. *FASEB J.* **2004,** 18, (1), 179-182.

12. Remsen, L. G.; McCormick, C. I.; Roman-Goldstein, S.; Nilaver, G.; Weissleder, R.; Bogdanov, A.; Hellström, K. E.; Hellström, I.; Kroll, R. A.; Neuwelt, E. A. MR of

Carcinoma-Specific Monoclonal Antibody Conjugated to Monocrystalline Iron Oxide Nanoparticles: The Potential for Noninvasive Diagnosis. *Am. J. Neuroradiol.* **1996,** 17, (3), 411-418.

13. Tiefenauer, L. X.; Kuehne, G.; Andres, R. Y. Antibody-Magnetite Nanoparticles: *In Vitro* Characterization of a Potential Tumor-Specific Contrast Agent for Magnetic Resonance Imaging. *Bioconjugate Chem.* **1993,** 4, (5), 347-352.

14. Toma, A.; Otsuji, E.; Kuriu, Y.; Okamoto, K.; Ichikawa, D.; Hagiwara, A.; Ito, H.; Nishimura, T.; Yamagishi, H. Monoclonal Antibody A7-Superparamagnetic Iron Oxide as Contrast Agent of MR Imaging of Rectal Carcinoma. *Br. J. Cancer* **2005,** 93, (1), 131-136.

15. Tsourkas, A.; Shinde-Patil, V. R.; Kelly, K. A.; Patel, P.; Wolley, A.; Allport, J. R.; Weissleder, R. In Vivo Imaging of Activated Endothelium Using an Anti-VCAM-1 Magnetooptical Probe. *Bioconjugate Chem.* **2005,** 16, (3), 576-581.

16. Weissleder, R.; Lee, A. S.; Fischman, A. J.; Reimer, P.; Shen, T.; Wilkinson, R.; Callahan, R. J.; Brady, T. J. Polyclonal Human Immunoglobulin G Labeled with Polymeric Iron Oxide: Antibody MR Imaging. *Radiology* **1991,** 181, (1), 245-249.

17. Weissleder, R.; Lee, A. S.; Khaw, B. A.; Shen, T.; Brady, T. J. Antimyosin-Labeled Monocrystalline Iron Oxide Allows Detection of Myocardial Infarct: MR Antibody Imaging. *Radiology* **1992,** 182, (2), 381-385.

18. Landmark, K. J.; DiMaggio, S.; Ward, J.; Kelly, C.; Vogt, S.; Hong, S.; Kotlyar, A.; Myc, A.; Thomas, T. P.; Penner-Hahn, J. E.*, et al.* Synthesis, Characterization, and *in Vitro* Testing of Superparamagnetic Iron Oxide Nanoparticles Targeted Using Folic Acid-Conjugated Dendrimers. *ACS Nano* **2008,** 2, (4), 773-783.

19. Shi, X.; Wang, S. H.; Swanson, S. D.; Ge, S.; Cao, Z.; Van Antwerp, M. E.; Landmark, K. J.; Baker, J. R., Jr. Dendrimer-Functionalized Shell-Crosslinked Iron Oxide Nanoparticles for *in-Vivo* Magnetic Resonance Imaging of Tumors. *Adv. Mater.* **2008,** 20, (9), 1671-1678.

20. Choi, H.; Choi, S. R.; Zhou, R.; Kung, H. F.; Chen, I.-W. Iron Oxide Nanoparticles as Magnetic Resonance Contrast Agent for Tumor Imaging Via Folate Receptor-Targeted Delivery. *Acad. Radiol.* **2004,** 11, (9), 996-1004.

21. Sonvico, F.; Mornet, S.; Vasseur, S.; Dubernet, C.; Jaillard, D.; Degrouard, J.; Hoebeke, J.; Duguet, E.; Colombo, P.; Couvreur, P. Folate-Conjugated Iron Oxide Nanoparticles for Solid Tumor Targeting as Potential Specific Magnetic Hyperthermia Mediators: Synthesis, Physicochemical Characterization, and in Vitro Experiments. *Bioconjugate Chem.* **2005,** 16, (5), 1181-1188.

22. Sun, C.; Sze, R.; Zhang, M. Folic Acid-PEG Conjugated Superparamagnetic Nanoparticles for Targeted Cellular Uptake and Detection by MRI. *J. Biomed. Mater. Res., Part A* **2006,** 78A, (3), 550-557.

23. Wang, S. H.; Shi, X.; Van Antwerp, M.; Cao, Z.; Swanson, S. D.; Bi, X.; Baker, J. R., Jr. Dendrimer-Functionalized Iron Oxide Nanoparticles for Specific Targeting and Imaging of Cancer Cells. *Adv. Funct. Mater.* **2007,** 17, (16), 3043-3050.

24. Zhang, Y.; Sun, C.; Kohler, N.; Zhang, M. Self-Assembled Coatings on Individual Monodisperse Magnetite Nanoparticles for Efficient Intracellular Uptake. *Biomed. Microdevices* **2004,** 6, (1), 33-40.

25. Zhang, Y.; Kohler, N.; Zhang, M. Surface Modification of Superparamagnetic Magnetite Nanoparticles and Their Intracellular Uptake. *Biomaterials* **2002,** 23, (7), 1553-1561.

26. Zhao, M.; Beauregard, D. A.; Loizou, L.; Davletov, B.; Brindle, K. M. Non-Invasive Detection of Apoptosis Using Magnetic Resonance Imaging and a Targeted Contrast Agent. *Nat. Med.* **2001,** 7, (11), 1241-1244.

27. Nahrendorf, M.; Jaffer, F. A.; Kelly, K. A.; Sosnovik, D. E.; Aikawa, E.; Libby, P.; Weissleder, R. Noninvasive Vascular Cell Adhesion Molecule-1 Imaging Identifies Inflammatory Activation of Cells in Atherosclerosis. *Circulation* **2006,** 114, (14), 1504-1511.

28. Sosnovik, D. E.; Schellenberger, E. A.; Nahrendorf, M.; Novikov, M. S.; Matsui, T.; Dai, G.; Reynolds, F.; Grazette, L.; Rosenzweig, A.; Weissleder, R.*, et al.* Magnetic Resonance Imaging of Cardiomyocyte Apoptosis with a Novel Magneto-Optical Nanoparticle. *Magn. Reson. Med.* **2005,** 54, (3), 718-724.

29. Schellenberger, E. A.; Sosnovik, D.; Weissleder, R.; Josephson, L. Magneto/Optical Annexin V, a Multimodal Protein. *Bioconjugate Chem.* **2004,** 15, (5), 1062-1067.

30. Kelly, K.; Nahrendorf, M.; Yu, A.; Reynolds, F.; Weissleder, R. In Vivo Phage Display Selection Yields Atherosclerotic Plaque Targeted Peptides for Imaging. *Mol. Imaging Biol.* **2006,** 8, (4), 201-207.

31. Moore, A.; Medarova, Z.; Potthast, A.; Dai, G. In Vivo Targeting of Underglycosylated MUC-1 Tumor Antigen Using a Multimodal Imaging Probe. *Cancer Res.* **2004,** 64, (5), 1821-1827.

32. Kelly, K. A.; Allport, J. R.; Tsourkas, A.; Shinde-Patil, V. R.; Josephson, L.; Weissleder, R. Detection of Vascular Adhesion Molecule-1 Expression Using a Novel Multimodal Nanoparticle. *Circ. Res.* **2005,** 96, (3), 327-336.

33. Weissleder, R.; Kelly, K.; Sun, E. Y.; Shtatland, T.; Josephson, L. Cell-Specific Targeting of Nanoparticles by Multivalent Attachment of Small Molecules. *Nat. Biotechnol.* **2005,** 23, (11), 1418-1423.

34. Reimer, P.; Weissleder, R.; Lee, A. S.; Wittenberg, J.; Brady, T. J. Receptor Imaging: Application to MR Imaging of Liver Cancer. *Radiology* **1990,** 177, (3), 729-734.

35. Weissleder, R.; Reimer, P.; Lee, A. S.; Wittenberg, J.; Brady, T. J. MR Receptor Imaging: Ultrasmall Iron Oxide Particles Targeted to Asialoglycoprotein Receptors. *Am. J. Roentgenol.* **1990,** 155, (6), 1161-1167.

36. Reimer, P.; Weissleder, R.; Wittenberg, J.; Brady, T. J. Receptor-Directed Contrast Agents for MR Imaging: Preclinical Evaluation with Affinity Assays. *Radiology* **1992,** 182, (2), 565-569.

37. Johansson, L. O.; Bjørnerud, A.; Ahlström, H. K.; Ladd, D. L.; Fujii, D. K. A Targeted Contrast Agent for Magnetic Resonance Imaging of Thrombus: Implications of Spatial Resolution. *J. Magn. Reson. Imaging* **2001,** 13, (4), 615-618.

38. Högemann, D.; Josephson, L.; Weissleder, R.; Basilion, J. P. Improvement of MRI Probes to Allow Efficient Detection of Gene Expression. *Bioconjugate Chem.* **2000,** 11, (6), 941-946.

39. Kresse, M.; Wagner, S.; Pfefferer, D.; Lawaczeck, R.; Elste, V.; Semmler, W. Targeting of Ultrasmall Superparamagnetic Iron Oxide (USPIO) Particles to Tumor Cells in Vivo by Using Transferrin Receptor Pathways. *Magn. Reson. Med.* **1998,** 40, (2), 236-242.

40. Moore, A.; Basilion, J. P.; Chiocca, E. A.; Weissleder, R. Measuring Transferrin Receptor Gene Expression by NMR Imaging. *Biochim. Biophys. Acta* **1998,** 1402, (3), 239-249.

41. Moore, A.; Josephson, L.; Bhorade, R. M.; Basilion, J. P.; Weissleder, R. Human Transferrin Receptor Gene as a Marker Gene for MR Imaging. *Radiology* **2001,** 221, (1), 244-250.

42. Weissleder, R.; Moore, A.; Mahmood, U.; Bhorade, R.; Benveniste, H.; Chiocca, E. A.; Basilion, J. P. In Vivo Magnetic Resonance Imaging of Transgene Expression. *Nat. Med.* **2000,** 6, (3), 351-354.

43. Leuschner, C.; Kumar, C.; Hansel, W.; Soboyejo, W.; Zhou, J.; Hormes, J. LHRH-Conjugated Magnetic Iron Oxide Nanoparticles for Detection of Breast Cancer Metastases. *Breast Cancer Res. Treat.* **2006,** 99, (2), 163-176.

44. Boutry, S.; Laurent, S.; Elst, L. V.; Muller, R. N. Specific E-Selectin Targeting with a Superparamagnetic MRI Contrast Agent. *Contrast Media Mol. Imaging* **2006,** 1, (1), 15-22.

45. Montet, X.; Weissleder, R.; Josephson, L. Imaging Pancreatic Cancer with a Peptide-Nanoparticle Conjugate Targeted to Normal Pancreas. *Bioconjugate Chem.* **2006,** 17, (4), 905-911.

46. Nasongkla, N.; Bey, E.; Ren, J.; Ai, H.; Khemtong, C.; Guthi, J. S.; Chin, S.-F.; Sherry, A. D.; Boothman, D. A.; Gao, J. Multifunctional Polymeric Micelles as Cancer-Targeted, MRI-Ultrasensitive Drug Delivery Systems. *Nano Lett.* **2006,** 6, (11), 2427-2430.

47. Kohler, N.; Sun, C.; Wang, J.; Zhang, M. Methotrexate-Modified Superparamagnetic Nanoparticles and Their Intracellular Uptake into Human Cancer Cells. *Langmuir* **2005,** 21, (19), 8858-8864.

48. Kohler, N.; Sun, C.; Fichtenholtz, A.; Gunn, J.; Fang, C.; Zhang, M. Methotrexate-Immobilized Poly(ethylene glycol) Magnetic Nanoparticles for MR Imaging and Drug Delivery. *Small* **2006,** 2, (6), 785-792.

49. Wadghiri, Y. Z.; Sigurdsson, E. M.; Sadowski, M.; Elliott, J. I.; Li, Y.; Scholtzova, H.; Tang, C. Y.; Aguinaldo, G.; Pappolla, M.; Duff, K.*, et al.* Detection of Alzheimer's Amyloid in Transgenic Mice Using Magnetic Resonance Microimaging. *Magn. Reson. Med.* **2003,** 50, (2), 293-302.

50. Sudimack, J.; Lee, R. J. Targeted Drug Delivery Via the Folate Receptor. *Adv. Drug Delivery Rev.* **2000,** 41, (2), 147-162.

51. Quintana, A.; Raczka, E.; Piehler, L.; Lee, I.; Myc, A.; Majoros, I.; Patri, A. K.; Thomas, T.; Mulé, J.; Baker, J. R., Jr. Design and Function of a Dendrimer-Based Therapeutic Nanodevice Targeted to Tumor Cells through the Folate Receptor. *Pharm. Res.* **2002,** 19, (9), 1310-1316.

52. Mornet, S.; Vasseur, S.; Grasset, F.; Duguet, E. Magnetic Nanoparticle Design for Medical Diagnosis and Therapy. *J. Mater. Chem.* **2004,** 14, (14), 2161-2175.

53. Artemov, D. Molecular Magnetic Resonance Imaging with Targeted Contrast Agents. *J. Cell. Biochem.* **2003,** 90, (3), 518-524.

54. Berry, C. C.; Curtis, A. S. G. Functionalisation of Magnetic Nanoparticles for Applications in Biomedicine. *J. Phys. D: Appl. Phys.* **2003,** 36, (13), R198-R206.

55. Weissleder, R. Molecular Imaging in Cancer. *Science* **2006,** 312, (5777), 1168-1171.

56. Šafařík, I.; Šafaříková, M. Magnetic Nanoparticles and Biosciences. *Monatsh. Chem.* **2002,** 133, (6), 737-759.

57. Lowenstam, H. A. Magnetite in Denticle Capping in Recent Chitons (*Polyplacophora*). *Geol. Soc. Am. Bull.* **1962,** 73, (4), 435-438.

58. Mizota, M.; Maeda, Y. Magnetite in the Radular Teeth of Chitons. *Hyperfine Interact.* **1986,** 29, (1), 1423-1426.

59. Crozier, W. J. "Homing" Behavior in Chiton. *Am. Nat.* **1921,** 55, (638), 276-281.

60. Thorne, M. J. Studies on Homing in the Chiton *Acanthozostera Gemmata*. *Aust. J. Mar. Freshwater Res.* **1968,** 19, (2), 151-160.

61. Johnsen, S.; Lohmann, K. J. Magnetoreception in Animals. *Phys. Today* **2008,** 61, (3), 29-35.

62. Schultheiss-Grassi, P. P.; Dobson, J. Magnetic Analysis of Human Brain Tissue. *BioMetals* **1999,** 12, (1), 67-72.

63. Brassart, J.; Kirschvink, J. L.; Phillips, J. B.; Borland, S. C. Ferromagnetic Material in the Eastern Red-Spotted Newt *Notophthalmus viridescens*. *J. Exp. Biol.* **1999,** 202, (22), 3155-3160.

64. Beason, R.; Dussourd, N.; Deutschlander, M. Behavioural Evidence for the Use of Magnetic Material in Magnetoreception by a Migratory Bird. *J. Exp. Biol.* **1995,** 198, (1), 141-146.

65. Beason, R.; Semm, P. Does the Avian Ophthalmic Nerve Carry Magnetic Navigational Information? *J. Exp. Biol.* **1996,** 199, (5), 1241-1244.

66. Beason, R. C.; Nichols, J. E. Magnetic Orientation and Magnetically Sensitive Material in a Transequatorial Migratory Bird. *Nature* **1984,** 309, (5964), 151-153.

67. Hanzlik, M.; Heunemann, C.; Holtkamp-Rötzler, E.; Winklhofer, M.; Petersen, N.; Fleissner, G. Superparamagnetic Magnetite in the Upper Beak Tissue of Homing Pigeons. *BioMetals* **2000,** 13, (4), 325-331.

68. Walcott, C.; Gould, J. L.; Kirschvink, J. L. Pigeons Have Magnets. *Science* **1979,** 205, (4410), 1027-1029.

69. Winklhofer, M.; Holtkamp-Rötzler, E.; Hanzlik, M.; Fleissner, G.; Petersen, N. Clusters of Superparamagnetic Magnetite Particles in the Upper-Beak Skin of Homing Pigeons: Evidence of a Magnetoreceptor? *Eur. J. Mineral.* **2001,** 13, 659-669.

70. Moore, A.; Freake, S. M.; Thomas, I. M. Magnetic Particles in the Lateral Line of the Atlantic Salmon (*Salmo salar* L.). *Philos. Trans. R. Soc. London, Ser. B* **1990,** 329, (1252), 11-15.

71. Diebel, C. E.; Proksch, R.; Green, C. R.; Neilson, P.; Walker, M. M. Magnetite Defines a Vertebrate Magnetoreceptor. *Nature* **2000,** 406, (6793), 299-302.

72. Mann, S.; Sparks, N. H.; Walker, M. M.; Kirschvink, J. L. Ultrastructure, Morphology and Organization of Biogenic Magnetite from Sockeye Salmon, *Oncorhynchus nerka*: Implications for Magnetoreception. *J. Exp. Biol.* **1988,** 140, (1), 35-49.

73. Walker, M. M.; Quinn, T. P.; Kirschvink, J. L.; Groot, C. Production of Single-Domain Magnetite Throughout Life by Sockeye Salmon, *Oncorhynchus nerka*. *J. Exp. Biol.* **1988,** 140, (1), 51-63.

74. Walker, M. M.; Kirschvink, J. L.; Chang, S. B. R.; Dizon, A. E. A Candidate Magnetic Sense Organ in the Yellowfin Tuna, *Thunnus albacares*. *Science* **1984,** 224, (4650), 751-753.

75. Gould, J. L.; Kirschvink, J. L.; Deffeyes, K. S. Bees Have Magnetic Remanence. *Science* **1978,** 201, (4360), 1026-1028.

76. Wajnberg, E.; Acosta-Avalos, D.; El-Jaick, L. J.; Abraçado, L.; Coelho, J. L. A.; Bakuzis, A. F.; Morais, P. C.; Esquivel, D. M. S. Electron Paramagnetic Resonance Study of the Migratory Ant *Pachycondyla marginata* Abdomens. *Biophys. J.* **2000,** 78, (2), 1018-1023.

77. Maher, B. A. Magnetite Biomineralization in Termites. *Proc. R. Soc. London, Ser. B* **1998,** 265, (1397), 733-737.

78. Zoeger, J.; Dunn, J. R.; Fuller, M. Magnetic Material in the Head of the Common Pacific Dolphin. *Science* **1981,** 213, (4510), 892-894.

79. Kirschvink, J. L.; Kobayashi-Kirschvink, A.; Woodford, B. J. Magnetite Biomineralization in the Human Brain. *Proc. Natl. Acad. Sci. U.S.A.* **1992,** 89, (16), 7683-7687.

80. Schultheiss-Grassi, P. P.; Wessiken, R.; Dobson, J. TEM Investigations of Biogenic Magnetite Extracted from the Human Hippocampus. *Biochim. Biophys. Acta* **1999,** 1426, (1), 212-216.

81. Dobson, J.; Grassi, P. Magnetic Properties of Human Hippocampal Tissue—Evaluation of Artefact and Contamination Sources. *Brain Res. Bull.* **1996,** 39, (4), 255-259.

82. Grassi-Schultheiss, P. P.; Heller, F.; Dobson, J. Analysis of Magnetic Material in the Human Heart, Spleen and Liver. *BioMetals* **1997,** 10, (4), 351-355.

83. Blakemore, R. Magnetotactic Bacteria. *Science* **1975,** 190, (4212), 377-379.

84. Frankel, R. B.; Blakemore, R. P.; Wolfe, R. S. Magnetite in Freshwater Magnetotactic Bacteria. *Science* **1979,** 203, (4387), 1355-1356.

85. Smith, M. J.; Sheehan, P. E.; Perry, L. L.; O'Connor, K.; Csonka, L. N.; Applegate, B. M.; Whitman, L. J. Quantifying the Magnetic Advantage in Magnetotaxis. *Biophys. J.* **2006,** 91, (3), 1098-1107.

86. Torres de Araujo, F. F.; Pires, M. A.; Frankel, R. B.; Bicudo, C. E. M. Magnetite and Magnetotaxis in Algae. *Biophys. J.* **1986,** 50, (2), 375-378.

87. Schüler, D.; Frankel, R. B. Bacterial Magnetosomes: Microbiology, Biomineralization and Biotechnological Applications. *Appl. Microbiol. Biotechnol.* **1999,** 52, (4), 464-473.

88. Phillips, J. B.; Adler, K.; Borland, S. C. True Navigation by an Amphibian. *Anim. Behav.* **1995,** 50, (3), 855-858.

89. Hyeon, T. Chemical Synthesis of Magnetic Nanoparticles. *Chem. Commun.* **2003**, (8), 927-934.

90. Neuberger, T.; Schopf, B.; Hofmann, H.; Hofmann, M.; von Rechenberg, B. Superparamagnetic Nanoparticles for Biomedical Applications: Possibilities and Limitations of a New Drug Delivery System. *J. Magn. Magn. Mater.* **2005,** 293, (1), 483-496.

91. Berkowitz, A. E.; Lahut, J. A.; Jacobs, I. S.; Levinson, L. M.; Forester, D. W. Spin Pinning at Ferrite-Organic Interfaces. *Phys. Rev. Lett.* **1975,** 34, (10), 594-597.

92. Lee, C. S.; Lee, H.; Westervelt, R. M. Microelectromagnets for the Control of Magnetic Nanoparticles. *Appl. Phys. Lett.* **2001,** 79, (20), 3308-3310.

93. Rishton, S. A.; Lu, Y.; Altman, R. A.; Marley, A. C.; Bian, X. P.; Jahnes, C.; Viswanathan, R.; Xiao, G.; Gallagher, W. J.; Parkin, S. S. P. Magnetic Tunnel Junctions Fabricated at Tenth-Micron Dimensions by Electron Beam Lithography. *Microelectron. Eng.* **1997,** 35, (1-4), 249-252.

94. Tartaj, P.; Morales, M. P.; Veintemillas-Verdaguer, S.; Gónzalez-Carreño, T.; Serna, C. J. The Preparation of Magnetic Nanoparticles for Applications in Biomedicine. *J. Phys. D: Appl. Phys.* **2003,** 36, (13), R182-R197.

95. Willard, M. A.; Kurihara, L. K.; Carpenter, E. E.; Calvin, S.; Harris, V. G. Chemically Prepared Magnetic Nanoparticles. *Int. Mater. Rev.* **2004,** 49, 125-170.

96. Kodama, R. H. Magnetic Nanoparticles. *J. Magn. Magn. Mater.* **1999,** 200, (1-3), 359-372.

97. Krishnan, K.; Pakhomov, A.; Bao, Y.; Blomqvist, P.; Chun, Y.; Gonzales, M.; Griffin, K.; Ji, X.; Roberts, B. Nanomagnetism and Spin Electronics: Materials, Microstructure and Novel Properties. *J. Mater. Sci.* **2006,** 41, (3), 793-815.

98. Lu, A. H.; Salabas, E. L.; Schüth, F. Magnetic Nanoparticles: Synthesis, Protection, Functionalization, and Application. *Angew. Chem. Int. Ed.* **2007,** 46, (8), 1222-1244.

99. Gupta, A. K.; Gupta, M. Synthesis and Surface Engineering of Iron Oxide Nanoparticles for Biomedical Applications. *Biomaterials* **2005,** 26, (18), 3995-4021.

100. Xu, C.; Sun, S. Monodisperse Magnetic Nanoparticles for Biomedical Applications. *Polym. Int.* **2007,** 56, (7), 821-826.

101. Gnanaprakash, G.; Mahadevan, S.; Jayakumar, T.; Kalyanasundaram, P.; Philip, J.; Raj, B. Effect of Initial pH and Temperature of Iron Salt Solutions on Formation of Magnetite Nanoparticles. *Mater. Chem. Phys.* **2007,** 103, (1), 168-175.

102. Bruce, I. J.; Taylor, J.; Todd, M.; Davies, M. J.; Borioni, E.; Sangregorio, C.; Sen, T. Synthesis, Characterisation and Application of Silica-Magnetite Nanocomposites. *J. Magn. Magn. Mater.* **2004,** 284, 145-160.

103. Iida, H.; Takayanagi, K.; Nakanishi, T.; Osaka, T. Synthesis of Fe_3O_4 Nanoparticles with Various Sizes and Magnetic Properties by Controlled Hydrolysis. *J. Colloid Interface Sci.* **2007,** 314, (1), 274-280.

104. Olowe, A. A.; Genin, J. M. R. The Mechanism of Oxidation of Ferrous Hydroxide in Sulphated Aqueous Media: Importance of the Initial Ratio of the Reactants. *Corros. Sci.* **1991,** 32, (9), 965-984.

105. Refait, P.; Genin, J. M. R. The Oxidation of Ferrous Hydroxide in Chloride-Containing Aqueous Media and Pourbaix Diagrams of Green Rust One. *Corros. Sci.* **1993,** 34, (5), 797-819.

106. Ishikawa, T.; Kumagai, M.; Yasukawa, A.; Kandori, K.; Nakayama, T.; Yuse, F. Influences of Metal Ions on the Formation of γ-FeOOH and Magnetite Rusts. *Corros. Sci.* **2002,** 44, (5), 1073-1086.

107. Kiyama, M. Conditions for the Formation of Fe_3O_4 by the Air Oxidation of $Fe(OH)_2$ Suspensions. *Bull. Chem. Soc. Jpn.* **1974,** 47, (7), 1646-1650.

108. Nedkov, I.; Merodiiska, T.; Kolev, S.; Krezhov, K.; Niarchos, D.; Moraitakis, E.; Kusano, Y.; Takada, J. Microstructure and Magnetic Behaviour of Nanosized Fe_3O_4 Powders and Polycrystalline Films. *Monatsh. Chem.* **2002,** 133, (6), 823-828.

109. Sugimoto, T.; Matijevic, E. Formation of Uniform Spherical Magnetite Particles by Crystallization from Ferrous Hydroxide Gels. *J. Colloid Interface Sci.* **1980,** 74, (1), 227-243.

110. Jeong, Y.-K.; Shin, D.-K.; Lee, H.-J.; Oh, K.-S.; Lee, J.-H.; Riu, D.-H. Nano Magnetite Particles Prepared under the Combined Addition of Urea and Ammonia. *Key Eng. Mater.* **2006,** 317-318, 203-206.

111. Kim, D. K.; Mikhaylova, M.; Zhang, Y.; Muhammed, M. Protective Coating of Superparamagnetic Iron Oxide Nanoparticles. *Chem. Mater.* **2003,** 15, (8), 1617-1627.

112. Gupta, A. K.; Curtis, A. S. G. Lactoferrin and Ceruloplasmin Derivatized Superparamagnetic Iron Oxide Nanoparticles for Targeting Cell Surface Receptors. *Biomaterials* **2004,** 25, (15), 3029-3040.

113. Wooding, A.; Kilner, M.; Lambrick, D. B. Studies of the Double Surfactant Layer Stabilization of Water-Based Magnetic Fluids. *J. Colloid Interface Sci.* **1991,** 144, (1), 236-242.

114. Deng, Y.; Wang, L.; Yang, W.; Fu, S.; Elaissari, A. Preparation of Magnetic Polymeric Particles Via Inverse Microemulsion Polymerization Process. *J. Magn. Magn. Mater.* **2003,** 257, (1), 69-78.

115. Sjögren, C. E.; Johansson, C.; Nævestad, A.; Sontum, P. C.; Briley-Sæbø, K.; Fahlvik, A. K. Crystal Size and Properties of Superparamagnetic Iron Oxide (SPIO) Particles. *Magn. Reson. Imaging* **1997,** 15, (1), 55-67.

116. Molday, R. S.; Mackenzie, D. Immunospecific Ferromagnetic Iron-Dextran Reagents for the Labeling and Magnetic Separation of Cells. *J. Immunol. Methods* **1982,** 52, (3), 353-367.

117. Liu, X.; Guan, Y.; Ma, Z.; Liu, H. Surface Modification and Characterization of Magnetic Polymer Nanospheres Prepared by Miniemulsion Polymerization. *Langmuir* **2004,** 20, (23), 10278-10282.

118. van Ewijk, G. A.; Vroege, G. J.; Philipse, A. P. Convenient Preparation Methods for Magnetic Colloids. *J. Magn. Magn. Mater.* **1999,** 201, (1-3), 31-33.

119. Fried, T.; Shemer, G.; Markovich, G. Ordered Two-Dimensional Arrays of Ferrite Nanoparticles. *Adv. Mater.* **2001,** 13, (15), 1158-1161.

120. Bee, A.; Massart, R.; Neveu, S. Synthesis of Very Fine Maghemite Particles. *J. Magn. Magn. Mater.* **1995,** 149, (1-2), 6-9.

121. Shen, L.; Laibinis, P. E.; Hatton, T. A. Bilayer Surfactant Stabilized Magnetic Fluids: Synthesis and Interactions at Interfaces. *Langmuir* **1999,** 15, (2), 447-453.

122. Elmore, W. C. Ferromagnetic Colloid for Studying Magnetic Structures. *Phys. Rev.* **1938,** 54, (4), 309-310.

123. Sato, T.; Iijima, T.; Seki, M.; Inagaki, N. Magnetic Properties of Ultrafine Ferrite Particles. *J. Magn. Magn. Mater.* **1987,** 65, (2-3), 252-256.

124. Khalafalla, S.; Reimers, G. Preparation of Dilution-Stable Aqueous Magnetic Fluids. *IEEE Trans. Magn.* **1980,** 16, (2), 178-183.

125. Pardoe, H.; Chua-anusorn, W.; St. Pierre, T. G.; Dobson, J. Structural and Magnetic Properties of Nanoscale Iron Oxide Particles Synthesized in the Presence of Dextran or Polyvinyl Alcohol. *J. Magn. Magn. Mater.* **2001,** 225, (1-2), 41-46.

126. Gazeau, F.; Bacri, J.-C.; Gendron, F.; Perzynski, R.; Raikher, Y. L.; Stepanov, V. I.; Dubois, E. Magnetic Resonance of Ferrite Nanoparticles: Evidence of Surface Effects. *J. Magn. Magn. Mater.* **1998,** 186, (1-2), 175-187.

127. Kim, D. K.; Zhang, Y.; Voit, W.; Rao, K. V.; Muhammed, M. Synthesis and Characterization of Surfactant-Coated Superparamagnetic Monodispersed Iron Oxide Nanoparticles. *J. Magn. Magn. Mater.* **2001,** 225, (1-2), 30-36.

128. Portet, D.; Denizot, B.; Rump, E.; Lejeune, J. J.; Jallet, P. Nonpolymeric Coatings of Iron Oxide Colloids for Biological Use as Magnetic Resonance Imaging Contrast Agents. *J. Colloid Interface Sci.* **2001,** 238, (1), 37-42.

129. Mikhaylova, M.; Kim, D. K.; Berry, C. C.; Zagorodni, A.; Toprak, M.; Curtis, A. S. G.; Muhammed, M. BSA Immobilization on Amine-Functionalized Superparamagnetic Iron Oxide Nanoparticles. *Chem. Mater.* **2004,** 16, (12), 2344-2354.

130. Lee, J.; Isobe, T.; Senna, M. Preparation of Ultrafine Fe_3O_4 Particles by Precipitation in the Presence of PVA at High pH. *J. Colloid Interface Sci.* **1996,** 177, (2), 490-494.

131. Babes, L.; Denizot, B.; Tanguy, G.; Le Jeune, J. J.; Jallet, P. Synthesis of Iron Oxide Nanoparticles Used as MRI Contrast Agents: A Parametric Study. *J. Colloid Interface Sci.* **1999,** 212, (2), 474-482.

132. Tronc, E.; Belleville, P.; Jolivet, J. P.; Livage, J. Transformation of Ferric Hydroxide into Spinel by Iron(II) Adsorption. *Langmuir* **1992,** 8, (1), 313-319.

133. Davies, K. J.; Wells, S.; Charles, S. W. The Effect of Temperature and Oleate Adsorption on the Growth of Maghemite Particles. *J. Magn. Magn. Mater.* **1993,** 122, (1-3), 24-28.

134. Fauconnier, N.; Pons, J. N.; Roger, J.; Bee, A. Thiolation of Maghemite Nanoparticles by Dimercaptosuccinic Acid. *J. Colloid Interface Sci.* **1997,** 194, (2), 427-433.

135. Kim, D. K.; Zhang, Y.; Kehr, J.; Klason, T.; Bjelke, B.; Muhammed, M. Characterization and MRI Study of Surfactant-Coated Superparamagnetic Nanoparticles Administered into the Rat Brain. *J. Magn. Magn. Mater.* **2001,** 225, (1-2), 256-261.

136. Kim, D. K.; Mikhaylova, M.; Wang, F. H.; Kehr, J.; Bjelke, B.; Zhang, Y.; Tsakalakos, T.; Muhammed, M. Starch-Coated Superparamagnetic Nanoparticles as MR Contrast Agents. *Chem. Mater.* **2003,** 15, (23), 4343-4351.

137. Massart, R. Preparation of Aqueous Magnetic Liquids in Alkaline and Acidic Media. *IEEE Trans. Magn.* **1981,** 17, (2), 1247-1248.

138. Tartaj, P.; Serna, C. J. Microemulsion-Assisted Synthesis of Tunable Superparamagnetic Composites. *Chem. Mater.* **2002,** 14, (10), 4396-4402.

139. Pileni, M. P. Nanosized Particles Made in Colloidal Assemblies. *Langmuir* **1997,** 13, (13), 3266-3276.

140. López-Pérez, J. A.; López-Quintela, M. A.; Mira, J.; Rivas, J.; Charles, S. W. Advances in the Preparation of Magnetic Nanoparticles by the Microemulsion Method. *J. Phys. Chem. B* **1997,** 101, (41), 8045-8047.

141. Dresco, P. A.; Zaitsev, V. S.; Gambino, R. J.; Chu, B. Preparation and Properties of Magnetite and Polymer Magnetite Nanoparticles. *Langmuir* **1999,** 15, (6), 1945-1951.

142. Feltin, N.; Pileni, M. P. New Technique for Synthesizing Iron Ferrite Magnetic Nanosized Particles. *Langmuir* **1997,** 13, (15), 3927-3933.

143. Gobe, M.; Kon-No, K.; Kandori, K.; Kitahara, A. Preparation and Characterization of Monodisperse Magnetite Sols in W/O Microemulsion. *J. Colloid Interface Sci.* **1983,** 93, (1), 293-295.

144. Gupta, A. K.; Wells, S. Surface-Modified Superparamagnetic Nanoparticles for Drug Delivery: Preparation, Characterization, and Cytotoxicity Studies. *IEEE Trans. Nanobiosci.* **2004,** 3, (1), 66-73.

145. Lee, K. M.; Sorensen, C. M.; Klabunde, K. J.; Hadjipanayis, G. C. Synthesis and Characterization of Stable Colloidal Fe_3O_4 Particles in Water-in-Oil Microemulsions. *IEEE Trans. Magn.* **1992,** 28, (5), 3180-3182.

146. López-Quintela, M. A.; Rivas, J. Chemical Reactions in Microemulsions: A Powerful Method to Obtain Ultrafine Particles. *J. Colloid Interface Sci.* **1993,** 158, (2), 446-451.

147. Santra, S.; Tapec, R.; Theodoropoulou, N.; Dobson, J.; Hebard, A.; Tan, W. Synthesis and Characterization of Silica-Coated Iron Oxide Nanoparticles in Microemulsion: The Effect of Nonionic Surfactants. *Langmuir* **2001,** 17, (10), 2900-2906.

148. Seip, C. T.; Carpenter, E. E.; O'Connor, C. J.; John, V. T.; Li, S. Magnetic Properties of a Series of Ferrite Nanoparticles Synthesized in Reverse Micelles. *IEEE Trans. Magn.* **1998,** 34, (4), 1111-1113.

149. Tartaj, P.; Serna, C. J. Synthesis of Monodisperse Superparamagnetic Fe/Silica Nanospherical Composites. *J. Am. Chem. Soc.* **2003,** 125, (51), 15754-15755.

150. Tartaj, P.; Tartaj, J. Microstructural Evolution of Iron-Oxide-Doped Alumina Nanoparticles Synthesized from Microemulsions. *Chem. Mater.* **2002,** 14, (2), 536-541.

151. Vidal-Vidal, J.; Rivas, J.; López-Quintela, M. A. Synthesis of Monodisperse Maghemite Nanoparticles by the Microemulsion Method. *Colloids Surf., A* **2006,** 288, (1-3), 44-51.

152. Gubin, S. P.; Koksharov, Y. A.; Khomutov, G. B.; Yurkov, G. Y. Magnetic Nanoparticles: Preparation, Structure and Properties. *Russ. Chem. Rev.* **2005,** 74, (6), 489-520.

153. Carpenter, E. E. Iron Nanoparticles as Potential Magnetic Carriers. *J. Magn. Magn. Mater.* **2001,** 225, (1-2), 17-20.

154. Kinoshita, T.; Seino, S.; Okitsu, K.; Nakayama, T.; Nakagawa, T.; Yamamoto, T. A. Magnetic Evaluation of Nanostructure of Gold-Iron Composite Particles Synthesized by a Reverse Micelle Method. *J. Alloys Compd.* **2003,** 359, (1-2), 46-50.

155. Cho, S. J.; Idrobo, J. C.; Olamit, J.; Liu, K.; Browning, N. D.; Kauzlarich, S. M. Growth Mechanisms and Oxidation Resistance of Gold-Coated Iron Nanoparticles. *Chem. Mater.* **2005,** 17, (12), 3181-3186.

156. Lin, J.; Zhou, W.; Kumbhar, A.; Wiemann, J.; Fang, J.; Carpenter, E. E.; O'Connor, C. J. Gold-Coated Iron (Fe@Au) Nanoparticles: Synthesis, Characterization, and Magnetic Field-Induced Self-Assembly. *J. Solid State Chem.* **2001,** 159, (1), 26-31.

157. Cho, S. J.; Kauzlarich, S. M.; Olamit, J.; Liu, K.; Grandjean, F.; Rebbouh, L.; Long, G. J. Characterization and Magnetic Properties of Core/Shell Structured Fe/Au Nanoparticles. *J. Appl. Phys.* **2004,** 95, (11, Pt. 2), 6804-6806.

158. Lin, X.-M.; Samia, A. C. S. Synthesis, Assembly and Physical Properties of Magnetic Nanoparticles. *J. Magn. Magn. Mater.* **2006,** 305, (1), 100-109.

159. Yu, W. W.; Falkner, J. C.; Yavuz, C. T.; Colvin, V. L. Synthesis of Monodisperse Iron Oxide Nanocrystals by Thermal Decomposition of Iron Carboxylate Salts. *Chem. Commun.* **2004**, (20), 2306-2307.

160. Rockenberger, J.; Scher, E. C.; Alivisatos, A. P. A New Nonhydrolytic Single-Precursor Approach to Surfactant-Capped Nanocrystals of Transition Metal Oxides. *J. Am. Chem. Soc.* **1999,** 121, (49), 11595-11596.

161. Li, Y.; Afzaal, M.; O'Brien, P. The Synthesis of Amine-Capped Magnetic (Fe, Mn, Co, Ni) Oxide Nanocrystals and Their Surface Modification for Aqueous Dispersibility. *J. Mater. Chem.* **2006,** 16, (22), 2175-2180.

162. Sun, S.; Zeng, H. Size-Controlled Synthesis of Magnetite Nanoparticles. *J. Am. Chem. Soc.* **2002,** 124, (28), 8204-8205.

163. Sun, S.; Zeng, H.; Robinson, D. B.; Raoux, S.; Rice, P. M.; Wang, S. X.; Li, G. Monodisperse MFe_2O_4 (M = Fe, Co, Mn) Nanoparticles. *J. Am. Chem. Soc.* **2004,** 126, (1), 273-279.

164. Hyeon, T.; Lee, S. S.; Park, J.; Chung, Y.; Na, H. B. Synthesis of Highly Crystalline and Monodisperse Maghemite Nanocrystallites without a Size-Selection Process. *J. Am. Chem. Soc.* **2001,** 123, (51), 12798-12801.

165. Redl, F. X.; Black, C. T.; Papaefthymiou, G. C.; Sandstrom, R. L.; Yin, M.; Zeng, H.; Murray, C. B.; O'Brien, S. P. Magnetic, Electronic, and Structural Characterization of

Nonstoichiometric Iron Oxides at the Nanoscale. *J. Am. Chem. Soc.* **2004,** 126, (44), 14583-14599.

166. Teng, X.; Yang, H. Effects of Surfactants and Synthetic Conditions on the Sizes and Self-Assembly of Monodisperse Iron Oxide Nanoparticles. *J. Mater. Chem.* **2004,** 14, (4), 774-779.

167. Jana, N. R.; Chen, Y.; Peng, X. Size- and Shape-Controlled Magnetic (Cr, Mn, Fe, Co, Ni) Oxide Nanocrystals Via a Simple and General Approach. *Chem. Mater.* **2004,** 16, (20), 3931-3935.

168. Park, J.; An, K.; Hwang, Y.; Park, J. G.; Noh, H. J.; Kim, J. Y.; Park, J. H.; Hwang, N. M.; Hyeon, T. Ultra-Large-Scale Syntheses of Monodisperse Nanocrystals. *Nat. Mater.* **2004,** 3, (12), 891-895.

169. Wang, J.; Sun, J.; Sun, Q.; Chen, Q. One-Step Hydrothermal Process to Prepare Highly Crystalline Fe_3O_4 Nanoparticles with Improved Magnetic Properties. *Mater. Res. Bull.* **2003,** 38, (7), 1113-1118.

170. Pankhurst, Q. A.; Connolly, J.; Jones, S. K.; Dobson, J. Applications of Magnetic Nanoparticles in Biomedicine. *J. Phys. D: Appl. Phys.* **2003,** 36, (13), R167-R181.

171. Lawaczeck, R.; Menzel, M.; Pietsch, H. Superparamagnetic Iron Oxide Particles: Contrast Media for Magnetic Resonance Imaging. *Appl. Organomet. Chem.* **2004,** 18, (10), 506-513.

172. Skomski, R. Nanomagnetics. *J. Phys.: Condens. Matter* **2003,** 15, (20), R841-R896.

173. Dennis, C. L.; Borges, R. P.; Buda, L. D.; Ebels, U.; Gregg, J. F.; Hehn, M.; Jouguelet, E.; Ounadjela, K.; Petej, I.; Prejbeanu, I. L.*, et al.* The Defining Length Scales of Mesomagnetism: A Review. *J. Phys.: Condens. Matter* **2002,** 14, (49), R1175-R1262.

174. Batlle, X.; Labarta, A. Finite-Size Effects in Fine Particles: Magnetic and Transport Properties. *J. Phys. D: Appl. Phys.* **2002,** 35, (6), R15-R42.

175. Leslie-Pelecky, D. L.; Rieke, R. D. Magnetic Properties of Nanostructured Materials. *Chem. Mater.* **1996,** 8, (8), 1770-1783.

176. Corot, C.; Robert, P.; Idee, J. M.; Port, M. Recent Advances in Iron Oxide Nanocrystal Technology for Medical Imaging. *Adv. Drug Delivery Rev.* **2006,** 58, (14), 1471-1504.

177. Bean, C. P. Hysteresis Loops of Mixtures of Ferromagnetic Micropowders. *J. Appl. Phys.* **1955,** 26, (11), 1381-1383.

178. Held, G. A.; Grinstein, G.; Doyle, H.; Sun, S.; Murray, C. B. Competing Interactions in Dispersions of Superparamagnetic Nanoparticles. *Phys. Rev. B: Condens. Matter Mater. Phys.* **2001,** 64, (1), 012408.

179. Vatta, L. L.; Sanderson, R. D.; Koch, K. R. Magnetic Nanoparticles: Properties and Potential Applications. *Pure Appl. Chem.* **2006,** 78, (9), 1793-1801.

180. Wilson, S. A.; Jourdain, R. P. J.; Zhang, Q.; Dorey, R. A.; Bowen, C. R.; Willander, M.; Wahab, Q. U.; Willander, M.; Al-hilli, S. M.; Nur, O*., et al.* New Materials for Micro-Scale Sensors and Actuators: An Engineering Review. *Mater. Sci. Eng., R* **2007,** 56, (1-6), 1-129.

181. Fannin, P. C.; Scaife, B. K. P.; Charles, S. W. The Measurement of the Frequency Dependent Susceptibility of Magnetic Colloids. *J. Magn. Magn. Mater.* **1988,** 72, (1), 95-108.

182. Kittel, C. Theory of the Structure of Ferromagnetic Domains in Films and Small Particles. *Phys. Rev.* **1946,** 70, (11-12), 965-971.

183. Harris, L. A.; Goff, J. D.; Carmichael, A. Y.; Riffle, J. S.; Harburn, J. J.; St. Pierre, T. G.; Saunders, M. Magnetite Nanoparticle Dispersions Stabilized with Triblock Copolymers. *Chem. Mater.* **2003,** 15, (6), 1367-1377.

184. Brown, W. F., Jr. Thermal Fluctuations of a Single-Domain Particle. *Phys. Rev.* **1963,** 130, (5), 1677-1686.

185. Brown, W. F., Jr. Relaxational Behavior of Fine Magnetic Particles. *J. Appl. Phys.* **1959,** 30, (4), S130-S132.

186. Lefebure, S.; Dubois, E.; Cabuil, V.; Neveu, S.; Massart, R. Monodisperse Magnetic Nanoparticles: Preparation and Dispersion in Water and Oils. *J. Mater. Res.* **1998,** 13, (10), 2975-2981.

187. Bacri, J.-C.; Perzynski, R.; Salin, D.; Cabuil, V.; Massart, R. Magnetic Colloidal Properties of Ionic Ferrofluids. *J. Magn. Magn. Mater.* **1986,** 62, (1), 36-46.

188. Coey, J. M. D. Noncollinear Spin Arrangement in Ultrafine Ferrimagnetic Crystallites. *Phys. Rev. Lett.* **1971,** 27, (17), 1140-1142.

189. Haneda, K.; Morrish, A. H. Vacancy Ordering in γ-Fe_2O_3 Small Particles. *Solid State Commun.* **1977,** 22, (12), 779-782.

190. Jun, Y. W.; Seo, J. W.; Cheon, J. Nanoscaling Laws of Magnetic Nanoparticles and Their Applicabilities in Biomedical Sciences. *Acc. Chem. Res.* **2008,** 41, (2), 179-189.

191. Kneller, E. F.; Luborsky, F. E. Particle Size Dependence of Coercivity and Remanence of Single-Domain Particles. *J. Appl. Phys.* **1963,** 34, (3), 656-658.

192. Kodama, R. H.; Berkowitz, A. E. Atomic-Scale Magnetic Modeling of Oxide Nanoparticles. *Phys. Rev. B: Condens. Matter Mater. Phys.* **1999,** 59, (9), 6321-6336.

193. Kodama, R. H.; Berkowitz, A. E.; McNiff, J. E. J.; Foner, S. Surface Spin Disorder in Ferrite Nanoparticles. *J. Appl. Phys.* **1997,** 81, (8), 5552-5557.

194. Linderoth, S.; Hendriksen, P. V.; Bodker, F.; Wells, S.; Davies, K.; Charles, S. W.; Morup, S. On Spin-Canting in Maghemite Particles. *J. Appl. Phys.* **1994,** 75, (10), 6583-6585.

195. Martínez, B.; Obradors, X.; Balcells, L.; Rouanet, A.; Monty, C. Low Temperature Surface Spin-Glass Transition in γ-Fe_2O_3 Nanoparticles. *Phys. Rev. Lett.* **1998,** 80, (1), 181-184.

196. Morales, M. P.; Serna, C. J.; Bødker, F.; Mørup, S. Spin Canting Due to Structural Disorder in Maghemite. *J. Phys.: Condens. Matter* **1997,** 9, (25), 5461-5467.

197. Morales, M. P.; Veintemillas-Verdaguer, S.; Montero, M. I.; Serna, C. J.; Roig, A.; Casas, L.; Martinez, B.; Sandiumenge, F. Surface and Internal Spin Canting in γ-Fe_2O_3 Nanoparticles. *Chem. Mater.* **1999,** 11, (11), 3058-3064.

198. Morrish, A. H.; Haneda, K.; Schurer, P. J. Surface Magnetic Structure of Small γ-Fe_2O_3 Particles. *J. Phys. Colloques* **1976,** 37, (6), 301-305.

199. Parker, F. T.; Foster, M. W.; Margulies, D. T.; Berkowitz, A. E. Spin Canting, Surface Magnetization, and Finite-Size Effects in γ-Fe_2O_3 Particles. *Phys. Rev. B: Condens. Matter Mater. Phys.* **1993,** 47, (13), 7885-7891.

200. Schmool, D. S.; Rocha, R.; Sousa, J. B.; Santos, J. A. M.; Kakazei, G. Evidence of Surface Anisotropy in Magnetic Nanoparticles. *J. Magn. Magn. Mater.* **2006,** 300, (1), e331-e334.

201. Jain, R. K. Transport of Molecules across Tumor Vasculature. *Cancer Metastasis Rev.* **1987,** 6, (4), 559-593.

202. Okuhata, Y. Delivery of Diagnostic Agents for Magnetic Resonance Imaging. *Adv. Drug Delivery Rev.* **1999,** 37, (1-3), 121-137.

203. Arruebo, M.; Fernández-Pacheco, R.; Ibarra, M. R.; Santamaría, J. Magnetic Nanoparticles for Drug Delivery. *Nano Today* **2007,** 2, (3), 22-32.

204. McNeil, S. E. Nanotechnology for the Biologist. *J. Leukocyte Biol.* **2005,** 78, (3), 585-594.

205. Chen, L.-T.; Weiss, L. The Role of the Sinus Wall in the Passage of Erythrocytes through the Spleen. *Blood* **1973,** 41, (4), 529-537.

206. Tartaj, P.; Morales, M. P.; Gonzalez-Carreno, T.; Veintemillas-Verdaguer, S.; Serna, C. J. Advances in Magnetic Nanoparticles for Biotechnology Applications. *J. Magn. Magn. Mater.* **2005,** 290-291, (Part 1), 28-34.

207. Azzazy, H. M. E.; Mansour, M. M. H.; Kazmierczak, S. C. Nanodiagnostics: A New Frontier for Clinical Laboratory Medicine. *Clin. Chem.* **2006,** 52, (7), 1238-1246.

208. Sridhar, S.; Amiji, M.; Shenoy, D.; Nagesha, D.; Weissig, V.; Fu, W., Nanosensing: Materials and Devices II. In *Proceedings of SPIE*, Islam, M. S.; Dutta, A. K., Eds. Boston, MA, 2005; Vol. 6008.

209. Dobson, J. Magnetic Nanoparticles for Drug Delivery. *Drug Dev. Res.* **2006,** 67, (1), 55-60.

210. Ritter, J. A.; Ebner, A. D.; Daniel, K. D.; Stewart, K. L. Application of High Gradient Magnetic Separation Principles to Magnetic Drug Targeting. *J. Magn. Magn. Mater.* **2004,** 280, (2-3), 184-201.

211. Torchilin, V. P. Drug Targeting. *Eur. J. Pharm. Sci.* **2000,** 11, (Suppl. 2), S81-S91.

212. Mosbach, K.; Schroder, U. Preparation and Application of Magnetic Polymers for Targeting of Drugs. *FEBS Lett.* **1979,** 102, (1), 112-116.

213. Senyei, A.; Widder, K.; Czerlinski, G. Magnetic Guidance of Drug-Carrying Microspheres. *J. Appl. Phys.* **1978,** 49, (6), 3578-3583.

214. Widder, K. J.; Senyei, A. E.; Scarpelli, D. G. Magnetic Microspheres: A Model System for Site Specific Drug Delivery in Vivo. *Proc. Soc. Exp. Biol. Med.* **1978,** 158, (2), 141-146.

215. Alexiou, C.; Arnold, W.; Klein, R. J.; Parak, F. G.; Hulin, P.; Bergemann, C.; Erhardt, W.; Wagenpfeil, S.; Lübbe, A. S. Locoregional Cancer Treatment with Magnetic Drug Targeting. *Cancer Res.* **2000,** 60, (23), 6641-6648.

216. Lübbe, A. S.; Alexiou, C.; Bergemann, C. Clinical Applications of Magnetic Drug Targeting. *J. Surg. Res.* **2001,** 95, (2), 200-206.

217. Lübbe, A. S.; Bergemann, C.; Brock, J.; McClure, D. G. Physiological Aspects in Magnetic Drug-Targeting. *J. Magn. Magn. Mater.* **1999,** 194, (1-3), 149-155.

218. Lübbe, A. S.; Bergemann, C.; Huhnt, W.; Fricke, T.; Riess, H.; Brock, J. W.; Huhn, D. Preclinical Experiences with Magnetic Drug Targeting: Tolerance and Efficacy. *Cancer Res.* **1996,** 56, (20), 4694-4701.

219. Lübbe, A. S.; Bergemann, C.; Riess, H.; Schriever, F.; Reichardt, P.; Possinger, K.; Matthias, M.; Dorken, B.; Herrmann, F.; Gurtler, R.*, et al.* Clinical Experiences with

Magnetic Drug Targeting: A Phase I Study with 4'-Epidoxorubicin in 14 Patients with Advanced Solid Tumors. *Cancer Res.* **1996,** 56, (20), 4686-4693.

220. Häfeli, U. O. Magnetically Modulated Therapeutic Systems. *Int. J. Pharm.* **2004,** 277, (1-2), 19-24.

221. Goodwin, S.; Peterson, C.; Hoh, C.; Bittner, C. Targeting and Retention of Magnetic Targeted Carriers (MTCs) Enhancing Intra-Arterial Chemotherapy. *J. Magn. Magn. Mater.* **1999,** 194, (1-3), 132-139.

222. Hassan, E. E.; Parish, R. C.; Gallo, J. M. Optimized Formulation of Magnetic Chitosan Microspheres Containing the Anticancer Agent, Oxantrazole. *Pharm. Res.* **1992,** 9, (3), 390-397.

223. Pulfer, S. K.; Ciccotto, S. L.; Gallo, J. M. Distribution of Small Magnetic Particles in Brain Tumor-Bearing Rats. *J. Neurooncol.* **1999,** 41, (2), 99-105.

224. Pulfer, S. K.; Gallo, J. M. Enhanced Brain Tumor Selectivity of Cationic Magnetic Polysaccharide Microspheres. *J. Drug. Target.* **1998,** 6, (3), 215-227.

225. Ström, V.; Hultenby, K.; Grüttner, C.; Teller, J.; Xu, B.; Holgersson, J. A Novel and Rapid Method for Quantification of Magnetic Nanoparticle-Cell Interactions Using a Desktop Susceptometer. *Nanotechnology* **2004,** 15, (5), 457-466.

226. Gallo, J. M.; Gupta, P. K.; Hung, C. T.; Perrier, D. G. Evaluation of Drug Delivery Following the Administration of Magnetic Albumin Microspheres Containing Adriamycin to the Rat. *J. Pharm. Sci.* **1989,** 78, (3), 190-194.

227. Goodwin, S. C.; Bittner, C. A.; Peterson, C. L.; Wong, G. Single-Dose Toxicity Study of Hepatic Intra-Arterial Infusion of Doxorubicin Coupled to a Novel Magnetically Targeted Drug Carrier. *Toxicol. Sci.* **2001,** 60, (1), 177-183.

228. Häfeli, U.; Pauer, G.; Failing, S.; Tapolsky, G. Radiolabeling of Magnetic Particles with Rhenium-188 for Cancer Therapy. *J. Magn. Magn. Mater.* **2001,** 225, (1-2), 73-78.

229. Häfeli, U. O.; Sweeney, S. M.; Beresford, B. A.; Humm, J. L.; Macklis, R. M. Effective Targeting of Magnetic Radioactive 90Y-Microspheres to Tumor Cells by an Externally Applied Magnetic Field. Preliminary *in Vitro* and *in Vivo* Results. *Nucl. Med. Biol.* **1995,** 22, (2), 147-155.

230. Johnson, J.; Kent, T.; Koda, J.; Peterson, C.; Rudge, S.; Tapolsky, G. The MTC Technology: A Platform Technology for the Site-Specific Delivery of Pharmaceutical Agents. *Eur. Cell. Mater.* **2002,** 3, (Suppl. 2), 12-15.

231. Mah, C.; Fraites, T. J., Jr.; Zolotukhin, I.; Song, S.; Flotte, T. R.; Dobson, J.; Batich, C.; Byrne, B. J. Improved Method of Recombinant AAV2 Delivery for Systemic Targeted Gene Therapy. *Mol. Ther.* **2002,** 6, (1), 106-112.

232. Rudge, S.; Peterson, C.; Vessely, C.; Koda, J.; Stevens, S.; Catterall, L. Adsorption and Desorption of Chemotherapeutic Drugs from a Magnetically Targeted Carrier (MTC). *J. Controlled Release* **2001,** 74, (1-3), 335-340.

233. Widder, K. J.; Morris, R. M.; Poore, G. A.; Howard, D. P.; Senyei, A. E. Selective Targeting of Magnetic Albumin Microspheres Containing Low-Dose Doxorubicin: Total Remission in Yoshida Sarcoma-Bearing Rats. *Eur. J. Cancer Clin. Oncol.* **1983,** 19, (1), 135-139.

234. Widder, K. J.; Senyei, A. E.; Ranney, D. F. *In Vitro* Release of Biologically Active Adriamycin by Magnetically Responsive Albumin Microspheres. *Cancer Res.* **1980,** 40, (10), 3512-3517.

235. Sonvico, F.; Dubernet, C.; Colombo, P.; Couvreur, P. Metallic Colloid Nanotechnology, Applications in Diagnosis and Therapeutics. *Curr. Pharm. Des.* **2005,** 11, 2091-2105.

236. Jeong, U.; Teng, X.; Wang, Y.; Yang, H.; Xia, Y. Superparamagnetic Colloids: Controlled Synthesis and Niche Applications. *Adv. Mater.* **2007,** 19, (1), 33-60.

237. Rudge, S. R.; Kurtz, T. L.; Vessely, C. R.; Catterall, L. G.; Williamson, D. L. Preparation, Characterization, and Performance of Magnetic Iron-Carbon Composite Microparticles for Chemotherapy. *Biomaterials* **2000,** 21, (14), 1411-1420.

238. Duguet, E.; Vasseur, S.; Mornet, S.; Goglio, G.; Demourgues, A.; Portier, J.; Grasset, F.; Veverka, P.; Pollert, E. Towards a Versatile Platform Based on Magnetic Nanoparticles for in Vivo Applications. *Bull. Mater. Sci.* **2006,** 29, (6), 581-586.

239. Bulte, J. W. M.; Kraitchman, D. L. Iron Oxide MR Contrast Agents for Molecular and Cellular Imaging. *NMR Biomed.* **2004,** 17, (7), 484-499.

240. Sunderland, C. J.; Steiert, M.; Talmadge, J. E.; Derfus, A. M.; Barry, S. E. Targeted Nanoparticles for Detecting and Treating Cancer. *Drug Dev. Res.* **2006,** 67, (1), 70-93.

241. Ito, A.; Shinkai, M.; Honda, H.; Kobayashi, T. Medical Application of Functionalized Magnetic Nanoparticles. *J. Biosci. Bioeng.* **2005,** 100, (1), 1-11.

242. Renshaw, P. F.; Owen, C. S.; Evans, A. E.; Leigh, J. S., Jr. Immunospecific NMR Contrast Agents. *Magn. Reson. Imaging* **1986,** 4, (4), 351-357.

243. Renshaw, P. F.; Owen, C. S.; McLaughlin, A. C.; Frey, T. G.; Leigh, J. S., Jr. Ferromagnetic Contrast Agents: A New Approach. *Magn. Reson. Med.* **1986,** 3, (2), 217-225.

244. Mornet, S.; Vasseur, S.; Grasset, F.; Veverka, P.; Goglio, G.; Demourgues, A.; Portier, J.; Pollert, E.; Duguet, E. Magnetic Nanoparticle Design for Medical Applications. *Prog. Solid State Chem.* **2006,** 34, (2-4), 237-247.

245. Thorek, D.; Chen, A.; Czupryna, J.; Tsourkas, A. Superparamagnetic Iron Oxide Nanoparticle Probes for Molecular Imaging. *Ann. Biomed. Eng.* **2006,** 34, (1), 23-38.

246. Saini, S.; Stark, D. D.; Hahn, P. F.; Wittenberg, J.; Brady, T. J.; Ferrucci, J. T., Jr. Ferrite Particles: A Superparamagnetic MR Contrast Agent for the Reticuloendothelial System. *Radiology* **1987,** 162, (1), 211-216.

247. Sahoo, S. K.; Labhasetwar, V. Nanotech Approaches to Drug Delivery and Imaging. *Drug Discovery Today* **2003,** 8, (24), 1112-1120.

248. Jain, R. K. Transport of Molecules, Particles, and Cells in Solid Tumors. *Annu. Rev. Biomed. Eng.* **1999,** 1, (1), 241-263.

249. Jain, R. K. Delivery of Molecular Medicine to Solid Tumors: Lessons from in Vivo Imaging of Gene Expression and Function. *J. Controlled Release* **2001,** 74, (1-3), 7-25.

250. Jain, R. K. Delivery of Novel Therapeutic Agents in Tumors: Physiological Barriers and Strategies. *J. Natl. Cancer Inst.* **1989,** 81, 570-576.

251. Brigger, I.; Dubernet, C.; Couvreur, P. Nanoparticles in Cancer Therapy and Diagnosis. *Adv. Drug Delivery Rev.* **2002,** 54, (5), 631-651.

252. Moghimi, S. M.; Hunter, A. C.; Murray, J. C. Long-Circulating and Target-Specific Nanoparticles: Theory to Practice. *Pharmacol. Rev.* **2001,** 53, (2), 283-318.

253. Tombach, B.; Reimer, P.; Bremer, C.; Allkemper, T.; Engelhardt, M.; Mahler, M.; Ebert, W.; Heindel, W. First-Pass and Equilibrium-MRA of the Aortoiliac Region with a Superparamagnetic Iron Oxide Blood Pool MR Contrast Agent (SH U 555 C): Results of a Human Pilot Study. *NMR Biomed.* **2004,** 17, (7), 500-506.

254. Taylor, A. M.; Panting, J. R.; Keegan, J.; Gatehouse, P. D.; Amin, D.; Jhooti, P.; Yang, G. Z.; McGill, S.; Burman, E. D.; Francis, J. M.*, et al.* Safety and Preliminary Findings with the Intravascular Contrast Agent NC100150 Injection for MR Coronary Angiography. *J. Magn. Reson. Imaging* **1999,** 9, (2), 220-227.

255. Wacker, F. K.; Wendt, M.; Ebert, W.; Hillenbrandt, C.; Wolf, K. J.; Lewin, J. S. Use of a Blood-Pool Contrast Agent for MR-Guided Vascular Procedures: Feasibility of Ultrasmall Superparamagnetic Iron Oxide Particles. *Acad. Radiol.* **2002,** 9, (11), 1251-1254.

256. Wagner, S.; Schnorr, J.; Pilgrimm, H.; Hamm, B.; Taupitz, M. Monomer-Coated Very Small Superparamagnetic Iron Oxide Particles as Contrast Medium for Magnetic Resonance Imaging: Preclinical in Vivo Characterization. *Invest. Radiol.* **2002,** 37, (4), 167-177.

257. Daldrup-Link, H. E.; Kaiser, A.; Helbich, T.; Werner, M.; Bjørnerud, A.; Link, T. M.; Rummeny, E. J. Macromolecular Contrast Medium (Feruglose) Versus Small

Molecular Contrast Medium (Gadopentetate) Enhanced Magnetic Resonance Imaging: Differentiation of Benign and Malignant Breast Lesions. *Acad. Radiol.* **2003,** 10, (11), 1237-1246.

258. Troprès, I.; Grimault, S.; Vaeth, A.; Grillon, E.; Julien, C.; Payen, J.-F.; Lamalle, L.; Décorps, M. Vessel Size Imaging. *Magn. Reson. Med.* **2001,** 45, (3), 397-408.

259. Troprès, I.; Lamalle, L.; Péoc'h, M.; Farion, R.; Usson, Y.; Décorps, M.; Rémy, C. In Vivo Assessment of Tumoral Angiogenesis. *Magn. Reson. Med.* **2004,** 51, (3), 533-541.

260. Turetschek, K.; Roberts, T. P. L.; Floyd, E.; Preda, A.; Novikov, V.; Shames, D. M.; Carter, W. O.; Brasch, R. C. Tumor Microvascular Characterization Using Ultrasmall Superparamagnetic Iron Oxide Particles (USPIO) in an Experimental Breast Cancer Model. *J. Magn. Reson. Imaging* **2001,** 13, (6), 882-888.

261. Dardzinski, B. J.; Schmithorst, V. J.; Holland, S. K.; Boivin, G. P.; Imagawa, T.; Watanabe, S.; Lewis, J. M.; Hirsch, R. MR Imaging of Murine Arthritis Using Ultrasmall Superparamagnetic Iron Oxide Particles. *Magn. Reson. Imaging* **2001,** 19, (9), 1209-1216.

262. Schmitz, S. A.; Coupland, S. E.; Gust, R.; Winterhalter, S.; Wagner, S.; Kresse, M.; Semmler, W.; Wolf, K. J. Superparamagnetic Iron Oxide-Enhanced MRI of Atherosclerotic Plaques in Watanabe Hereditable Hyperlipidemic Rabbits. *Invest. Radiol.* **2000,** 35, (8), 460-471.

263. Ruehm, S. G.; Corot, C.; Vogt, P.; Kolb, S.; Debatin, J. F. Magnetic Resonance Imaging of Atherosclerotic Plaque with Ultrasmall Superparamagnetic Particles of Iron Oxide in Hyperlipidemic Rabbits. *Circulation* **2001,** 103, (3), 415-422.

264. Dousset, V.; Delalande, C.; Ballarino, L.; Quesson, B.; Seilhan, D.; Coussemacq, M.; Thiaudiére, E.; Brochet, B.; Canioni, P.; Caillé, J. M. In Vivo Macrophage Activity Imaging in the Central Nervous System Detected by Magnetic Resonance. *Magn. Reson. Med.* **1999,** 41, (2), 329-333.

265. Beckmann, N.; Cannet, C.; Fringeli-Tanner, M.; Baumann, D.; Pally, C.; Bruns, C.; Zerwes, H.-G.; Andriambeloson, E.; Bigaud, M. Macrophage Labeling by SPIO as an Early Marker of Allograft Chronic Rejection in a Rat Model of Kidney Transplantation. *Magn. Reson. Med.* **2003,** 49, (3), 459-467.

266. Metz, S.; Lohr, S.; Settles, M.; Beer, A.; Woertler, K.; Rummeny, E.; Daldrup–Link, H. Ferumoxtran-10-Enhanced MR Imaging of the Bone Marrow before and after Conditioning Therapy in Patients with Non-Hodgkin Lymphomas. *Eur. Radiol.* **2006,** 16, (3), 598-607.

267. Daldrup-Link, H.; Rummeny, E.; Ihssen, B.; Kienast, J.; Link, T. Iron-Oxide-Enhanced MR Imaging of Bone Marrow in Patients with Non-Hodgkin's Lymphoma:

Differentiation between Tumor Infiltration and Hypercellular Bone Marrow. *Eur. Radiol.* **2002,** 12, (6), 1557-1566.

268. Stark, D. D.; Weissleder, R.; Elizondo, G.; Hahn, P. F.; Saini, S.; Todd, L. E.; Wittenberg, J.; Ferrucci, J. T. Superparamagnetic Iron Oxide: Clinical Application as a Contrast Agent for MR Imaging of the Liver. *Radiology* **1988,** 168, (2), 297-301.

269. Elizondo, G.; Weissleder, R.; Stark, D. D.; Guerra, J.; Garza, J.; Fretz, C. J.; Todd, L. E.; Ferrucci, J. T. Hepatic Cirrhosis and Hepatitis: MR Imaging Enhanced with Superparamagnetic Iron Oxide. *Radiology* **1990,** 174, (3), 797-801.

270. Fujita, T.; Ito, K.; Honjo, K.; Okazaki, H.; Matsumoto, T.; Matsunaga, N. Detection of Hepatocellular Carcinoma: Comparison of T2-Weighted Breath-Hold Fast Spin-Echo Sequences and High-Resolution Dynamic MR Imaging with a Phased-Array Body Coil. *J. Magn. Reson. Imaging* **1999,** 9, (2), 274-279.

271. Reimer, P.; Balzer, T. Ferucarbotran (Resovist): A New Clinically Approved RES-Specific Contrast Agent for Contrast-Enhanced MRI of the Liver: Properties, Clinical Development, and Applications. *Eur. Radiol.* **2003,** 13, (6), 1266-1276.

272. Sharma, R.; Saini, S.; Ros, P. R.; Hahn, P. F.; Small, W. C.; de Lange, E. E.; Stillman, A. E.; Edelman, R. R.; Runge, V. M.; Outwater, E. K.*, et al.* Safety Profile of Ultrasmall Superparamagnetic Iron Oxide Ferumoxtran-10: Phase II Clinical Trial Data. *J. Magn. Reson. Imaging* **1999,** 9, (2), 291-294.

273. Harisinghani, M. G.; Barentsz, J.; Hahn, P. F.; Deserno, W. M.; Tabatabaei, S.; van de Kaa, C. H.; de la Rosette, J.; Weissleder, R. Noninvasive Detection of Clinically Occult Lymph-Node Metastases in Prostate Cancer. *N. Engl. J. Med.* **2003,** 348, (25), 2491-2499.

274. Nguyen, B. C.; Stanford, W.; Thompson, B. H.; Rossi, N. P.; Kernstine, K. H.; Kern, J. A.; Robinson, R. A.; Amorosa, J. K.; Mammone, J. F.; Outwater, E. K. Multicenter Clinical Trial of Ultrasmall Superparamagnetic Iron Oxide in the Evaluation of Mediastinal Lymph Nodes in Patients with Primary Lung Carcinoma. *J. Magn. Reson. Imaging* **1999,** 10, (3), 468-473.

275. Michel, S. C. A.; Keller, T. M.; Frohlich, J. M.; Fink, D.; Caduff, R.; Seifert, B.; Marincek, B.; Kubik-Huch, R. A. Preoperative Breast Cancer Staging: MR Imaging of the Axilla with Ultrasmall Superparamagnetic Iron Oxide Enhancement. *Radiology* **2002,** 225, (2), 527-536.

276. Bremer, C.; Allkemper, T.; Baermig, J.; Reimer, P. RES-Specific Imaging of the Liver and Spleen with Iron Oxide Particles Designed for Blood Pool MR-Angiography. *J. Magn. Reson. Imaging* **1999,** 10, (3), 461-467.

277. Simon, G. H.; Raatschen, H.-J.; Wendland, M. F.; von Vopelius-Feldt, J.; Fu, Y.; Chen, M.-H.; Daldrup-Link, H. E. Ultrasmall Superparamagnetic Iron-Oxide-Enhanced

MR Imaging of Normal Bone Marrow in Rodents: Original Research. *Acad. Radiol.* **2005,** 12, (9), 1190-1197.

278. Bachmann, R.; Kreft, B.; Dombrowski, F.; Block, W.; Öksendal, A.; Schild, H. Enhanced Tumor Detection in the Presence of Liver Cirrhosis: Experimental Study on the Diagnostic Value of a Superparamagnetic Iron Oxide MR Imaging Contrast Agent (NSR 0430). *J. Magn. Reson. Imaging* **1999,** 9, (2), 251-256.

279. Weissleder, R.; Elizondo, G.; Wittenberg, J.; Lee, A. S.; Josephson, L.; Brady, T. J. Ultrasmall Superparamagnetic Iron Oxide: An Intravenous Contrast Agent for Assessing Lymph Nodes with MR Imaging. *Radiology* **1990,** 175, (2), 494-498.

280. Weissleder, R.; Elizondo, G.; Wittenberg, J.; Rabito, C. A.; Bengele, H. H.; Josephson, L. Ultrasmall Superparamagnetic Iron Oxide: Characterization of a New Class of Contrast Agents for MR Imaging. *Radiology* **1990,** 175, (2), 489-493.

281. Weissleder, R.; Heautot, J. F.; Schaffer, B. K.; Nossiff, N.; Papisov, M. I.; Bogdanov, A., Jr.; Brady, T. J. MR Lymphography: Study of a High-Efficiency Lymphotrophic Agent. *Radiology* **1994,** 191, (1), 225-230.

282. Bordat, C.; Sich, M.; Réty, F.; Bouet, O.; Cournot, G.; Cuénod, C. A.; Clément, O. Distribution of Iron Oxide Nanoparticles in Rat Lymph Nodes Studied Using Electron Energy Loss Spectroscopy (EELS) and Electron Spectroscopic Imaging (ESI). *J. Magn. Reson. Imaging* **2000,** 12, (3), 505-509.

283. Guimaraes, R.; Clément, O.; Bittoun, J.; Carnot, F.; Frija, G. MR Lymphography with Superparamagnetic Iron Nanoparticles in Rats: Pathologic Basis for Contrast Enhancement. *Am. J. Roentgenol.* **1994,** 162, (1), 201-207.

284. Weinmann, H. J.; Ebert, W.; Misselwitz, B.; Schmitt-Willich, H. Tissue-Specific MR Contrast Agents. *Eur. J. Radiol.* **2003,** 46, (1), 33-44.

285. Konda, S.; Aref, M.; Wang, S.; Brechbiel, M.; Wiener, E. Specific Targeting of Folate–Dendrimer MRI Contrast Agents to the High Affinity Folate Receptor Expressed in Ovarian Tumor Xenografts. *Magn. Reson. Mater. Phys., Biol. Med.* **2001,** 12, (2), 104-113.

286. Häfeli, U. O.; Pauer, G. J. In Vitro and in Vivo Toxicity of Magnetic Microspheres. *J. Magn. Magn. Mater.* **1999,** 194, (1-3), 76-82.

287. Müller, R.; Steinmetz, H.; Hiergeist, R.; Gawalek, W. Magnetic Particles for Medical Applications by Glass Crystallisation. *J. Magn. Magn. Mater.* **2004,** 272-276, (Part 2), 1539-1541.

288. Babincová, M.; Sourivong, P.; Leszczynska, D.; Babinec, P. Blood-Specific Whole-Body Electromagnetic Hyperthermia. *Med. Hypotheses* **2000,** 55, (6), 459-460.

289. Wada, S.; Yue, L.; Tazawa, K.; Furuta, I.; Nagae, H.; Takemori, S.; Minamimura, T. New Local Hyperthermia Using Dextran Magnetite Complex (DM) for Oral Cavity: Experimental Study in Normal Hamster Tongue. *Oral Dis.* **2001,** 7, (3), 192-195.

290. Barrett, T.; Kobayashi, H.; Brechbiel, M.; Choyke, P. L. Macromolecular MRI Contrast Agents for Imaging Tumor Angiogenesis. *Eur. J. Radiol.* **2006,** 60, (3), 353-366.

291. Anzai, Y. Superparamagnetic Iron Oxide Nanoparticles: Nodal Metastases and Beyond. *Top. Magn. Reson. Imaging* **2004,** 15, (2), 103-111.

292. Arbab, A. S.; Bashaw, L. A.; Miller, B. R.; Jordan, E. K.; Bulte, J. W. M.; Frank, J. A. Intracytoplasmic Tagging of Cells with Ferumoxides and Transfection Agent for Cellular Magnetic Resonance Imaging after Cell Transplantation: Methods and Techniques. *Transplantation* **2003,** 76, (7), 1123-1130.

293. Vadala, M. L.; Zalich, M. A.; Fulks, D. B.; St. Pierre, T. G.; Dailey, J. P.; Riffle, J. S. Cobalt-Silica Magnetic Nanoparticles with Functional Surfaces. *J. Magn. Magn. Mater.* **2005,** 293, (1), 162-170.

294. Wormuth, K. Superparamagnetic Latex Via Inverse Emulsion Polymerization. *J. Colloid Interface Sci.* **2001,** 241, (2), 366-377.

295. Connolly, J.; St. Pierre, T. G.; Rutnakornpituk, M.; Riffle, J. S. Silica Coating of Cobalt Nanoparticles Increases Their Magnetic and Chemical Stability for Biomedical Applications. *Eur. Cell. Mater.* **2002,** 3, (2), 106-109.

296. Cushing, B. L.; Kolesnichenko, V. L.; O'Connor, C. J. Recent Advances in the Liquid-Phase Syntheses of Inorganic Nanoparticles. *Chem. Rev.* **2004,** 104, (9), 3893-3946.

297. Chan, D. C. F.; Kirpotin, D. B.; Bunn, P. A. Synthesis and Evaluation of Colloidal Magnetic Iron Oxides for the Site-Specific Radiofrequency-Induced Hyperthermia of Cancer. *J. Magn. Magn. Mater.* **1993,** 122, (1-3), 374-378.

298. Stiriba, S.-E.; Frey, H.; Haag, R. Dendritic Polymers in Biomedical Applications: From Potential to Clinical Use in Diagnostics and Therapy. *Angew. Chem. Int. Ed.* **2002,** 41, (8), 1329-1334.

299. Shukla, R.; Thomas, T. P.; Peters, J.; Kotlyar, A.; Myc, A.; Baker, J. R., Jr. Tumor Angiogenic Vasculature Targeting with PAMAM Dendrimer-RGD Conjugates. *Chem. Commun.* **2005**, (46), 5739-5741.

300. Hong, S.; Bielinska, A. U.; Mecke, A.; Keszler, B.; Beals, J. L.; Shi, X.; Balogh, L.; Orr, B. G.; Baker, J. R., Jr.; Banaszak Holl, M. M. Interaction of Poly(amidoamine) Dendrimers with Supported Lipid Bilayers and Cells: Hole Formation and the Relation to Transport. *Bioconjugate Chem.* **2004,** 15, (4), 774-782.

301. Thomas, T. P.; Patri, A. K.; Myc, A.; Myaing, M. T.; Ye, J. Y.; Norris, T. B.; Baker, J. R., Jr. In Vitro Targeting of Synthesized Antibody-Conjugated Dendrimer Nanoparticles. *Biomacromolecules* **2004,** 5, (6), 2269-2274.

302. Majoros, I. J.; Keszler, B.; Woehler, S.; Bull, T.; Baker, J. R., Jr. Acetylation of Poly(amidoamine) Dendrimers. *Macromolecules* **2003,** 36, (15), 5526-5529.

303. Esfand, R.; Tomalia, D. A. Poly(amidoamine) (PAMAM) Dendrimers: From Biomimicry to Drug Delivery and Biomedical Applications. *Drug Discovery Today* **2001,** 6, (8), 427-436.

304. Baker, J. R., Jr.; Quintana, A.; Piehler, L.; Banaszak Holl, M.; Tomalia, D.; Raczka, E. The Synthesis and Testing of Anti-Cancer Therapeutic Nanodevices. *Biomed. Microdevices* **2001,** 3, (1), 61-69.

305. Hong, S.; Leroueil, P. R.; Majoros, I. J.; Orr, B. G.; Baker, J. R., Jr.; Banaszak Holl, M. M. The Binding Avidity of a Nanoparticle-Based Multivalent Targeted Drug Delivery Platform. *Chem. Biol.* **2007,** 14, (1), 107-115.

306. Kukowska-Latallo, J. F.; Candido, K. A.; Cao, Z.; Nigavekar, S. S.; Majoros, I. J.; Thomas, T. P.; Balogh, L. P.; Khan, M. K.; Baker, J. R., Jr. Nanoparticle Targeting of Anticancer Drug Improves Therapeutic Response in Animal Model of Human Epithelial Cancer. *Cancer Res.* **2005,** 65, (12), 5317-5324.

307. Majoros, I. J.; Myc, A.; Thomas, T.; Mehta, C. B.; Baker, J. R., Jr. PAMAM Dendrimer-Based Multifunctional Conjugate for Cancer Therapy: Synthesis, Characterization, and Functionality. *Biomacromolecules* **2006,** 7, (2), 572-579.

308. Majoros, I. J.; Thomas, T. P.; Mehta, C. B.; Baker, J. R., Jr. Poly(amidoamine) Dendrimer-Based Multifunctional Engineered Nanodevice for Cancer Therapy. *J. Med. Chem.* **2005,** 48, (19), 5892-5899.

309. Myc, A.; Majoros, I. J.; Thomas, T. P.; Baker, J. R., Jr. Dendrimer-Based Targeted Delivery of an Apoptotic Sensor in Cancer Cells. *Biomacromolecules* **2007,** 8, (1), 13-18.

310. Thomas, T. P.; Majoros, I. J.; Kotlyar, A.; Kukowska-Latallo, J. F.; Bielinska, A.; Myc, A.; Baker, J. R., Jr. Targeting and Inhibition of Cell Growth by an Engineered Dendritic Nanodevice. *J. Med. Chem.* **2005,** 48, (11), 3729-3735.

311. Thomas, T. P.; Myaing, M. T.; Ye, J. Y.; Candido, K.; Kotlyar, A.; Beals, J.; Cao, P.; Keszler, B.; Patri, A. K.; Norris, T. B.*, et al.* Detection and Analysis of Tumor Fluorescence Using a Two-Photon Optical Fiber Probe. *Biophys. J.* **2004,** 86, (6), 3959-3965.

312. Patri, A. K.; Myc, A.; Beals, J.; Thomas, T. P.; Bander, N. H.; Baker, J. R., Jr. Synthesis and in Vitro Testing of J591 Antibody-Dendrimer Conjugates for Targeted Prostate Cancer Therapy. *Bioconjugate Chem.* **2004,** 15, (6), 1174-1181.

313. Leroueil, P. R.; Hong, S.; Mecke, A.; Baker, J. R., Jr.; Orr, B. G.; Banaszak Holl, M. M. Nanoparticle Interaction with Biological Membranes: Does Nanotechnology Present a Janus Face? *Acc. Chem. Res.* **2007,** 40, (5), 335-342.

314. Storm, G.; Belliot, S. O.; Daemen, T.; Lasic, D. D. Surface Modification of Nanoparticles to Oppose Uptake by the Mononuclear Phagocyte System. *Adv. Drug Delivery Rev.* **1995,** 17, (1), 31-48.

315. Weitman, S. D.; Weinberg, A. G.; Coney, L. R.; Zurawski, V. R.; Jennings, D. S.; Kamen, B. A. Cellular Localization of the Folate Receptor: Potential Role in Drug Toxicity and Folate Homeostasis. *Cancer Res.* **1992,** 52, (23), 6708-6711.

316. Ross, J. F.; Chaudhuri, P. K.; Ratnam, M. Differential Regulation of Folate Receptor Isoforms in Normal and Malignant Tissues in Vivo and in Established Cell Lines. Physiologic and Clinical Implications. *Cancer* **1994,** 73, (9), 2432-2443.

317. Miotti, S.; Canevari, S.; Menard, S.; Mezzanzanica, D.; Porro, G.; Pupa, S. M.; Regazzoni, M.; Tagliabue, E.; Colnaghi, M. I. Characterization of Human Ovarian Carcinoma-Associated Antigens Defined by Novel Monoclonal Antibodies with Tumor-Restricted Specificity. *Int. J. Cancer* **1987,** 39, (3), 297-303.

318. Veggian, R.; Fasolato, S.; Menard, S.; Minucci, D.; Pizzetti, P.; Regazzoni, M.; Tagliabue, E.; Colnaghi, M. I. Immunohistochemical Reactivity of a Monoclonal Antibody Prepared against Human Ovarian Carcinoma on Normal and Pathological Female Genital Tissues. *Tumori* **1989,** 75, (5), 510-513.

319. Campbell, I. G.; Jones, T. A.; Foulkes, W. D.; Trowsdale, J. Folate-Binding Protein Is a Marker for Ovarian Cancer. *Cancer Res.* **1991,** 51, (19), 5329-5338.

320. Stella, B.; Arpicco, S.; Peracchia, M. T.; Desmaële, D.; Hoebeke, J.; Renoir, M.; D'Angelo, J.; Cattel, L.; Couvreur, P. Design of Folic Acid-Conjugated Nanoparticles for Drug Targeting. *J. Pharm. Sci.* **2000,** 89, (11), 1452-1464.

321. Lu, Y.; Low, P. S. Folate-Mediated Delivery of Macromolecular Anticancer Therapeutic Agents. *Adv. Drug Delivery Rev.* **2002,** 54, (5), 675-693.

CHAPTER 2

SYNTHESIS OF ORGANIC- AND DENDRIMER-COATED IRON OXIDE NANOPARTICLES

2.1 Introduction

2.1.1 Poly(amidoamine) (PAMAM) Dendrimers

Our group has demonstrated success using poly(amidoamine) (PAMAM) dendrimers conjugated with FA to target tumors both *in vitro* and *in vivo*.[1-9] PAMAM dendrimers are biocompatible, cascade-branched macromolecules with highly flexible surface chemistry that facilitates functionalization. The PAMAM dendrimers used in this work are unique in that the surfaces were completely neutralized by capping with acetyl groups following the covalent attachment of several molecules of both folic acid and 6-TAMRA dye. Folic acid is the targeting moiety; the dye allows optical tracking of the devices, and the neutral surface minimizes non-specific interactions with cells.[1, 5, 10-13] Targeting efficacy is further augmented by the multivalent effect—multiple FA moieties simultaneously interacting with multiple receptors—exhibited by the dendrimer-FA conjugates.[2]

2.1.2 Iron Oxide Nanoparticles

For use in biomedical applications, magnetic nanoparticles should possess uniform, carefully controlled physicochemical and magnetic properties since the

particles' behavior critically depends on these characteristics.[14-17] Indeed, it is only justifiable to refer to the singular behavior of the particles if they are monodisperse; otherwise, "particles' behaviors" is more appropriate. Synthesizing monodisperse populations of highly crystalline magnetic nanoparticles is a very complicated task.[18] Size control is challenging because the high surface energy of nanoparticles favors agglomeration and nonuniform growth both immediately following formation of nucleation centers and as the particles age in solution.[19] Nucleation occurs to restore thermodynamic equilibrium when the reaction solution becomes supersaturated with precursors or their decomposition products.[20] The growth of small particles is dominated by this process as precursor molecules react and condense. As particles become larger, they grow at the expense of other particles through Ostwald ripening: material is removed and redistributed among particles.[20] The key to forming monodisperse particles is, therefore, to separate nucleation and growth: a single burst of nucleation followed by slow, steady growth of the nuclei.[21, 22] This can be accomplished by using a single pure precursor that exhibits a sharp decomposition temperature and injecting it into a suitable surfactant solution.[20, 21] The surfactant immediately caps the nucleation centers as they form and modulates their growth.

Initial iron oxide nanoparticle syntheses were conducted following the procedure published by Rockenberger *et al*. It was discovered, however, that the product particles were difficult to purify and redissolve following purification; other groups reported similar problems with handling.[23] The nanoparticles were readily precipitated by adding several excess volumes of more polar solvents miscible with the organic dispersion media, e.g. acetone and ethanol; flocculation was evident as the liquid went from clear

and brown to turbid and brown. However, the precipitated particles did not settle very well even when a rare-earth magnet was used to facilitate the process. Once the particles were finally magnetically isolated from the supernatant, purification by rinsing with the precipitating solvent made the majority of the particles insoluble. This suggests that the amine surfactants used were very weakly interacting with the particles' surfaces and could therefore be stripped away *via* simple solvent washes.

I hypothesized that oleic acid would increase the particles' stability and make them more tractable. Experimentation verified this hypothesis. Recent literature also provides support as it indicates oleic acid is the optimal capping agent for iron oxide nanoparticles.[24, 25] This is presumably due to the strong coordination of carboxylic acids to nanoscale metal oxide surfaces[26] as well as a particular feature of oleic acid: the kink in its aliphatic hydrocarbon tail at the double bond.[27]

2.2 Reagents and Materials

Reagents were used as obtained from commercial sources. Hexanes (HPLC grade), dimethyl sulfoxide (DMSO, ≥99.8%), methanol (MeOH, HPLC grade), hydrochloric acid (certified ACS Plus) and acetone (≥99.5%) were purchased from Fisher Scientific (Chicago, IL); 6-carboxytetramethylrhodamine, succinimidyl ester *single isomer* (6-TAMRA, 6T) was from Molecular Probes, Inc. (Eugene, OR). Ferric chloride hexahydrate ($FeCl_3 \cdot 6H_2O$, ≥98%) and folic acid (FA, 98%) were acquired from Sigma (St. Louis, MO). Chloroform (≥99.8%), cupferron (97%), acetic anhydride (99.5%), *N*-(3-dimethylaminopropyl)-*N*′-ethylcarbodiimide hydrochloride (EDC, 98%), triethylamine (Et_3N, ≥99.5%), octylamine (99%), trioctylamine (98%), oleic acid (technical grade, 90%) and sodium bicarbonate (>99.5%) were from Sigma-Aldrich

(Milwaukee, WI). Amine-terminated generation 5 PAMAM dendrimers (G5-NH_2) were purchased from Dendritech (Midland, MI) and purified *via* dialysis and ultrafiltration.[3, 10] The polymer was checked for the presence of trailing generations by HPLC,[5, 28] and characterized by GPC[5, 29] and MALDI-TOF[30, 31] to establish the molecular weight. The number of primary amine terminal functional groups was determined to be 110 by potentiometric titration.[4, 30] Throughout the experiments unless otherwise specified, ultrapure water with a resistivity of at least 18 MΩ·cm was used as produced by a Milli-Q purification system (Millipore; Bedford, MA).

2.3 Dendrimer Conjugation

The PAMAM dendrimers used in this study were modified according to previously published protocols. Acetylation was conducted on G5-NH_2 to neutralize an average of 73% (82 out of 110) of the dendrimers' amine termini to produce G5-Ac(82).[5, 29] This step is essential for minimizing non-specific interactions with cells.[1, 5, 10-13] Next, EDC coupling was employed to conjugate the targeting moiety, folic acid, at an average of 5 molecules per dendrimer to yield G5-NH_2(23)-Ac(82)-FA(5).[6, 32] 6-TAMRA dye labels were added at three equivalents per dendrimer primary amine, producing G5-NH_2(20)-Ac(82)-FA(5)-6T(3).[9] Finally, the dendrimers were allowed to react with excess acetic anhydride to convert any remaining surface amines to acetamide groups, resulting in G5-Ac(102)-FA(5)-6T(3).[5, 29] Surface functionalization was quantified and purity evaluated following each step using several complementary techniques: peak integrations from proton nuclear magnetic resonance spectroscopy (^{1}H NMR), molecular weight changes from MALDI-TOF mass spectrometry, and using absorbance calibration curves with UV–visible (UV–vis) spectroscopy.[2, 5, 9, 10, 28, 29]

2.4 Iron Oxide Nanoparticle Synthesis

The following procedures were adapted from the work published by Rockenberger *et al*.[33]

2.4.1 Ferric Cupferron Precursor ($FeCup_3$)

Magnetic stirring was used in the preparation of all solutions unless otherwise noted. In a typical synthesis, a clear, light brown aqueous cupferron solution was prepared by dissolving 3.005 g of cupferron in 100 mL deionized tap water (DI water). A 280 mL volume of 1% hydrochloric acid was prepared in a separate flask to dissolve 1.136 g of ferric chloride hexahydrate. Once the $FeCl_3 \cdot 6H_2O$ had completely dissolved to form a clear, yellow solution, the solution was further acidified by slowly adding 140 mL concentrated HCl; the liquid turned a brighter yellow but remained clear. It was then diluted by the slow addition of 525 mL DI water and placed in a refrigerator under Parafilm at 4°C for 15 min to cool. After cooling, the acidic iron chloride solution was rapidly stirred while the cupferron solution was added dropwise from a burette. The stirred solution initially became turned clear red. As more cupferron solution was added, the red color grew deeper until the solution became turbid due to the formation of a red-brown precipitate. Once addition of the cupferron solution was complete, the precipitate was allowed to settle for 15 min before isolating it *via* Büchner funnel vacuum filtration. The solid was washed on the filter paper with several mL of water to remove unreacted cupferron. The filter paper was then placed in a beaker and rinsed thoroughly with 140 mL of chloroform to extract the solid and form a dark red solution. A separation funnel was used to isolate the organic phase from any residual water. Crystallization was then conducted to obtain pure ferric cupferron ($FeCup_3$). The organic solution was

concentrated to approximately 5 mL using a rotary evaporator with a bath temperature of 40°C. Crystallization often spontaneously began upon removal of the flask from the rotary evaporator. If this did not happen, several drops of hexanes were added until white wisps appeared in the dark red concentrated solution. In either case, the resulting mixture was placed in the original flask under Parafilm in a refrigerator at 4°C. After an incubation period of around 24 h, the mother liquor was discarded, and the resulting dark red $FeCup_3$ crystals were rinsed using cold hexanes, dried under a nitrogen stream, collected and weighed. Typical yields were around 80% with respect to iron.

2.4.2 Nanoparticle Synthesis

2.4.2.1 Solution Preparation

Reaction solutions were generally prepared 24 h prior to actual nanoparticle synthesis. First, an oil bath was set up to stir at 60°C, and a wax bath was set up to stir at 100°C. Next, the $FeCup_3$ precursor was dissolved in octylamine to make a clear, dark red 0.3 M solution; with typical yields, around 10 mL octylamine was required. The resulting solution was transferred into a 50 mL two-neck round-bottom flask containing a stir bar; one neck was capped with a septum (preferably white rubber), and a needle valve was connected to the other neck. Finally, 2.5 mL of oleic acid and 8 mL of trioctylamine were mixed in a 100 mL two-neck round-bottom flask containing a stir bar to form a clear, colorless solution. One of the flask's necks was capped with a septum (preferably white rubber); a condenser and needle valve were attached to the other neck. Teflon tape was used to secure the connection between the flask and the condenser.

Both the 25 mL and 100 mL apparatus were attached to a vacuum line to remove residual air and moisture. The flask containing the solution of oleic acid in trioctylamine was set stirring in the 100°C wax bath; the flask containing the $FeCup_3$ solution in octylamine was set stirring in the 60°C oil bath. Drying and degassing were accomplished by cracking the needle valves six times: once every 15 min over a 1.5 h period. The $FeCup_3$ solution in octylamine was found to readily bump when heated and opened to dynamic vacuum, so special care was taken to slowly open the needle valve and not leave it open for too long. Although there was no discernible change in the color or turbidity of the $FeCup_3$ solution following the degassing procedure, the oleic acid/trioctylamine solution became light yellow. After degassing, both apparatus were backfilled with Ar once cooled and sealed.

2.4.2.2 Rapid Injection and Thermal Decomposition

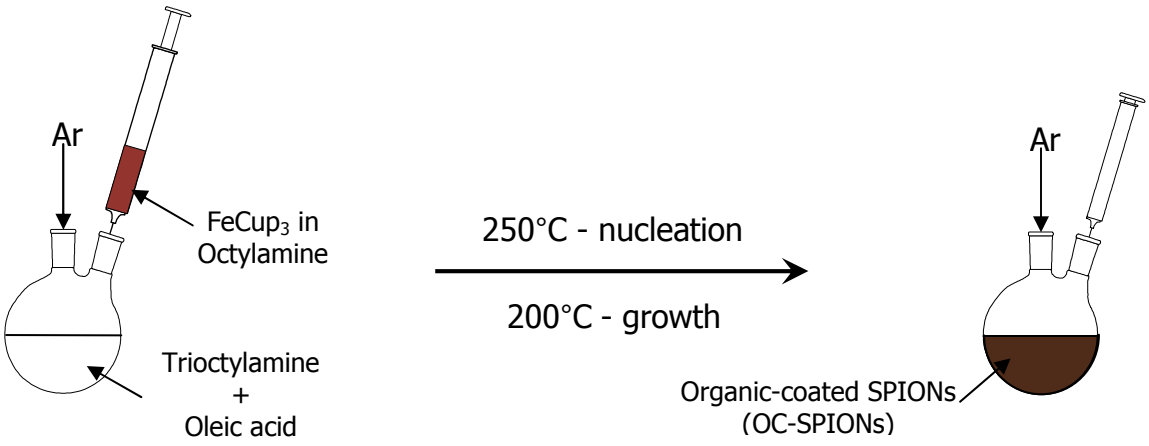

Figure 2.1 - A schematic of the OC-SPION synthesis.

The flask containing the solution of oleic acid in trioctylamine (Figure 2.1) was placed in a sand bath within a heating mantle that was plugged into an adjustable voltage transformer. A mercury thermometer was placed in the sand with its bulb adjacent to the

flask at liquid level. The apparatus was opened to flowing Ar, and condenser water flow and rapid stirring were started before supplying heat. Temperature adjustments were made by incremental changes on the voltage transformer dial. These adjustments were made slowly over 2-3 h to ensure thermal equilibration so the thermometer reading accurately reflected the liquid temperature. As the reading neared 250°C a 5 mL all-plastic syringe was fitted with an 18-gauge needle onto which about a 4.5" piece of thin-walled Teflon tubing was then threaded. Once the reading reached 250°C, the needle valve stem on the $FeCup_3$ apparatus was removed, and the syringe was purged by inserting the tubing into the valve neck and drawing and expelling several aliquots of the Ar blanket. The valve was replaced before removing the septum on the apparatus' flask and using the purged syringe to draw out a 4.8 mL portion of the 0.3 M $FeCup_3$ solution. Bubbles were removed by inverting the syringe and expelling the void volume and any excess liquid back into the flask; the liquid in the tubing was also drained back in by detaching it from the needle with the opposite end still hanging in the flask. After resealing the flask with the septum, the $FeCup_3$ solution was rapidly injected into the hot stirring 0.75 M solution of oleic acid in trioctylamine (Figure 2.1). After reducing the temperature to 200°C and aging for 30 minutes, the clear, black reaction liquid was allowed to cool to room temperature under argon flow. Once cool, stirring was stopped, and a rare-earth magnet was applied to the flask for 15 minutes to collect and hold any magnetic precipitate. The supernatant was then magnetically decanted into a new flask and stored under a nitrogen blanket. Aliquots were taken as needed from this stock solution. Particles were precipitated by adding 3-fold volume excess of acetone and immediately settled by applying a rare-earth magnet. The magnet was used to hold the

particles while decanting the clear, dark brown-yellow supernatant. Fresh acetone was then added, the mixture was agitated, and the particles were again settled using a rare-earth magnet and held with it while the supernatant was decanted. This process was repeated until the supernatant was clear and colorless. The cleaned organic-coated SPIONs (OC-SPIONs) were dried in a nitrogen stream and then dissolved in chloroform for surface modification.

2.5 Magnetite Nanoparticle Surface Modification

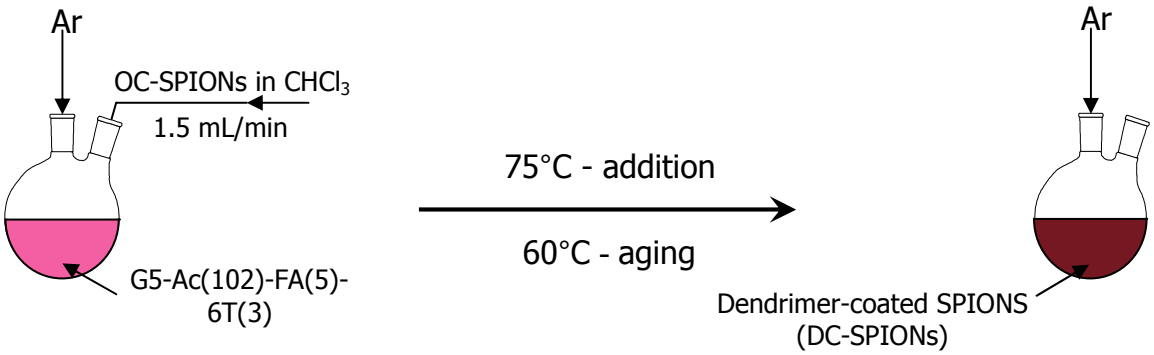

Figure 2.2 - A schematic of the phase transfer operation of OC-SPIONs leading to DC-SPIONs.

A 3.4 mg portion of G5-Ac(102)-FA(5)-6T(3) was dissolved in 1 mL of DMSO (Figure 2.2). The solution was thoroughly degassed *via* 5 cycles of standard freeze-pump-thaw protocol and then placed under flowing Ar. A syringe purged with nitrogen was used to gather a dispersion of 5 mg OC-SPIONs in 1 mL chloroform. The dendrimer solution was heated to 75°C, and the nanoparticles in chloroform were added dropwise at a rate of 1.5 mL/min (Figure 2.2). After the syringe was emptied, the reaction temperature was reduced to 60°C, and stirring was continued for 12 hours under steady Ar flow. Heat was then removed, and the clear, dark brown/pink liquid product cooled and was transferred to a vial. The dendrimer-coated SPIONs (DC-SPIONs) were isolated

from free dendrimer using precipitation and magnetic separation; this purification was performed on individual 150 μL aliquots of the reaction solution to the total volume of ~1.5 mL. A threefold volume excess of acetone was added to the aliquot. The mixture was gently agitated, and the resulting precipitate was gathered and held with a rare-earth magnet while removing the supernatant using a pipet. DMSO (150 μL) was added to redissolve the particles. This was followed by precipitation with a 4-fold volume excess of acetone, agitation, and magnetic separation as before. The particles were then dried under a nitrogen stream and dissolved in 100 μL water. The resulting 1 mL of stock solution was determined by inductively coupled plasma optical emission spectroscopy (ICP-OES) to have an iron concentration of 0.66 mg Fe/mL.

2.6 References

1. Baker, J. R., Jr.; Quintana, A.; Piehler, L.; Banaszak Holl, M.; Tomalia, D.; Raczka, E. The Synthesis and Testing of Anti-Cancer Therapeutic Nanodevices. *Biomed. Microdevices* **2001,** 3, (1), 61-69.

2. Hong, S.; Leroueil, P. R.; Majoros, I. J.; Orr, B. G.; Baker, J. R., Jr.; Banaszak Holl, M. M. The Binding Avidity of a Nanoparticle-Based Multivalent Targeted Drug Delivery Platform. *Chem. Biol.* **2007,** 14, (1), 107-115.

3. Kukowska-Latallo, J. F.; Candido, K. A.; Cao, Z.; Nigavekar, S. S.; Majoros, I. J.; Thomas, T. P.; Balogh, L. P.; Khan, M. K.; Baker, J. R., Jr. Nanoparticle Targeting of Anticancer Drug Improves Therapeutic Response in Animal Model of Human Epithelial Cancer. *Cancer Res.* **2005,** 65, (12), 5317-5324.

4. Majoros, I. J.; Myc, A.; Thomas, T.; Mehta, C. B.; Baker, J. R., Jr. PAMAM Dendrimer-Based Multifunctional Conjugate for Cancer Therapy: Synthesis, Characterization, and Functionality. *Biomacromolecules* **2006,** 7, (2), 572-579.

5. Majoros, I. J.; Thomas, T. P.; Mehta, C. B.; Baker, J. R., Jr. Poly(amidoamine) Dendrimer-Based Multifunctional Engineered Nanodevice for Cancer Therapy. *J. Med. Chem.* **2005,** 48, (19), 5892-5899.

6. Myc, A.; Majoros, I. J.; Thomas, T. P.; Baker, J. R., Jr. Dendrimer-Based Targeted Delivery of an Apoptotic Sensor in Cancer Cells. *Biomacromolecules* **2007,** 8, (1), 13-18.

7. Quintana, A.; Raczka, E.; Piehler, L.; Lee, I.; Myc, A.; Majoros, I.; Patri, A. K.; Thomas, T.; Mulé, J.; Baker, J. R., Jr. Design and Function of a Dendrimer-Based Therapeutic Nanodevice Targeted to Tumor Cells through the Folate Receptor. *Pharm. Res.* **2002,** 19, (9), 1310-1316.

8. Thomas, T. P.; Majoros, I. J.; Kotlyar, A.; Kukowska-Latallo, J. F.; Bielinska, A.; Myc, A.; Baker, J. R., Jr. Targeting and Inhibition of Cell Growth by an Engineered Dendritic Nanodevice. *J. Med. Chem.* **2005,** 48, (11), 3729-3735.

9. Thomas, T. P.; Myaing, M. T.; Ye, J. Y.; Candido, K.; Kotlyar, A.; Beals, J.; Cao, P.; Keszler, B.; Patri, A. K.; Norris, T. B*., et al.* Detection and Analysis of Tumor Fluorescence Using a Two-Photon Optical Fiber Probe. *Biophys. J.* **2004,** 86, (6), 3959-3965.

10. Hong, S.; Bielinska, A. U.; Mecke, A.; Keszler, B.; Beals, J. L.; Shi, X.; Balogh, L.; Orr, B. G.; Baker, J. R., Jr.; Banaszak Holl, M. M. Interaction of Poly(amidoamine) Dendrimers with Supported Lipid Bilayers and Cells: Hole Formation and the Relation to Transport. *Bioconjugate Chem.* **2004,** 15, (4), 774-782.

11. Leroueil, P. R.; Hong, S.; Mecke, A.; Baker, J. R., Jr.; Orr, B. G.; Banaszak Holl, M. M. Nanoparticle Interaction with Biological Membranes: Does Nanotechnology Present a Janus Face? *Acc. Chem. Res.* **2007,** 40, (5), 335-342.

12. Patri, A. K.; Myc, A.; Beals, J.; Thomas, T. P.; Bander, N. H.; Baker, J. R., Jr. Synthesis and in Vitro Testing of J591 Antibody-Dendrimer Conjugates for Targeted Prostate Cancer Therapy. *Bioconjugate Chem.* **2004,** 15, (6), 1174-1181.

13. Shukla, R.; Thomas, T. P.; Peters, J.; Kotlyar, A.; Myc, A.; Baker, J. R., Jr. Tumor Angiogenic Vasculature Targeting with PAMAM Dendrimer-RGD Conjugates. *Chem. Commun.* **2005**, (46), 5739-5741.

14. Corot, C.; Robert, P.; Idee, J. M.; Port, M. Recent Advances in Iron Oxide Nanocrystal Technology for Medical Imaging. *Adv. Drug Delivery Rev.* **2006,** 58, (14), 1471-1504.

15. Kodama, R. H. Magnetic Nanoparticles. *J. Magn. Magn. Mater.* **1999,** 200, (1-3), 359-372.

16. Krishnan, K.; Pakhomov, A.; Bao, Y.; Blomqvist, P.; Chun, Y.; Gonzales, M.; Griffin, K.; Ji, X.; Roberts, B. Nanomagnetism and Spin Electronics: Materials, Microstructure and Novel Properties. *J. Mater. Sci.* **2006,** 41, (3), 793-815.

17. Tartaj, P.; Morales, M. P.; Veintemillas-Verdaguer, S.; Gónzalez-Carreño, T.; Serna, C. J. The Preparation of Magnetic Nanoparticles for Applications in Biomedicine. *J. Phys. D: Appl. Phys.* **2003,** 36, (13), R182-R197.

18. Sugimoto, T. Preparation of Monodispersed Colloidal Particles. *Adv. Colloid Interface Sci.* **1987,** 28, 65-108.

19. Tartaj, P.; Morales, M. P.; Gonzalez-Carreno, T.; Veintemillas-Verdaguer, S.; Serna, C. J. Advances in Magnetic Nanoparticles for Biotechnology Applications. *J. Magn. Magn. Mater.* **2005,** 290-291, (Part 1), 28-34.

20. Willard, M. A.; Kurihara, L. K.; Carpenter, E. E.; Calvin, S.; Harris, V. G. Chemically Prepared Magnetic Nanoparticles. *Int. Mater. Rev.* **2004,** 49, 125-170.

21. Xu, C.; Sun, S. Monodisperse Magnetic Nanoparticles for Biomedical Applications. *Polym. Int.* **2007,** 56, (7), 821-826.

22. Hyeon, T. Chemical Synthesis of Magnetic Nanoparticles. *Chem. Commun.* **2003**, (8), 927-934.

23. Rajamathi, M.; Ghosh, M.; Seshadri, R. Hydrolysis and Amine-Capping in a Glycol Solvent as a Route to Soluble Maghemite γ-Fe_2O_3 Nanoparticles. *Chem. Commun.* **2002**, (10), 1152-1153.

24. Cushing, B. L.; Kolesnichenko, V. L.; O'Connor, C. J. Recent Advances in the Liquid-Phase Syntheses of Inorganic Nanoparticles. *Chem. Rev.* **2004,** 104, (9), 3893-3946.

25. Willis, A. L.; Turro, N. J.; O'Brien, S. Spectroscopic Characterization of the Surface of Iron Oxide Nanocrystals. *Chem. Mater.* **2005,** 17, (24), 5970-5975.

26. Li, Y.; Afzaal, M.; O'Brien, P. The Synthesis of Amine-Capped Magnetic (Fe, Mn, Co, Ni) Oxide Nanocrystals and Their Surface Modification for Aqueous Dispersibility. *J. Mater. Chem.* **2006,** 16, (22), 2175-2180.

27. Tadmor, R.; Rosensweig, R. E.; Frey, J.; Klein, J. Resolving the Puzzle of Ferrofluid Dispersants. *Langmuir* **2000,** 16, (24), 9117-9120.

28. Islam, M. T.; Shi, X.; Balogh, L.; Baker, J. R., Jr. HPLC Separation of Different Generations of Poly(amidoamine) Dendrimers Modified with Various Terminal Groups. *Anal. Chem.* **2005,** 77, (7), 2063-2070.

29. Majoros, I. J.; Keszler, B.; Woehler, S.; Bull, T.; Baker, J. R., Jr. Acetylation of Poly(amidoamine) Dendrimers. *Macromolecules* **2003,** 36, (15), 5526-5529.

30. Shi, X.; Lesniak, W.; Islam, M. T.; Muñiz, M. C.; Balogh, L. P.; Baker, J. R., Jr. Comprehensive Characterization of Surface-Functionalized Poly(amidoamine) Dendrimers with Acetamide, Hydroxyl, and Carboxyl Groups. *Colloids Surf., A* **2006,** 272, (1-2), 139-150.

31. Woller, E. K.; Walter, E. D.; Morgan, J. R.; Singel, D. J.; Cloninger, M. J. Altering the Strength of Lectin Binding Interactions and Controlling the Amount of Lectin Clustering Using Mannose/Hydroxyl-Functionalized Dendrimers. *J. Am. Chem. Soc.* **2003,** 125, (29), 8820-8826.

32. Wiener, E. C.; Konda, S.; Shadron, A.; Brechbiel, M.; Gansow, O. Targeting Dendrimer-Chelates to Tumors and Tumor Cells Expressing the High-Affinity Folate Receptor. *Invest. Radiol.* **1997,** 32, (12), 748-754.

33. Rockenberger, J.; Scher, E. C.; Alivisatos, A. P. A New Nonhydrolytic Single-Precursor Approach to Surfactant-Capped Nanocrystals of Transition Metal Oxides. *J. Am. Chem. Soc.* **1999,** 121, (49), 11595-11596.

CHAPTER 3

CHARACTERIZATION OF ORGANIC- AND DENDRIMER-COATED IRON OXIDE NANOPARTICLES

3.1 Introduction

Nanoparticles are complex entities, and their efficacy in biomedical applications critically depends on their physicochemical and magnetic characteristics. These properties should thus be determined to both predict their suitability for particular uses and facilitate understanding of the results of their application.[1, 2] Size, surface characteristics and magnetic properties are among the most influential factors influencing performance,[3] so these were examined using transmission electron microscopy, X-ray photoelectron spectroscopy, and a superconducting quantum interference device, respectively.

3.2 Methods

3.2.1 Transmission Electron Microscopy (TEM)

Specimens for TEM were prepared by releasing a drop of OC-SPIONs in chloroform or a drop of DC-SPION dispersion in water onto 400-mesh copper grids coated by ultrathin carbon support films (Ted Pella; Redding, CA). Once the grids were dry, images were acquired using a Philips CM-12 microscope operating at an accelerating potential difference of 120 kV.

3.2.2 X-ray Photoelectron Spectroscopy (XPS)

XPS samples were prepared on substrates cut from a sheet of indium foil (0.127 mm thick, 99.99%; Sigma-Aldrich; Milwaukee, WI). A drop of OC-SPIONs in chloroform or the aqueous DC-SPION dispersion was placed on the foil, and the solvent was allowed to evaporate in a fume hood. Analysis was conducted using an ESCA PHI-5000C (Physical Electronics; Chanhassen, MN) using Mg Kα X-rays (1253.6 eV) and a pass energy of 23.50 eV. Thorough descriptions of the experimental apparatus have been previously published.[4, 5]

3.2.3 Superconducting QUantum Interference Device (SQUID) Magnetometry

A Quantum Design (San Diego, CA) MPMS-5 SQUID magnetometer was used to investigate the dependence of sample magnetic moment on applied magnetic field. The specimen was a known volume (~30 μL) of a concentrated aqueous DC-SPION dispersion in a quartz tube. Residual air was removed from the liquid *via* six cycles of standard freeze-pump-thaw techniques before flame-sealing the tube while under vacuum using an oxygen/propane type 3A blowpipe with adjustable burn stoichiometry; an OX-2 (single 0.055”-diameter hole) or OX-1 (single 0.042”-diameter hole) tip worked best.

Inductively coupled plasma optical emission spectroscopy was employed to obtain the normalized magnetic moment with respect to iron. Poly(methylpentene) (PMP) volumetric flasks (Fisher Scientific; Chicago, IL) and ultrapure water with a resistivity of at least 18 MΩ·cm were used for all solution preparations. Iron and yttrium 1000 ppm elemental standard solutions (100 mL size) were obtained from GFS Chemicals (Powell, OH). A 625 μL aliquot of each of these solutions was added to separate 25 mL PMP flasks that were then filled to the line with water to make 25 ppm

solutions of Fe and Y. One mL of the Y solution was added to every sample and calibration standard solution prepared to serve as a 1 ppm internal standard. Calibration standards of 5, 1, and 0.1 ppm Fe (all 1 ppm Y) were made along with a 1 ppm Y blank (no Fe). A 50 μL sample of DC-SPION stock solution was diluted to 25 mL by adding 1 mL of the 25 ppm Y solution and adding water for the remaining volume. For analysis, the 371.029 nm line was used for Y, and the 238.204 nm and 239.562 nm lines were used for Fe. Three replicates were run for each measurement, and the Fe content was taken as the average of the mean values for each Fe line obtained over the three replicates.

3.3 Results and Discussion

3.3.1 Nanoparticle Synthesis and Surface Modification

The TEM micrograph in Figure 3.1A shows the structural characteristics of the magnetite nanoparticles as synthesized in organic media; the particles are consistent in size and shape with a mean diameter of 7.6 ± 0.7 nm (relative standard deviation of 8.9% for n = 72). Such uniformity is desirable since it facilitates determination of the connection between the individual particles and their collective behavior. This is especially useful when evaluating their suitability for use in biological applications. My novel phase transfer method leverages the benefits of nanocrystal synthesis in organic solvents, namely superior control over phase, shape, size, and size distribution, and provided a single step to achieving water solubility and enhanced functionality. This is accomplished using G5 dendrimers functionalized with an average of 102 acetamide groups (Ac), 5 molecules of FA, and 3 molecules of 6-TAMRA dye (6T): G5-Ac(102)-FA(5)-6T(3).

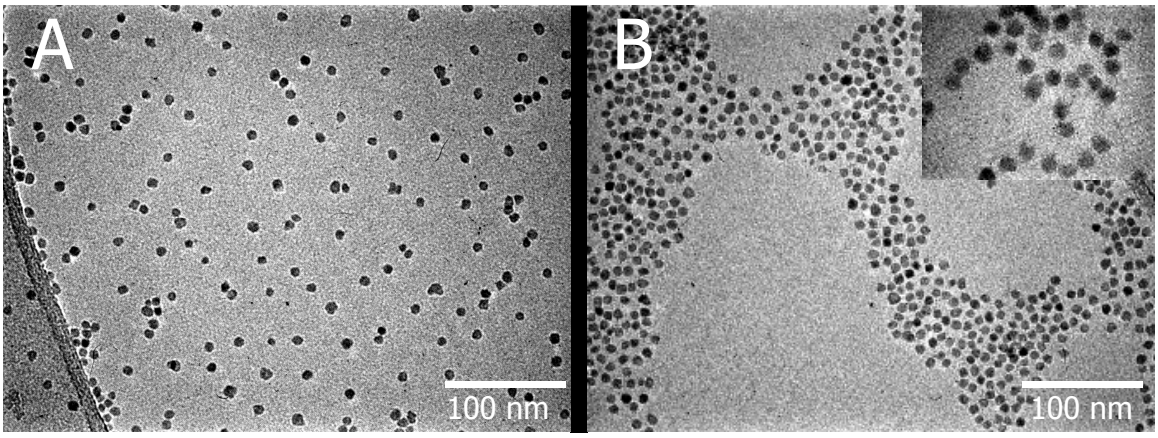

Figure 3.1 - Transmission electron micrographs of magnetite nanocrystals. The OC-SPIONs are shown in (A); panel (B) displays the DC-SPIONs. The inset of (B) is a higher-resolution image of the same DC-SPIONs clearly showing that size and shape uniformity are maintained. Although drying induces particle grouping, the DC-SPIONs remain isolated and do not form multi-particle aggregates.

I hypothesize that the dendrimers effect phase transfer by displacing the fatty acid ligands whose carboxylate groups are initially coordinated to the OC-SPIONs' surfaces.[6, 7] Since every folic acid moiety on the surrounding dendrimers has a free carboxylate group and there are multiple folic acids per dendrimer, the free carboxylates of some of the folic acid groups likely accomplish this suface exchange and coordinate to the surface through multidentate interactions. Such a linkage between nanoparticle and dendrimer would be consistent with the many literature examples of carboxylates coordinating to the surfaces of nanoscale metal oxides.[8, 9] Furthermore, my parallel attempts to produce a control particle using acetylated dendrimers functionalized with 6-TAMRA but without folic acid failed to yield stable, water-soluble SPIONs: G5-Ac(107)-6T(3) did not produce successful phase transfer whereas treatment with G5-Ac(102)-FA(5)-6T(3) did.

Figure 3.1B clearly demonstrates that the magnetite nanoparticles' structural quality is maintained upon treatment with G5-Ac(102)-FA(5)-6T(3) and dispersion in

water. It is important to note that there is no guarantee of size and shape uniformity being maintained upon phase transfer.[10-12] Indeed, the concerns of phase transfer operations and place exchange reactions are that significant aggregation and/or changes in particle size and shape can occur. The inset gives a clearer indication that the particles do not form fused aggregates even after drying in air. Further evidence that the iron oxide cores remain isolated was demonstrated by lyophilizing and redissolving an aliquot of the aqueous DC-SPION suspension.

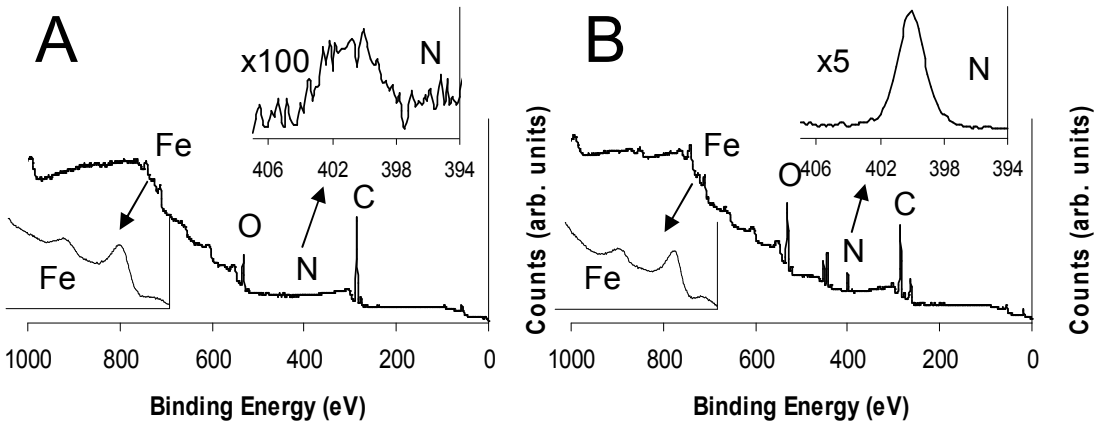

Figure 3.2 - X-ray photoelectron spectroscopy survey scans of (A) OC-SPIONs and (B) DC-SPIONs. The insets demonstrate that although no significant changes occur in the iron region of the spectra, there is a tremendous increase in nitrogen signal from (A) to (B), corresponding to dendrimers displacing the organic shell and binding to the nanoparticles' surfaces. Analysis of the nitrogen 1s and iron 2p core levels indicates an approximately 20:1 ratio of dendrimers to nanoparticles.

The solubility properties of the particles provide strong evidence of surface modification by the hydrophilic dendrimers. Comparing the XPS spectra for the OC-SPIONs and the DC-SPIONs provides further support for this conclusion. Figure 3.2 depicts survey scans for the capped magnetite cores both before (Figure 3.2A) and after

(Figure 3.2B) phase-transfer reaction with G5-Ac(102)-FA(5)-6T(3). The iron regions of both scans are nearly identical, but their nitrogen signatures differ significantly. Although the nitrogen spectrum in Figure 3.2A shows little more than noise, the same region in Figure 3.2B displays a strong signal attributed to the over five-hundred nitrogens in the amides and amines that compose the dendrimer backbone. No distinct peaks are seen for the heterocyclic nitrogens in the conjugated folic acid molecules either for the coated particles or even for neat G5-Ac(102)-FA(5)-6T(3). This is not surprising considering the approximately 100:3 theoretical ratio of aliphatic to heterocyclic nitrogen atoms and the expected overlap of the nitrogen 1s core levels.

3.3.2 Magnetic Properties

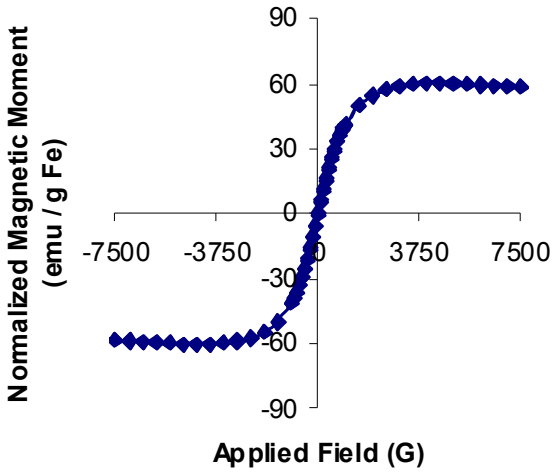

Figure 3.3 - Magnetization curve for DC-SPIONs. The data—taken at 37°C using a Quantum Design SQUID magnetometer—show that the particles are superparamagnetic with a rapid approach to saturation.

For their ultimate use as targeted contrast agents for MRI, it is critical that the iron oxide nanoparticles retain their favorable magnetic properties after coating them with dendrimers. The TEM results from Figure 3.1B demonstrate that the sizes of the DC-

SPIONs are unchanged from the OC-SPIONs and that the particles do not form fused aggregates, strongly suggesting that their magnetic properties would be unchanged. SQUID data (Figure 3.3) show that the DC-SPIONs rapidly approach a saturation magnetization of 60 emu/g Fe, compared to the bulk value of 90 emu/g Fe. Their size and the negligible hysteresis observed in their magnetic profile suggest that the DC-SPIONs are superparamagnetic. Neglecting anisotropy and assuming perfect monodispersity permit the DC-SPIONs to be modeled as a collection of magnetic moments whose behavior is described by the Langevin function:

$$M(H) = M_s \left(\coth\left(\frac{\mu H}{k_B T} \right) - \frac{k_B T}{\mu H} \right) \tag{3.1}$$

where M_s is the saturation magnetization, H is the applied magnetic field, k_B is Boltzmann's constant, T is the absolute temperature, and μ is the magnetic moment of a particle in the ensemble.[13, 14] This treatment is valid even considering interactions between particles.[15-17] A fit of Eq. (3.1) to the magnetization data yields the magnetic moment for a DC-SPION on the order of 10^{-16} erg/G or 10^4 μ_B, where μ_B, the Bohr magneton, is 9.3×10^{-21} erg/G. This demonstrates that the particles are superparamagnetic versus merely paramagnetic since paramagnetic moments are generally only a few μ_B.[13] These factors mean the particles are capable of providing substantial contrast in MR images even at modest clinical field strengths.

3.4 References

1. Corot, C.; Robert, P.; Idee, J. M.; Port, M. Recent Advances in Iron Oxide Nanocrystal Technology for Medical Imaging. *Adv. Drug Delivery Rev.* **2006,** 58, (14), 1471-1504.

2. Lawaczeck, R.; Menzel, M.; Pietsch, H. Superparamagnetic Iron Oxide Particles: Contrast Media for Magnetic Resonance Imaging. *Appl. Organomet. Chem.* **2004,** 18, (10), 506-513.

3. Neuberger, T.; Schopf, B.; Hofmann, H.; Hofmann, M.; von Rechenberg, B. Superparamagnetic Nanoparticles for Biomedical Applications: Possibilities and Limitations of a New Drug Delivery System. *J. Magn. Magn. Mater.* **2005,** 293, (1), 483-496.

4. Lee, S.; Makan, S.; Banaszak Holl, M. M.; McFeely, F. R. Synthetic Control of Solid/Solid Interfaces: Analysis of Three New Silicon/Silicon Oxide Interfaces by Soft X-Ray Photoemission. *J. Am. Chem. Soc.* **1994,** 116, (26), 11819-11826.

5. Greeley, J. N.; Meeuwenberg, L. M.; Banaszak Holl, M. M. Surface Infrared Studies of Silicon/Silicon Oxide Interfaces Derived from Hydridosilsesquioxane Clusters. *J. Am. Chem. Soc.* **1998,** 120, (31), 7776-7782.

6. Bronstein, L. M.; Huang, X.; Retrum, J.; Schmucker, A.; Pink, M.; Stein, B. D.; Dragnea, B. Influence of Iron Oleate Complex Structure on Iron Oxide Nanoparticle Formation. *Chem. Mater.* **2007,** 19, (15), 3624-3632.

7. Li, Y.; Afzaal, M.; O'Brien, P. The Synthesis of Amine-Capped Magnetic (Fe, Mn, Co, Ni) Oxide Nanocrystals and Their Surface Modification for Aqueous Dispersibility. *J. Mater. Chem.* **2006,** 16, (22), 2175-2180.

8. Harris, L. A.; Goff, J. D.; Carmichael, A. Y.; Riffle, J. S.; Harburn, J. J.; St. Pierre, T. G.; Saunders, M. Magnetite Nanoparticle Dispersions Stabilized with Triblock Copolymers. *Chem. Mater.* **2003,** 15, (6), 1367-1377.

9. Lattuada, M.; Hatton, T. A. Functionalization of Monodisperse Magnetic Nanoparticles. *Langmuir* **2007,** 23, (4), 2158-2168.

10. Wang, Y.; Teng, X.; Wang, J. S.; Yang, H. Solvent-Free Atom Transfer Radical Polymerization in the Synthesis of Fe_2O_3@Polystyrene Core-Shell Nanoparticles. *Nano Lett.* **2003,** 3, (6), 789-793.

11. Yu, W. W.; Chang, E.; Sayes, C. M.; Drezek, R.; Colvin, V. L. Aqueous Dispersion of Monodisperse Magnetic Iron Oxide Nanocrystals through Phase Transfer. *Nanotechnology* **2006,** 17, (17), 4483-4487.

12. Boal, A. K.; Das, K.; Gray, M.; Rotello, V. M. Monolayer Exchange Chemistry of γ-Fe_2O_3 Nanoparticles. *Chem. Mater.* **2002,** 14, (6), 2628-2636.

13. Dennis, C. L.; Borges, R. P.; Buda, L. D.; Ebels, U.; Gregg, J. F.; Hehn, M.; Jouguelet, E.; Ounadjela, K.; Petej, I.; Prejbeanu, I. L.*, et al.* The Defining Length Scales of Mesomagnetism: A Review. *J. Phys.: Condens. Matter* **2002,** 14, (49), R1175-R1262.

14. Kim, D. K.; Zhang, Y.; Kehr, J.; Klason, T.; Bjelke, B.; Muhammed, M. Characterization and MRI Study of Surfactant-Coated Superparamagnetic Nanoparticles Administered into the Rat Brain. *J. Magn. Magn. Mater.* **2001,** 225, (1-2), 256-261.

15. Bradbury, A.; Menear, K.; O'Grady, K.; Chantrell, R. W. Magnetic Size Determination for Interacting Fine Particle Systems. *IEEE Trans. Magn.* **1984,** 20, (5), 1846-1848.

16. Chantrell, R. W.; Popplewell, J.; Charles, S. W. Measurements of Particle Size Distribution Parameters in Ferrofluids. *IEEE Trans. Magn.* **1978,** 14, (5), 975-977.

17. Bacri, J.-C.; Perzynski, R.; Salin, D.; Cabuil, V.; Massart, R. Magnetic Colloidal Properties of Ionic Ferrofluids. *J. Magn. Magn. Mater.* **1986,** 62, (1), 36-46.

CHAPTER 4

IN VITRO EXPERIMENTS WITH DENDRIMER-COATED IRON OXIDE NANOPARTICLES

4.1 Introduction

Having synthesized and characterized monodisperse, water-soluble magnetite nanocrystals protected by functionalized dendrimers, the composite particles' behavior was investigated *in vitro*. The main point of the investigation was to demonstrate folic acid receptor-mediated targeting of the devices. It was critical to show binding and/or internalization of complete devices by separately tracking properties unique to the dendrimer coatings and the iron oxide cores using two distinct but complementary methods and showing agreement between the results. In addition to providing the targeting moiety, the dendrimers were also functionalized with 6-TAMRA dye molecules for tracking by UV–visible fluorescence using flow cytometry analysis. The magnetite cores were tracked *via* elemental X-ray fluorescence from constituent iron atoms using a novel technique at Argonne National Lab (ANL): X-ray fluorescence (XRF) microscopy.

4.2 XRF Microscopy and Synchrotron Radiation

X-ray fluorescence spectroscopy employs X-radiation to liberate core-shell electrons from atoms in a sample and create vacancies in their electronic structures. Atoms are not stable in such states and will relax by various mechanisms. In the pathway

leveraged by XRF analysis, an electron from a higher orbital drops in energy to fill the vacancy. The energy difference is emitted in the form of an X-ray photon whose energy is characteristic of the emitting atom, and the total number of photons emitted is proportional to the atom's abundance in the sample. Therefore, a sample's elemental content can be quantitatively determined using an energy dispersive detector and counting the number of X-ray photons collected at signature energies. X-ray fluorescence microscopy is the application of this technique with high spatial resolution, employing an X-ray microbeam to sequentially excite minute regions the sample, collecting the emitted photons at each point, and using the data to generate maps of the spatial distribution of the elements composing the sample. Although XRF microscopy can, in principle, be performed using standard laboratory X-ray sources, the technique's utility is significantly enhanced using X-rays from a synchrotron, as the high brightness is needed to enable high spatial resolution combined with sufficient elemental sensitivity.[1]

4.2.1 Synchrotron Radiation and Its Production

Synchrotron radiation is emitted by charged particles moving at nearly light speed and undergoing transverse acceleration.[2] The phenomenon naturally occurs for all charged particles under such conditions, but it is generally induced for the purposes of scientific experimentation using electrons traveling in a storage ring. Electrons are chosen over heavier particles to maximize the radiated power since it varies as the inverse fourth power of the particle mass.[3]

Before reaching the storage ring, electrons must be liberated from a substance and accelerated to the appropriate speed. This is typically accomplished in two stages. The first stage employs a linear accelerator (linac): generally a cavity subjected to high-

frequency electromagnetic waves whose electric fields provide the accelerating force. Electrons are periodically injected in bunches into this cavity with a timing that ensures the electric field they experience is opposite their intended direction of travel.[3] Although this is an effective method, the cavity length that would be required to accelerate the electrons to their final desired speed is practically impossible to implement. So once the electrons leave the linear accelerator, they enter a device called a booster synchrotron in which they circulate until reaching the speed desired for the storage ring. The booster synchrotron consists of one or more radio-frequency (RF) cavities and magnets with adjustable field strength. As the electron bunches travel around the booster they emit electromagnetic radiation and thus lose energy. The RF cavities inject energy to negate these losses as well as provide a surplus that is added to the particles' kinetic energy. As the particles' speed periodically increases, the magnets' strength must be synchronously increased in proportion to this speed to keep the particles traveling on the same fixed path.[3] This situation is very similar to what occurs in the electrons' final destination: the storage ring. Bending magnets along the storage ring keep the particles moving along a fixed trajectory, but the RF cavities only impart enough energy to replace that which is lost as radiation.

Synchrotron radiation can be extracted along lines tangent to the storage ring parallel to the length of the bending magnet, but modern facilities are optimized for the use of insertion devices. Insertion devices (IDs) are arrays of magnets through which the electrons pass as they traverse the storage ring. Without producing any net deflection, IDs alter the beam's path while it is passing through for the enhanced production of synchrotron radiation. There are different kinds of IDs, but undulators are the most

important type for XRF microscopy applications. An undulator is a line of periodic array of electromagnets. The arrangement and strength of the magnets are engineered to force electrons traveling through the device to undergo numerous small-amplitude sinusoidal oscillations, thus emitting synchrotron radiation many times along its length. Constructive interference increases the brightness with a flux output theoretically proportional to the square of the number of oscillations.[4, 5] The brilliance of the emitted light—a parameter describing its intensity and directionality[6]—at its fundamental frequency is about 1000 times that of the output from a bending magnet.[7]

4.2.2 XRF Microscopy Using Synchrotron Radiation

Several of the key characteristics of synchrotron radiation, particularly from undulators, make it an ideal source of X-rays for trace elemental analysis of microscopic samples. Because the radiating electrons are moving at relativistic speeds, the electromagnetic energy they emit is concentrated into an extremely narrow cone that is tangent to the particles' path.[2] The resulting high directionality and high collimation afford a very brilliant beam that can deliver high photon flux to small sample areas;[1, 8] this is essential for successful practical application of the tecnhnique.[9, 10] Synchrotron X-ray beams also have quantitatively well-defined characteristics that facilitate the planning and execution of experiments and enhance their accuracy and sensitivity.[2, 8] Sensitivity is also improved by the nearly total linear polarization of the light in the orbital plane, which reduces the background of scattered X-rays in certain directions.[1, 8, 11] Scattering events are minimized along the direction of polarization whereas photoemission is isotropic, so the detector can be strategically placed for optimal results.

4.2.3 XRF Microscopy at Argonne National Lab (ANL)

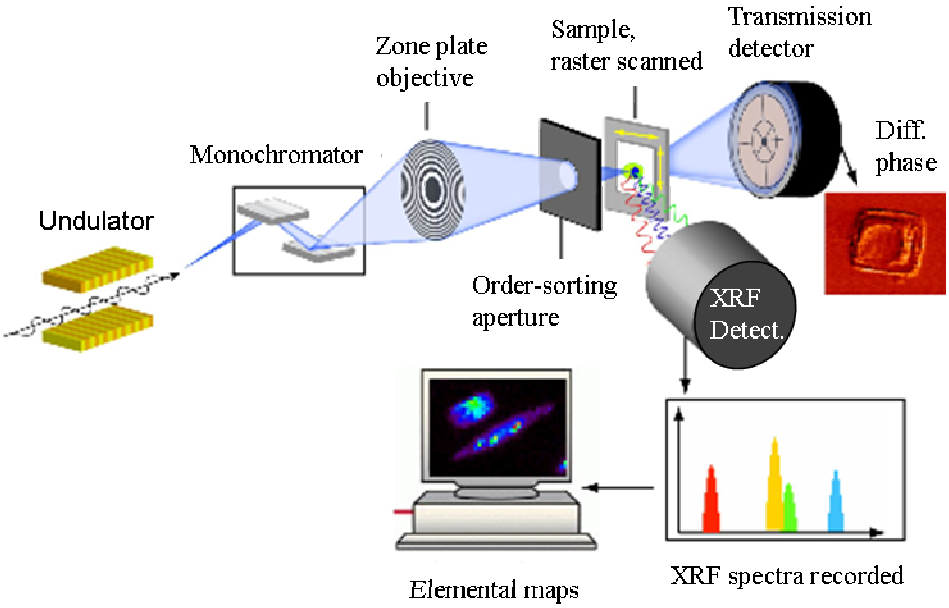

Figure 4.1 - A schematic of the experimental setup for X-ray fluorescence microscopy on beamline 2-ID-E at Advanced Photon Source, Argonne National Lab. Image courtesy of and used with permission of Dr. Stefan Vogt.

The storage ring at ANL is called the Advanced Photon Source (APS),[7] and the electrons it contains are generated by a hot cathode at 1100ºC.[12] The liberated electrons are first fed into a linac that brings them up to an energy of 450 MeV for injection into the booster synchrotron.[12] The electrons leave the booster and enter the storage ring with an energy ~7 GeV.[13] There are many straight sections along the ring that are fitted with insertion devices; the synchrotron radiation that is emitted along the length of these sections is allowed to leave the storage ring and pass to stations called beamlines where experiments are conducted. A typical experimental setup for XRF microscopy on beamline 2-ID-E and its key components are displayed in Figure 4.1.[14] Electrons in the storage ring pass through an undulator to generate a beam of synchrotron radiation that is monochromatized at the front end of the beamline so it can be focused by the zone plate.

To minimize noise from any unfocused light, the beam is further refined using an order-sorting aperture that only passes focused X-rays.[14] The beam finally illuminates the sample at a spot size around 0.15 μm^2, exciting atoms of the sample's constituent elements in a microscopic area to produce a spectrum of fluorescent X-rays that are detected and analyzed. This process is repeated for the entire region of interest as precision stepper motors move the sample so that different areas are irradiated. Data acquired for a range of elements over the entire region of interest are ultimately recombined to generate elemental maps.

4.3 Reagents and Materials

Reagents were used as obtained from commercial sources. ProLong Gold with DAPI was from Molecular Probes, Inc. (Eugene, OR). Epithelial cancer cells of the KB line were obtained from American Type Culture Collection (ATCC; Rockville, MD); Dr. J. Mulé at the University of Michigan kindly proffered the head and neck squamous cell carcinoma line, UM-SCC-38.[15] Cell culture media, antibiotics, and supplies were purchased from Gibco BRL (Gaithersburg, MD).

4.4 Methods

4.4.1 Cell Culture

Human epidermoid carcinoma cells (KB) and squamous carcinoma cells (UM-SCC-38) were maintained at 37°C and 5% CO_2 in RPMI 1640 media supplemented with 10% heat-inactivated fetal bovine serum (FBS) and 1% penicillin/streptomycin. While the UM-SCC-38 cells were maintained in folate-rich media, the KB cell batch was cultured as two distinct populations by growing one half of the batch in folate-rich media

and the other half in folate-deficient media. Although KB cells express the folate receptor in normal media (KB-FAR), the receptor density increases on cells grown in environments with low folic acid concentration (KB-FAR+, upregulated).[16-19] To study the targeting capabilities of the dendrimer-coated magnetic nanoparticles, KB-FAR, KB-FAR+, and UM-SCC-38 cells were seeded in 24-well plates with 500 μL of serum-free media and allowed to grow into a monolayer over a 48-hour period. The neat media were aspirated and replaced by 200 μL media with dendrimer-coated nanoparticle concentrations of 50, 100 and 200 nM in separate wells for 24-hour incubation; 200 nM G5-Ac(102)-FA(5)-6T(3) served as the control. Wells for KB-FAR were supplemented with folic acid at a final concentration of 40 μM; blocking studies of KB-FAR+ by free folate were conducted *via* 15-minute pre-incubation at the same concentration. One-hour incubation was performed the next day using an identical setup on the other halves of the same plates such that the cells from both conditions could be simultaneously harvested. Every condition for the two time points had two replicates: one for flow analysis and the other for iron content measurements. Once incubation was complete, the media were aspirated; the cells were rinsed twice with phosphate-buffered saline (PBS) and were detached by incubating in trypsin-EDTA for 15 minutes. The content of each well was collected in a separate flow tube with complete media being added to halt trypsin's enzymatic activity. The resulting suspensions were then centrifuged for 5 minutes at 2000 rpm to form cell pellets. After aspirating the supernatants, 500 μL fresh PBS was added to each tube, and the tubes were agitated to form suspensions before repeating centrifugation. Each tube's supernatant was aspirated, and 500 μL of a 2% buffered paraformaldehyde solution was added to each pellet to fix the cells. The pellets were

agitated into suspension and allowed to sit for 15 minutes before centrifugation. Aspiration, PBS washing, and centrifugation were performed twice before ultimately suspending the fixed cells in 500 μL neat PBS.

4.4.2 Flow Cytometry

Flow cytometry was conducted at the University of Michigan Cancer Center (Ann Arbor, MI) on a FACSDiVa high-speed cell sorter (Becton, Dickinson & Co.; Franklin Lakes, NJ) using an argon laser to excite the 6-TAMRA labels. Cell samples were prepared for analysis as already described.

4.4.3 Confocal Microscopy

KB KB-FAR+ cells were plated in glass-bottomed Petri dishes with folate-deficient media. Each dish's media were aspirated and replaced by 500 μL of the appropriate concentration of DC-SPIONs or G5-Ac(102)-FA(5)-6T(3) in serum-free media. Incubation was conducted for 1 hour at 37ºC. All media were aspirated; the cells were washed twice with 1 mL of PBS and then fixed by incubation in 1 mL 2% buffered paraformaldehyde for 10 minutes at room temperature. Aspiration and PBS washing were again conducted twice. After aspirating the final PBS wash, ProLong Gold—an antifade reagent with DAPI to stain nuclei—was added. Confocal experiments were conducted on a Zeiss LSM 510 confocal microscope using a C-Apochromat 63x objective with a 1.2 NA and water immersion. Each image includes a color layer of red fluorescence from the 6-TAMRA, blue fluorescence from the DAPI, and differential interference contrast (DIC) of all cells in view. 6-TAMRA images were acquired using HeNe laser excitation at 543nm, with emission detected at wavelengths >560nm. DAPI

images were acquired using Ar laser excitation at 364nm, with emission detected at wavelengths between 385 and 470nm.

4.4.4 X-ray Fluorescence (XRF) Microscopy

Cell samples for elemental analysis were prepared on silicon nitride (Si_3N_4) windows (membrane thickness: 500 nm; Silson Ltd.; Blisworth, Northampton, England). A drop of fixed cells suspended in PBS was deposited on the window and allowed to dry in a biological safety cabinet. Several water rinses were then conducted to remove salt crystals remaining from the evaporated buffer since the crystals make it difficult to locate target cells in addition to raising the background level of fluorescent X-rays.[9] After thoroughly drying, the Si_3N_4 windows were collected and placed into a desiccator for storage and transportation to the Advanced Photon Source (APS; Argonne, IL). Once at the APS the windows were mounted on kinematic sample holders. Cells of interest were located on the Si_3N_4 windows using a visible light microscope (Leica DMXRE; Leica Microsystems; Wetzlar, Germany) equipped with a motorized, high-precision *x*/*y*-stage (Ludl Bioprecision; Hawthorne, NY). The cells were selected from random locations on the silicon nitride windows and inspected to verify that they had remained intact during sample preparation. Any burst cells were eliminated as candidates for XRF analysis. Another cell was then randomly selected and observed for integrity until the desired total was reached. It should be noted that there are no evident morphological differences between cells with high iron content versus cells with low iron content. Specimen positions were recorded and used to locate the same cells for elemental analysis *via* X-ray fluorescence on the 2-ID-E beamline at the APS. Samples were illuminated with a 10 keV X-ray beam focused to a 0.3 μm x 0.5 μm spot using Fresnel zone plates (Xradia;

Concord, CA). X-ray fluorescence corresponding to elements with atomic number Z = 13 (Al) through Z = 30 (Zn) was detected using an Ultra-LEGe energy dispersive Ge-detector (Be window thickness: 24 μm; single-element area: 100 mm^2; Canberra; Meriden, CT) as the sample was raster-scanned through the beam spot. A complete X-ray fluorescence spectrum was acquired at every scan position for subsequent processing. Elemental concentrations were calculated using thin-film samples NBS-1832 and NBS-1833 from the National Institute of Standards and Technology (NIST; Gaithersburg, MD) as calibration standards. MAPS software—developed by Stefan Vogt and Martin de Jonge—was used to evaluate all acquired spectra, produce elemental maps, and calculate iron content per cell.[20]

4.5 Results and Discussion

4.5.1 KB Cells

KB cells are a human epidermoid carcinoma having a variable level of expression of receptors for the vitamin, folic acid (FA). This variation can be induced by simply varying the concentration of FA in the cells' growth media and allowing time for the cells to adjust. Normal KB cells (KB-FAR) have a minimal expression of the folic acid receptor when maintained in FA-rich media. However, the cells will upregulate their folic-acid-receptor expression when starved of the vitamin.[16-19] They overexpress the receptor (KB-FAR+) to increase their chances of proliferation. With less FA available in their environment due to its lower presence, competition for the vitamin with other cells, or some combination of factors, KB cells are more likely to survive by enhancing folic-acid-receptor expression. It is interesting to note that the process is dynamic and

reversible: normal KB cells can be programmed to upregulate and returned to normal repeatedly by appropriately adjusting the presence of FA in their growth media. These properties make the KB line ideal for use as a tumor model to assess folic-acid-mediated targeting; that is why they were used in this study and in other work done by our group.

4.5.2 UM-SCC-38 Cells

UM-SCC-38 is a squamous cell carcinoma line developed at the University of Michigan that does not express folic acid receptors.[15] Therefore, it provides a useful negative control—in addition to normal KB cells—to elucidate the intrinsic binding of DC-SPIONs.

4.5.3 Fluorescence Data

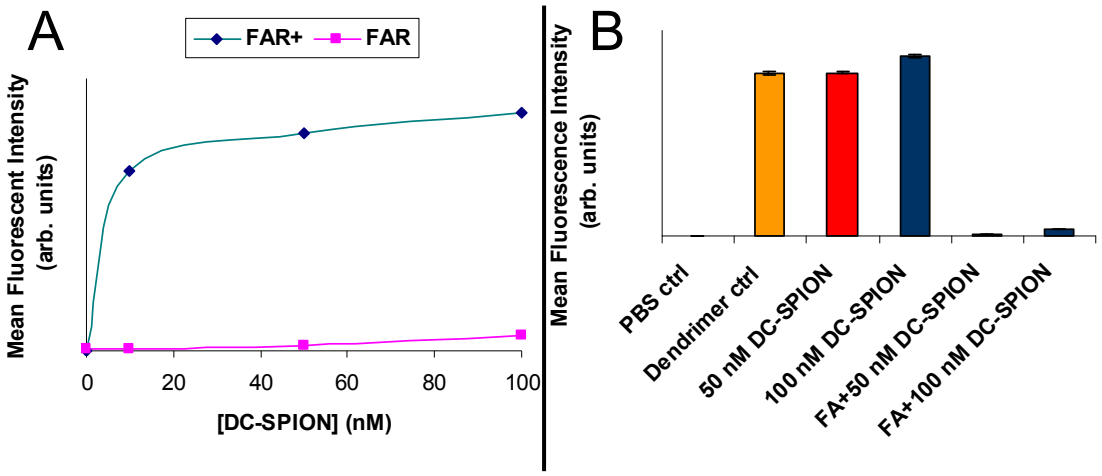

Figure 4.2 - Flow cytometry data for KB cells incubated with DC-SPIONs and the corresponding controls. Error bars indicate the standard error of the mean. Panel (A) shows binding saturation for KB-FAR+ cells with DC-SPIONs and a slight increase in nonspecific binding for KB-FAR cells over the concentration range. Data in panel (B) implicate the folate receptor as the binding mediator since cells incubated with free folic acid before DC-SPION addition exhibit significantly reduced fluorescence. Free folic acid added in large excess occupies the cells' receptors for the vitamin and thus inhibits subsequent cell interaction with DC-SPIONs.

The 6-TAMRA dye molecules present in the DC-SPIONs were used to track particle association with the KB cells over various experimental conditions. Samples were sorted using flow cytometry, and data among groups were compared to investigate receptor-mediated targeting of the devices. The results shown in Figure 4.2A demonstrate successful targeted binding and/or uptake of the devices as the fluorescence intensity is much higher for KB-FAR+ than for KB-FAR. The saturation seen for KB-FAR+ also suggests site-specific binding versus non-specific interactions. Similar saturation data were previously observed for the FA-targeted dendrimers alone.[18, 21, 22] The internal dendrimer control for the current experiments, consisting of G5-Ac(102)-FA(5)-6T(3), showed identical behavior to the DC-SPIONs (Figure 4.2B). Data from the blocking studies (Figure 4.2B) confirm site-specific binding and clearly implicate the folate receptor as the means of cell-particle interaction. A vast excess of free folic acid in the growth media prior to treatment with DC-SPIONs occupies the KB cells' FA receptors, thus inhibiting interaction with the FA ligands. The role of FA-receptor targeting was further explored by conducting a comparative study using the KB cell line and a cell line that does not express FA receptors, UM-SCC-38.[15] The KB-FAR+ cells showed a 5.7-fold increase in mean fluorescence whereas the UM-SCC-38 cells showed no increase in mean fluorescence.

4.5.4 Iron Content Analysis

XRF microscopy was used to determine cellular iron content and to confirm that targeting of the DC-SPIONs caused enhanced binding and/or uptake of iron into the cells as opposed to only binding and/or uptake of the dendrimers themselves. The mean data for 17 cells in each group are summarized in Figure 4.3. KB-FAR+ cells clearly had the

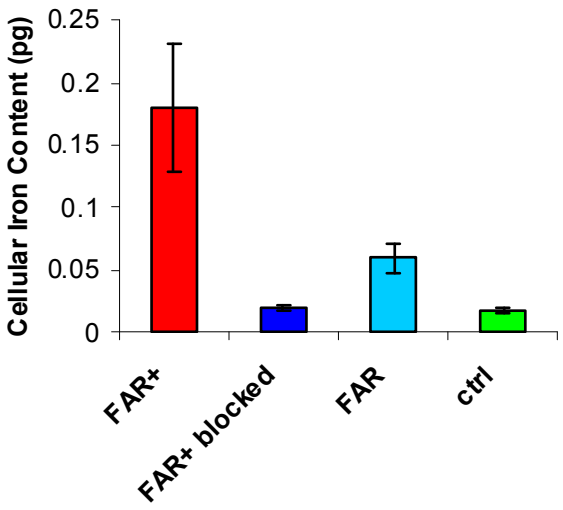

Figure 4.3 - Average cellular iron content as determined by XRF microscopy for different samples. Error bars indicate the standard error of the mean. The largest amount of DC-SPIONs was clearly delivered to KB-FAR+ cells. As expected from the flow cytometry data, KB-FAR cells exhibited significantly lower iron content than KB-FAR+ cells although the level was higher than that of KB-FAR+ blocked cells and the blank control. Statistical analysis using Mann-Whitney U tests showed the iron contents of the KB-FAR+ and KB-FAR+ blocked populations and the KB-FAR+ and control populations to be significantly different with 99% confidence. Similarly, the iron contents of the KB-FAR+ and KB-FAR populations are significantly different with 80% confidence. Taken together, these data demonstrate targeting mediated by the folic acid receptor of the DC-SPIONs to tumor cells.

highest iron loading while KB-FAR+ blocked and the blank control were the lowest and exhibited identical content to within experimental error. One picogram of iron translates to approximately 10^6 particles and—assuming a cell volume of 3.5 pL—a corresponding average cellular concentration of ~475 nM particles or ~5 mM Fe. For the 50 nM KB-FAR+ DC-SPION condition this means that between 5 and 10% of the available iron as nanoparticles was bound to or taken up by the cells.

In this study, I report on two methods for measuring the uptake of the DC-SPIONs into the cells and quantification at the individual cell level in both cases. Receptor-mediated targeting of DC-SPIONs is strongly supported by both iron XRF

microscopy and 6-TAMRA fluorescence. Details for the entire collection of cells analyzed using XRF microscopy are shown in Figure 4.4. A striking aspect of this figure is the large degree of variation in iron content per cell. However, this degree of variation

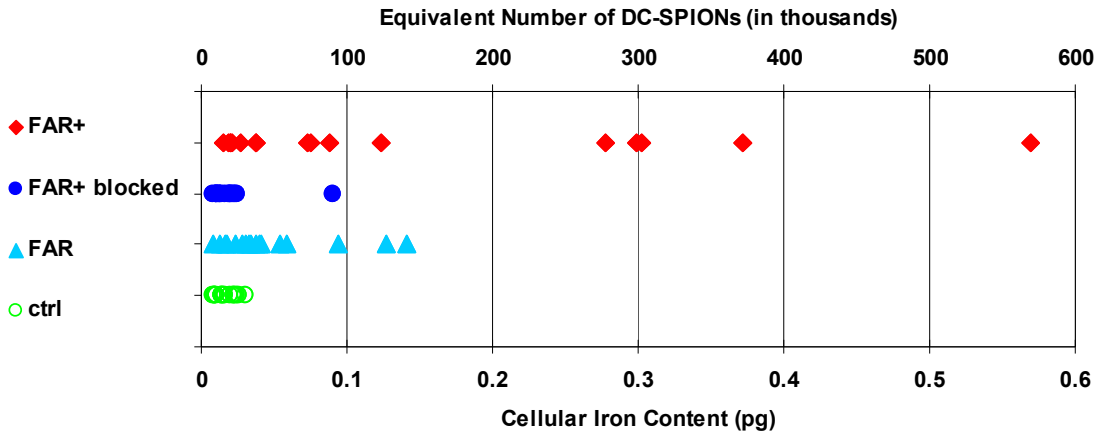

Figure 4.4 - Iron content for the 17 cells from each experimental group of 50 nM DC-SPION incubation analyzed by XRF microscopy. The primary abscissa (bottom) shows actual iron content in picograms, while the secondary abscissa (top) depicts the equivalent number of DC-SPIONs corresponding to a given mass of iron. There are about 10^6 DC-SPIONs in one picogram of iron. The amount of native iron in the untreated controls corresponds to an average of 10^4 DC-SPIONs.

is consistent with the distribution of uptake measured for the large populations of cells by flow cytometry as shown in Figure 4.5. Although direct comparisons between XRF microscopy and flow cytometry data are obfuscated by several factors, it is still useful to numerically express and analyze the widths of the data distributions observed from these two techniques in this study to at least illustrate qualitative similarities in their variations. The range of the average values for uptake as measured by fluorescence intensity is typically given as the standard error of the mean (SEM). For the data reported in Figure 4.5 this yields 2400 ± 20 (0.83% relative SEM, n = 9385) and 2400 ± 20 (0.83% relative

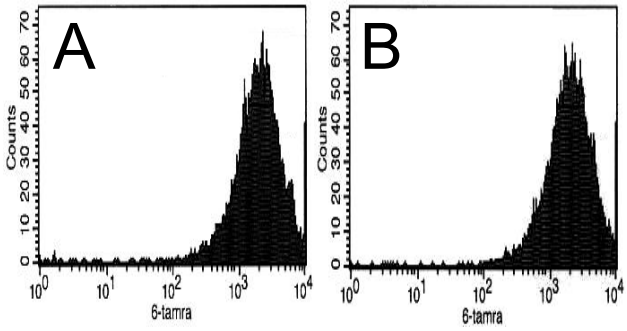

Figure 4.5 - Flow cytometry data distributions for G5-Ac(102)-FA(5)-6T(3) alone (A) and for the same dendrimers coupled to magnetite nanoparticles, DC-SPION (B). Note that the abscissa is a log scale for 6-TAMRA fluorescent intensity, and the ordinate is a linear scale for counts. The distributions are quantitatively identical and reveal a large variation in binding through their ~75% relative standard deviations.

SEM, n = 9324) for the targeted dendrimer alone and for the DC-SPIONs, respectively. However, considering the standard deviations (SD) of these data one obtains 2400 ± 1800 (75% relative SD) and 2400 ± 1800 (75% relative SD). The relative SEM and relative SD for the DC-SPIONs from the flow data can be compared to that obtained by XRF microscopy for the 17 KB-FAR+ cells, which are 28% (180 ± 50 fg Fe/cell) and 100% (200 ± 200 fg Fe/cell), respectively. The elevated values for the SEM and SD for the XRF microscopy experiments versus the flow cytometry experiments are attributable to the much smaller number of cells measured by this method as compared to flow cytometry. Non-parametric methods are required for statistical analysis since my samples are small and fail both the F-test for equal variances and the Shapiro-Wilks test for normality. Using Mann-Whitney U tests reveals that the KB-FAR+ population's iron content is significantly different from those of the KB-FAR+ blocked, KB-FAR, and control populations with 99%, 80%, and 99% confidence, respectively.

Mindful of the data distribution, it is interesting to compare representative XRF microscopy images (iron maps) for cells from each population as depicted in Figure 4.6.

Hot spots—localized masses of iron—that are substantially greater than the cell's inherent iron content are evident in the upregulated cells (Figure 4.6A). All upregulated cells with high nanoparticle content display these hot spots whereas similar KB-FAR+ blocked (Figure 4.6B) and KB-FAR (Figure 4.6C) cells show less localized distributions.

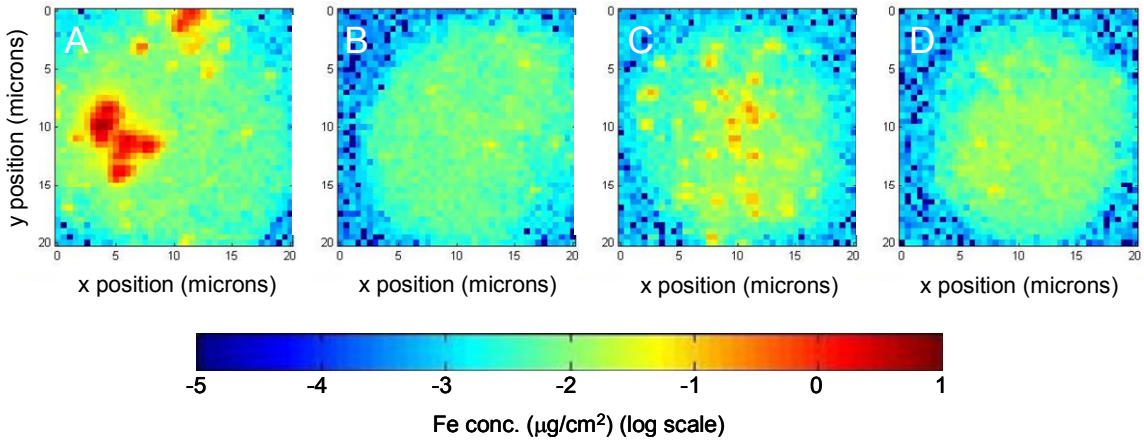

Figure 4.6 - Representative false-color XRF microscopy images showing iron content for a KB cell from each of four populations: (A) KB-FAR+ with 50nM DC-SPIONs, (B) KB-FAR+ with 50nM DC-SPIONs + free FA, (C) KB-FAR with 50nM DC-SPIONs, and (D) untreated control. All incubations were for 1 h. The qualitative feature of localized points of high iron concentration in (A) is obvious; these pockets overwhelm the signal from the cell's endogenous iron background.

With an average of 60 molecules of 6-TAMRA per DC-SPION and 10^6 DC-SPIONs per picogram of iron, the amount of iron in these cells corresponds to several million 6-TAMRA molecules, which is well above the estimated optical detection threshold of 10^4 dye molecules. Furthermore, the punctate distribution of iron observed in the high-iron KB-FAR+ cells is similar to the clustering of fluorescence seen in the central-slice confocal microscopy images (Figure 4.7) and suggests DC-SPIONs are contained within intracellular vesicles.[23] Additional evidence for internalization is provided *via* analysis revealing a high autocorrelation between zinc and iron. This is significant since zinc is a

transition metal typically associated with the clathrin-coated pits that are part of the receptor-mediated endocytosis pathway.[24] Furthermore, analysis of z-stack confocal microscopy images for 50 nM DC-SPIONs (Figure 4.8, column A) and 100 nM G5-Ac(102)-FA(5)-6T(3) (Figure 4.8, column B) shows that the majority of the fluorescence from the nanoparticles occurs in the middle of the cells versus their tops or bottoms. Thus both G5-Ac(102)-FA(5)-6T(3) alone and the composite DC-SPIONs are undoubtedly internalized by the cells.

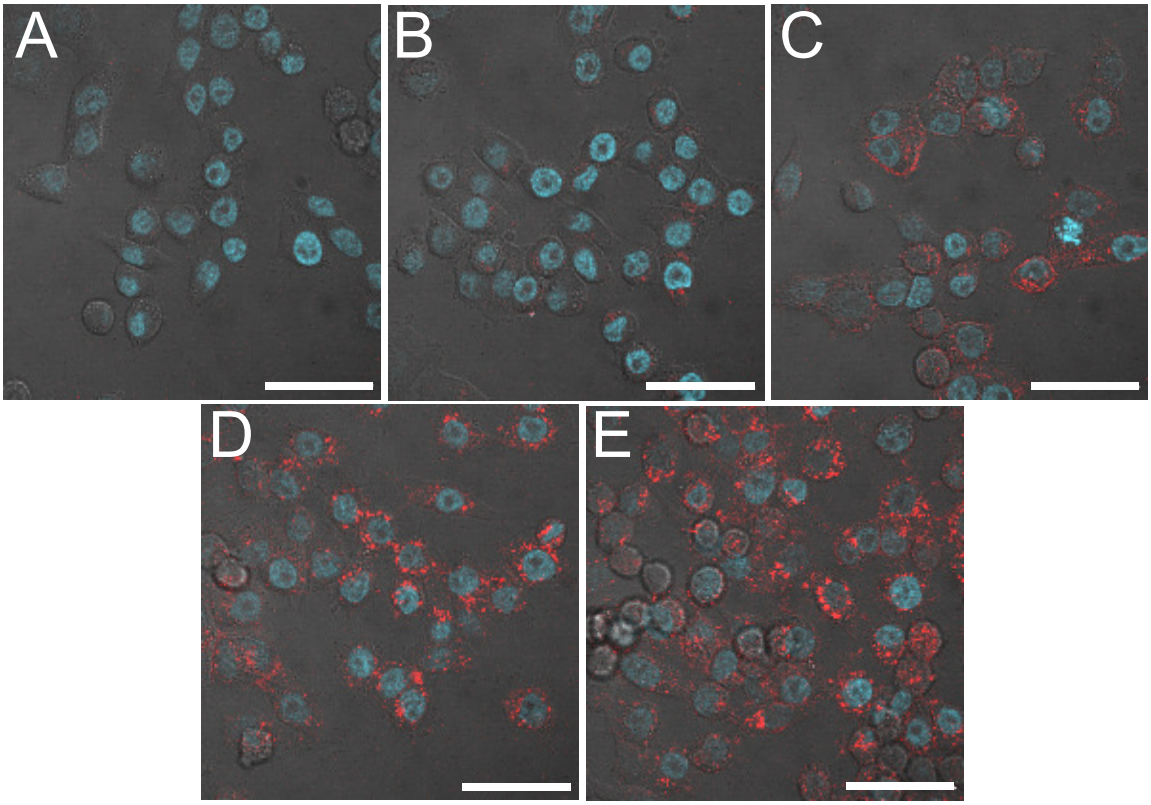

Figure 4.7 - Confocal microscopy images of five experimental conditions demonstrating internalization of DC-SPIONs; scale bars are 40 μm. All images are for KB cells after 1 h incubation at 37ºC. Nuclei are visible in blue due to DAPI staining; red fluorescence comes from the 6-TAMRA dye conjugated to neat dendrimers and dendrimers on the surface of DC-SPIONs. The PBS control for KB-FAR+ (A) shows only background fluorescence, and the KB-FAR+ blocked sample (B) exhibits a signal just slightly above this background. Whereas the signal for neat G5-Ac(102)-FA(5)-6T(3) with KB-FAR+ (C) is largely concentrated on the cells' exteriors, the fluorescence for 50 nM (D) and 100 nM (E) DC-SPIONs is clearly intracellular and appears in clusters, correlating nicely with the XRF microscopy data for iron. Images taken by Christopher V. Kelly.

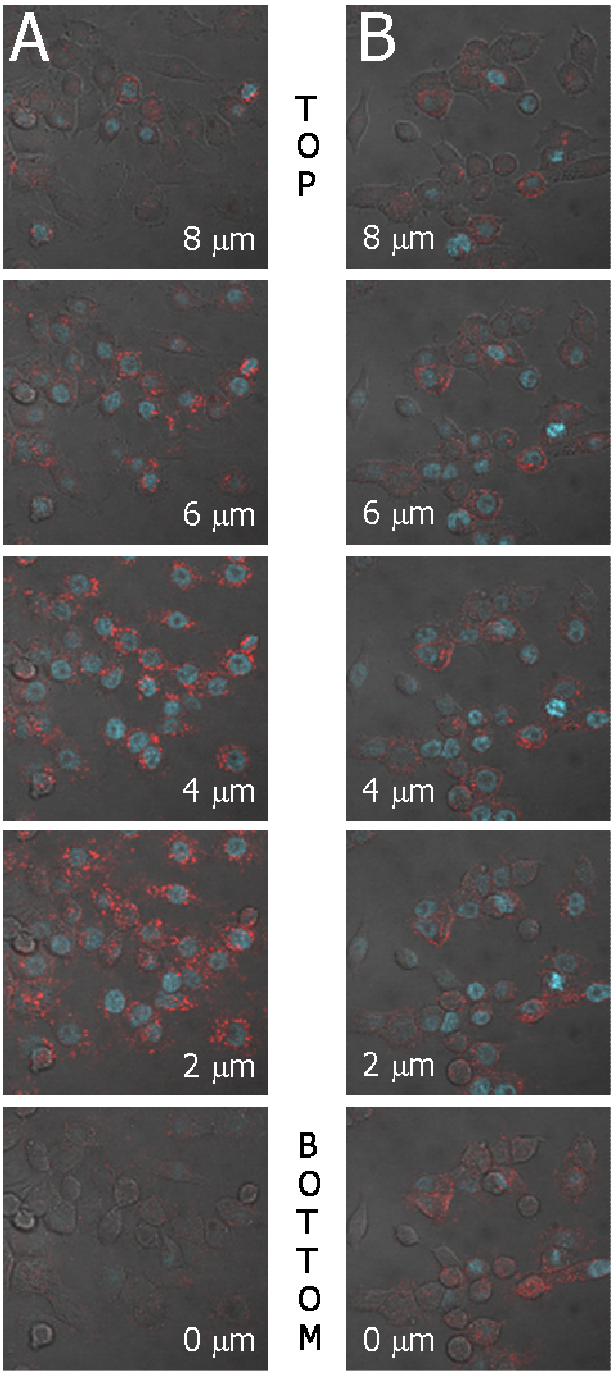

Figure 4.8 - Confocal microscopy z-stacks depicting internalization of 50 nM DC-SPIONs (column A); the positive control using neat 100 nM G5-Ac(102)-FA(5)-6T(3) is also shown for comparison (column B). Slices were taken from the sample dish surface (BOTTOM) to the top of the cellular monolayer (TOP); consecutive images in each column are separated by 2 microns. The enhanced fluorescence for the 50 nM DC-SPIONs seen in the middle of the stack shows that the majority of them are within the cells versus bound to the surfaces. Images taken by Christopher V. Kelly.

The data presented in this thesis employing DC-SPIONs provide a unique perspective on uptake distribution because iron is quantified on the cellular level and correlated to the entire population of cells characterized by flow cytometry. Previous publications on the topic of targeted delivery of iron oxide particles report intracellular iron content based on acid digestion of bulk samples and subsequent analysis by inductively coupled plasma optical emission spectroscopy (ICP-OES),[25-29] atomic emission spectroscopy (AES),[30] or colorimetric assay.[31] The reported values vary widely. Kresse and co-workers indicate uptake of around 2.8 pg Fe/cell for SPIONs targeted to human epidermoid carcinoma cells (A 431) using the iron chelating protein, transferrin, following 2 hours of incubation.[30] Leuschner and collaborators report approximately 150 pg Fe/cell after 30 minutes of incubating genetically modified human breast cancer cells (MDA-MB-435S) with SPIONs at a concentration of 0.3 mg Fe/mL; the particles accomplished specific binding *via* luteinizing hormone releasing hormone (LHRH) moieties grafted on their surfaces.[31] Finally, Zhang *et al*. have targeted SPIONs using methotrexate (MTX), yielding about 43, 35, and 70 pg Fe/cell for 9L glioma, human cervical adenocarcinoma (HeLa), and human breast cancer cells (MCF-7), respectively, after 2 hours of incubation.[25, 26] They have also employed folic acid as a ligand to target SPIONs to HeLa and BT20 cells. Uptake of approximately 1.4 pg Fe/cell was achieved for HeLa cells after 4 hours of incubation.[27] The first study for BT20 cells showed up to 85 pg Fe/cell after 4 days, while subsequent work yielded around 700 pg Fe/cell over the same period.[28, 29] The above set of previously published measurements all characterize iron uptake as an average quantity for a bulk population of cells. I have shown in this research that iron uptake per cell actually varies widely, as would be expected for a FA-

targeted system.[17, 18, 22, 32] It will be of interest for future studies to see if variation in uptake for magnetic contrast agents is a common behavior for agents targeted to receptors involved in endocytosis.

4.6 References

1. Adams, F.; Vincze, L.; Vekemans, B., Synchrotron Radiation for Microscopic X-Ray Fluorescence Analysis. In *X-Ray Spectrometry: Recent Technological Advances*, Tsuji, K.; Injuk, J.; van Grieken, R., Eds. Wiley: Chichester, West Sussex, England, 2004; pp 344-353.

2. Koch, E.-E.; Eastman, D. E.; Farge, Y., Synchrotron Radiation – a Powerful Tool in Science. In *Handbook on Synchrotron Radiation*, Koch, E.-E., Ed. Elsevier: New York, NY, 1983; Vol. 1A, pp 1-63.

3. Brefeld, W.; Gürtler, P., Synchrotron Radiation Sources. In *Handbook on Synchrotron Radiation*, Ebashi, S.; Koch, M.; Rubenstein, E., Eds. Elsevier: New York, NY, 1991; Vol. 4, pp 271-296.

4. Ortiz, W. A. Wigglers and Undulators as Synchrotron Radiation Sources. In *Synchrotron Light: Applications and Related Instrumentation*, Proceedings of the I Workshop, Teaneck, NJ, 1989; Craievich, A., Ed. World Scientific: Teaneck, NJ, 1989; pp 15-23.

5. Weihreter, E., Basic Design Considerations for Compact Storage Ring. In *Compact Synchrotron Light Sources*, Series on Synchrotron Radiation Techniques and Applications; World Scientific: River Edge, NJ, 1996; Vol. 3, pp 27-48.

6. Insertion Devices & Brilliance | Advanced Photon Source. http://aps.anl.gov/About/APS_Overview/insertion_devices.html (accessed April 13, 2008).

7. Watanabe, M.; Isoyama, G., New Synchrotron Radiation Sources. In *X-Ray Spectrometry: Recent Technological Advances*, Tsuji, K.; Injuk, J.; Grieken, R. v., Eds. Wiley: Chichester, West Sussex, England, 2004; pp 29-47.

8. Iida, A.; Gohshi, Y., Trace Element Analysis by X-Ray Fluorescence. In *Handbook on Synchrotron Radiation*, Ebashi, S.; Koch, M.; Rubenstein, E., Eds. Elsevier: New York, NY, 1991; Vol. 4, pp 309-348.

9. Twining, B. S.; Baines, S. B.; Fisher, N. S.; Maser, J.; Vogt, S.; Jacobsen, C.; Tovar-Sanchez, A.; Sañudo-Wilhelmy, S. A. Quantifying Trace Elements in Individual Aquatic Protist Cells with a Synchrotron X-Ray Fluorescence Microprobe. *Anal. Chem.* **2003,** 75, (15), 3806-3816.

10. Paunesku, T.; Vogt, S.; Maser, J.; Lai, B.; Woloschak, G. X-Ray Fluorescence Microprobe Imaging in Biology and Medicine. *J. Cell. Biochem.* **2006,** 99, (6), 1489-1502.

11. Yun, W.; Ice, G., X-Ray Microbeam and Microscopy Techniques with Hard X-Rays. In *Third-Generation Hard X-Ray Synchrotron Radiation Sources: Source*

Properties, Optics, and Experimental Techniques, Mills, D. M., Ed. Wiley: New York, NY, 2002; pp 125-177.

12. Linear Accelerator | Advanced Photon Source. http://aps.anl.gov/About/APS_Overview/linac.html (accessed April 13, 2008).

13. Booster Synchrotron | Advanced Photon Source. http://aps.anl.gov/About/APS_Overview/booster.html (accessed April 13, 2008).

14. Vogt, S. X-Ray Fluorescence Mapping. http://www.aps.anl.gov/Xray_Science_Division/Xray_Microscopy_and_Imaging/Science_and_Research/Techniques/Xray_Fluorescence_Mapping/index.html (accessed April 13, 2008).

15. Myc, A.; Majoros, I. J.; Thomas, T. P.; Baker, J. R., Jr. Dendrimer-Based Targeted Delivery of an Apoptotic Sensor in Cancer Cells. *Biomacromolecules* **2007,** 8, (1), 13-18.

16. Ross, J. F.; Chaudhuri, P. K.; Ratnam, M. Differential Regulation of Folate Receptor Isoforms in Normal and Malignant Tissues in Vivo and in Established Cell Lines. Physiologic and Clinical Implications. *Cancer* **1994,** 73, (9), 2432-2443.

17. Baker, J. R., Jr.; Quintana, A.; Piehler, L.; Banaszak Holl, M.; Tomalia, D.; Raczka, E. The Synthesis and Testing of Anti-Cancer Therapeutic Nanodevices. *Biomed. Microdevices* **2001,** 3, (1), 61-69.

18. Thomas, T. P.; Majoros, I. J.; Kotlyar, A.; Kukowska-Latallo, J. F.; Bielinska, A.; Myc, A.; Baker, J. R., Jr. Targeting and Inhibition of Cell Growth by an Engineered Dendritic Nanodevice. *J. Med. Chem.* **2005,** 48, (11), 3729-3735.

19. Leamon, C. P.; Low, P. S. Delivery of Macromolecules into Living Cells: A Method That Exploits Folate Receptor Endocytosis. *Proc. Natl. Acad. Sci. U.S.A.* **1991,** 88, (13), 5572-5576.

20. Vogt, S. Maps: A Set of Software Tools for Analysis and Visualization of 3D X-Ray Fluorescence Data Sets. *J. Phys. IV* **2003,** 104, 635-638.

21. Hong, S.; Leroueil, P. R.; Majoros, I. J.; Orr, B. G.; Baker, J. R., Jr.; Banaszak Holl, M. M. The Binding Avidity of a Nanoparticle-Based Multivalent Targeted Drug Delivery Platform. *Chem. Biol.* **2007,** 14, (1), 107-115.

22. Quintana, A.; Raczka, E.; Piehler, L.; Lee, I.; Myc, A.; Majoros, I.; Patri, A. K.; Thomas, T.; Mulé, J.; Baker, J. R., Jr. Design and Function of a Dendrimer-Based Therapeutic Nanodevice Targeted to Tumor Cells through the Folate Receptor. *Pharm. Res.* **2002,** 19, (9), 1310-1316.

23. Dubé, D.; Francis, M.; Leroux, J. C.; Winnik, F. M. Preparation and Tumor Cell Uptake of Poly(N-Isopropylacrylamide) Folate Conjugates. *Bioconjugate Chem.* **2002,** 13, (3), 685-692.

24. Remacle, A.; Murphy, G.; Roghi, C. Membrane Type I-Matrix Metalloproteinase (MT1-MMP) Is Internalised by Two Different Pathways and Is Recycled to the Cell Surface. *J. Cell Sci.* **2003,** 116, (19), 3905-3916.

25. Kohler, N.; Sun, C.; Fichtenholtz, A.; Gunn, J.; Fang, C.; Zhang, M. Methotrexate-Immobilized Poly(ethylene glycol) Magnetic Nanoparticles for MR Imaging and Drug Delivery. *Small* **2006,** 2, (6), 785-792.

26. Kohler, N.; Sun, C.; Wang, J.; Zhang, M. Methotrexate-Modified Superparamagnetic Nanoparticles and Their Intracellular Uptake into Human Cancer Cells. *Langmuir* **2005,** 21, (19), 8858-8864.

27. Sun, C.; Sze, R.; Zhang, M. Folic Acid-PEG Conjugated Superparamagnetic Nanoparticles for Targeted Cellular Uptake and Detection by MRI. *J. Biomed. Mater. Res., Part A* **2006,** 78A, (3), 550-557.

28. Zhang, Y.; Kohler, N.; Zhang, M. Surface Modification of Superparamagnetic Magnetite Nanoparticles and Their Intracellular Uptake. *Biomaterials* **2002,** 23, (7), 1553-1561.

29. Zhang, Y.; Sun, C.; Kohler, N.; Zhang, M. Self-Assembled Coatings on Individual Monodisperse Magnetite Nanoparticles for Efficient Intracellular Uptake. *Biomed. Microdevices* **2004,** 6, (1), 33-40.

30. Kresse, M.; Wagner, S.; Pfefferer, D.; Lawaczeck, R.; Elste, V.; Semmler, W. Targeting of Ultrasmall Superparamagnetic Iron Oxide (USPIO) Particles to Tumor Cells in Vivo by Using Transferrin Receptor Pathways. *Magn. Reson. Med.* **1998,** 40, (2), 236-242.

31. Leuschner, C.; Kumar, C.; Hansel, W.; Soboyejo, W.; Zhou, J.; Hormes, J. LHRH-Conjugated Magnetic Iron Oxide Nanoparticles for Detection of Breast Cancer Metastases. *Breast Cancer Res. Treat.* **2006,** 99, (2), 163-176.

32. Patri, A. K.; Myc, A.; Beals, J.; Thomas, T. P.; Bander, N. H.; Baker, J. R., Jr. Synthesis and in Vitro Testing of J591 Antibody-Dendrimer Conjugates for Targeted Prostate Cancer Therapy. *Bioconjugate Chem.* **2004,** 15, (6), 1174-1181.

CHAPTER 5

CONCLUSIONS

5.1 Overview

The progression of clinical medicine toward earlier detection and treatment of disease and perhaps even its prevention requires developing new techniques or refining or supplementing current technology. Magnetic resonance imaging (MRI), currently one of the most ubiquitous and powerful contemporary diagnostic methods,[1-4] is anticipated to be a primary tool in realizing the objectives of this new paradigm.[5, 6] It is a noninvasive, tomographic technique, without the hazards of ionizing radiation, that provides anatomical and physiological data from deep within the body through three-dimensional images with nearly microscopic resolution.[5, 7-10] Although it was originally hoped that MRI would be able to accomplish early detection when used unaided, it soon became obvious that its sensitivity is too low when relying upon inherent contrast mechanisms within the body.[2-4, 11] This prompted the development of contrast agents, such as chelated paramagnetic ions and the more recent advent of superparamagnetic particles, particularly nanoscale iron oxides.

Superparamagnetic iron oxide nanoparticles (SPIONs) supersede the paramagnetic chelates in many ways. They have been shown to naturally occur in many animals and are currently the only inorganic particulate contrast agents approved for *in vivo* human applications; more formulations are now in Phase-III trials.[4, 12, 13] Iron oxides

are biodegradable and exhibit neither acute nor chronic toxicity.[14-17] SPIONs have a large contrast effect per metal center,[18] so they are able to generate sufficient contrast in low doses versus their paramagnetic counterparts: nM SPIONs (μM Fe) versus mM Gd.[16, 19, 20] Furthermore, the body has established methods to metabolize the excess iron introduced by the particles.[15, 18, 21-24]

SPIONs are biocompatible and offer outstanding performance as MRI contrast agents, but their full potential can only be realized by directing them to regions of interest and having them accumulate there.[7, 25, 26] It has been shown that SPIONs can be directed *in vivo* using an external magnet.[27-37] However, such a targeting mode has proven difficult and requires knowing the desired location *a priori*. A more powerful approach is the passive targeting method that relies on the judicious adjustment of the particles' physicochemical characteristics to influence their biodistribution following intravenous administration. The particles are sequestered by phagocytic cells in the body and accrue mainly in healthy regions of the primary and secondary organs of the reticuloendothelial system (RES): the liver, spleen, lymph nodes, and bone marrow.[24, 38-55] SPIONs with longer circulation can even be found at sites of inflammation following their internalization by macrophages[56-60] or can gather in tumors *via* the enhanced permeation and retention (EPR) effect.[61-64]

Passive targeting has been clinically proven, and magnetic targeting is still being pursued, but the "clinician's dream" is an actively targeted contrast agent with a high specificity for cancer markers that accumulates wherever the malignant cells are in the body.[15, 65] Many approaches to active targeting of SPIONs have been documented, including peptides, hormones, antibodies, proteins, therapeutics, and nutrients, such as

folic acid (FA).[8, 10, 25, 26, 66-107] Antibodies are inherently immunogenic and are also bulky; both properties are believed to inhibit internalization of attached structures. Although none of the other approaches suffer from these particular drawbacks, nutrient pathways are attractive since they are directly linked to proliferation and thus in principle will cause increased uptake of the imaging agent, thereby yielding greater signal for the most aggressive tumor cells. The folic acid receptor (FAR) is overexpressed in a wide variety of human cancers, as FA is a key precursor in DNA base synthesis and is thus required for tumor cell proliferation. Folic acid receptors are therefore internalized and recycled to the surface for gathering the vitamin,[74, 76, 108] a process that is highly advantageous since it should enable active loading of SPIONs, leading to MRI contrast enhancement that facilitates earlier disease detection.[3, 7, 9, 66, 109]

5.2 Summary

The research presented in this thesis is part of a larger effort to develop multimodal nanoparticles: a novel and promising avenue for probing and treating disease and evaluating treatment efficacy using a single platform.[3, 5, 8, 10, 16, 92-96, 110-112] Its foundation is our group's successful use of poly(amidoamine) (PAMAM) dendrimers conjugated with FA to target tumors both *in vitro* and *in vivo*.[113-123] For the generation 5 (G5) dendrimers used in this work, an average of five FA molecules per polymer unit were covalently attached to leverage the multivalent effect.[3, 92, 97, 114, 124-127] On average, three molecules of 6-TAMRA (6T) dye were also linked through peptide bonds, and the dendrimers' remaining amine termini were neutralized by capping with acetyl groups (Ac). The dendrimers, denoted G5-Ac(102)-FA(5)-6T(3), were thus specially modified to bear folic acid moieties for multivalent targeting, 6-TAMRA dye molecules for

tracking *via* optical fluorescence, and a neutral surface to minimize nonspecific interactions with cells.[113, 117, 122, 123, 128, 129] These functionalized dendrimers were synthesized to transfer high-quality SPIONs from organic to aqueous media, protect them, and impart targeting and an optical fluorescent tag in a single step.

Organic-coated SPIONs (OC-SPIONs) were synthesized by the nonhydrolytic procedure published by Rockenberger *et al*. with a slight but important modification. The original synthesis used trioctylamine as a coordinating solvent without any other ligands present,[130] but particles produced this way were not tractable. Oleic acid was thus added to the reaction mixture as a surfactant; doing so enhanced the resulting particles' stability during purification and handling. This experimental result agrees with recent work that indicates oleic acid is the optimal stabilizer for iron oxide nanoparticles.[131, 132]

G5-Ac(102)-FA(5)-6T(3) were used to transfer the hydrophobic OC-SPIONs from organic to aqueous media to produce dendrimer-coated SPIONs (DC-SPIONs). Transmission electron microscopy (TEM) experiments verified that the DC-SPIONs maintained the narrow size and shape distribution afforded by the thermolytic organic synthesis. Superconducting quantum interference device (SQUID) measurements demonstrated that the DC-SPIONs were highly magnetic, exhibiting a saturation magnetization around 60 emu/g versus the bulk value of 90 emu/g. Results from X-ray photoelectron spectroscopy (XPS) experiments were consistent with a dendrimer coating replacing the fatty acid ligands.

DC-SPIONs were tested for targeting *in vitro* using KB cells overexpressing the folic acid receptor (FAR) as a model system. Targeting was verified through the correlation between cellular association as measured by two distinct and complementary

methods: UV–visible (UV–visible) fluorescence for the dendrimers using 6-TAMRA and X-ray fluorescence (XRF) microscopy for iron in the iron oxide particles. Confocal microscopy images, including z-stacks, verified that the DC-SPIONs were internalized in a manner similar to the free targeted dendrimers. Previous similar studies either did not quantify iron uptake[8, 66, 68-71, 106] or did so on bulk samples,[25, 26, 72-76] but the work presented in this dissertation is unique in demonstrating and quantifying uptake of DC-SPIONs at the single-cell level using the novel XRF microscopy technique. Such analysis confirms specific targeting of DC-SPIONs and reveals fascinating features and variations that cannot be discerned by bulk analysis.

A wide distribution of uptake was observed when tracking elemental fluorescence from iron using XRF microscopy. However, the breadth of this distribution was consistent with that obtained when examining uptake by tracking UV–visible fluorescence with flow cytometry. It is critical to recognize that the abscissa of counts versus intensity plots from flow is logarithmic. Therefore, seemingly narrow, symmetric distributions are actually broad and skewed. Although this is not really significant for bulk analyses, it becomes critically important when analyzing individual cells. It is also interesting to note that the width of the distribution obtained for DC-SPIONs is indistinguishable from that of free G5-Ac(102)-FA(5)-6T(3): the uptake behavior for the dendrimers alone and when they are anchored to the iron oxide nanoparticle surfaces is the same.

5.3 Future Work

Given the successful *in vitro* work with DC-SPIONs, animal studies with them are worth pursuing. A small animal's reticuloendothelial system rapidly clears SPIONs:

the blood half-life is generally around 10% of that in a human.[16, 133] Hence the contrast agent dose for a small animal typically exceeds the average clinical dose for a human, 1 mg Fe/kg, by an order of magnitude or more.[16] Although the majority of studies on targeted SPION contrast agents in small animals used amounts consistent with these expectations,[26, 68-70, 79, 83, 88, 91, 92, 95, 96, 101, 104, 105, 107, 134] several studies report success using smaller quantities.[8, 86, 87, 93, 97, 99, 106, 135, 136]

Considering the wide variation in the amounts of iron used per kg animal body weight (0.25 kg was assumed as the average weight when absolute doses were given), it is reasonable to try animal studies at various doses. Assuming a yield of ~0.7 mg Fe per batch of DC-SPIONs, around 0.5 mg Fe would remain for injection after an aliquot was taken for SQUID, MRI, TEM, and XPS measurements, and iron content analysis by inductively coupled plasma optical emission spectroscopy (ICP-OES). The product of each synthesis should be characterized separately at least until inter-batch consistency has been established after multiple repetitions of the protocol. If necessary to maximize usable material, one of the magnetic characterization steps can justifiably be omitted. The MRI experiments to assess the r1 and r2 relaxivities of the DC-SPION batch should take priority over the SQUID measurements since r1 and r2 are more directly relevant to *in vivo* studies.

Three dosages should be adequate for a pilot study: 0.125, 0.25, and 0.5 mg Fe. For a single mouse at each level, this requires a total of six DC-SPION syntheses. A single OC-SPION preparation will provide plenty of SPIONs; dendrimer availability will be the limiting factor. Following the current protocol, a total of 20.4 mg G5-Ac(102)-

FA(5)-6T(3) is needed. The functionalized dendrimers should be prepared in a single batch.

Based on previous work, immunodeficient NOD.CB17-SCID mice (Charles River Laboratories; Wilmington, MA) with KB tumor xenografts are suitable models.[67, 115] At least seven animals are necessary for the pilot study: one untreated control and six animals to receive DC-SPIONs, two at each dose. One of the animals in each treated pair will be a negative control, receiving free folic acid prior to DC-SPION injection. Injection should be performed once the tumors reach a volume of 0.6 ± 0.15 cm^3, staggered such that each animal can be imaged at multiple post-injection time points: 1 h, 4 h, 8 h, 24 h, 48 h, and 7 d.

Moving toward a more proactive approach to medicine is critical to enhance the survival of individuals faced with cancer. Current approaches cannot reliably detect cancer early enough to avoid painful and expensive treatments that often fail. The results of this research and many other contemporary studies provide the impetus to continue investigating magnetic nanoparticles as actively targeted MRI contrast agents. Leveraging the magnetic properties of SPIONs and the flexible surface chemistry of dendrimers should be thoroughly investigated to produce multimodal devices, customized for individual patients, capable of detecting and treating disease as well as reporting on the efficacy of the treatment. With talented interdisciplinary teams, such as the scientists collaborating in the Michigan Nanotechnology Institute for Medicine and Biological Sciences (MNiMBS), there is much reason to be hopeful about the future of nanoscience and its applications to clinical medicine.

5.4 References

1. Jun, Y. W.; Choi, J. S.; Cheon, J. Heterostructured Magnetic Nanoparticles: Their Versatility and High Performance Capabilities. *Chem. Commun.* **2007**, (12), 1203-1214.

2. Duguet, E.; Vasseur, S.; Mornet, S.; Goglio, G.; Demourgues, A.; Portier, J.; Grasset, F.; Veverka, P.; Pollert, E. Towards a Versatile Platform Based on Magnetic Nanoparticles for in Vivo Applications. *Bull. Mater. Sci.* **2006,** 29, (6), 581-586.

3. Mornet, S.; Vasseur, S.; Grasset, F.; Duguet, E. Magnetic Nanoparticle Design for Medical Diagnosis and Therapy. *J. Mater. Chem.* **2004,** 14, (14), 2161-2175.

4. Mornet, S.; Vasseur, S.; Grasset, F.; Veverka, P.; Goglio, G.; Demourgues, A.; Portier, J.; Pollert, E.; Duguet, E. Magnetic Nanoparticle Design for Medical Applications. *Prog. Solid State Chem.* **2006,** 34, (2-4), 237-247.

5. Morawski, A. M.; Lanza, G. A.; Wickline, S. A. Targeted Contrast Agents for Magnetic Resonance Imaging and Ultrasound. *Curr. Opin. Biotechnol.* **2005,** 16, (1), 89-92.

6. Sosnovik, D. E.; Weissleder, R. Emerging Concepts in Molecular MRI. *Curr. Opin. Biotechnol.* **2007,** 18, (1), 4-10.

7. Artemov, D. Molecular Magnetic Resonance Imaging with Targeted Contrast Agents. *J. Cell. Biochem.* **2003,** 90, (3), 518-524.

8. Huh, Y.-M.; Jun, Y.; Song, H.-T.; Kim, S.; Choi, J. S.; Lee, J.-H.; Yoon, S.; Kim, K.-S.; Shin, J.-S.; Suh, J.-S.*, et al.* In Vivo Magnetic Resonance Detection of Cancer by Using Multifunctional Magnetic Nanocrystals. *J. Am. Chem. Soc.* **2005,** 127, (35), 12387-12391.

9. Weissleder, R. Molecular Imaging in Cancer. *Science* **2006,** 312, (5777), 1168-1171.

10. Schellenberger, E. A.; Sosnovik, D.; Weissleder, R.; Josephson, L. Magneto/Optical Annexin V, a Multimodal Protein. *Bioconjugate Chem.* **2004,** 15, (5), 1062-1067.

11. Kim, D. K.; Mikhaylova, M.; Zhang, Y.; Muhammed, M. Protective Coating of Superparamagnetic Iron Oxide Nanoparticles. *Chem. Mater.* **2003,** 15, (8), 1617-1627.

12. Häfeli, U. O.; Pauer, G. J. In Vitro and in Vivo Toxicity of Magnetic Microspheres. *J. Magn. Magn. Mater.* **1999,** 194, (1-3), 76-82.

13. Müller, R.; Steinmetz, H.; Hiergeist, R.; Gawalek, W. Magnetic Particles for Medical Applications by Glass Crystallisation. *J. Magn. Magn. Mater.* **2004,** 272-276, (Part 2), 1539-1541.

14. Gupta, A. K.; Gupta, M. Synthesis and Surface Engineering of Iron Oxide Nanoparticles for Biomedical Applications. *Biomaterials* **2005,** 26, (18), 3995-4021.

15. Weinmann, H. J.; Ebert, W.; Misselwitz, B.; Schmitt-Willich, H. Tissue-Specific MR Contrast Agents. *Eur. J. Radiol.* **2003,** 46, (1), 33-44.

16. Corot, C.; Robert, P.; Idee, J. M.; Port, M. Recent Advances in Iron Oxide Nanocrystal Technology for Medical Imaging. *Adv. Drug Delivery Rev.* **2006,** 58, (14), 1471-1504.

17. Babincová, M.; Sourivong, P.; Leszczynska, D.; Babinec, P. Blood-Specific Whole-Body Electromagnetic Hyperthermia. *Med. Hypotheses* **2000,** 55, (6), 459-460.

18. Bulte, J. W. M.; Kraitchman, D. L. Iron Oxide MR Contrast Agents for Molecular and Cellular Imaging. *NMR Biomed.* **2004,** 17, (7), 484-499.

19. Renshaw, P. F.; Owen, C. S.; Evans, A. E.; Leigh, J. S., Jr. Immunospecific NMR Contrast Agents. *Magn. Reson. Imaging* **1986,** 4, (4), 351-357.

20. Renshaw, P. F.; Owen, C. S.; McLaughlin, A. C.; Frey, T. G.; Leigh, J. S., Jr. Ferromagnetic Contrast Agents: A New Approach. *Magn. Reson. Med.* **1986,** 3, (2), 217-225.

21. Arbab, A. S.; Bashaw, L. A.; Miller, B. R.; Jordan, E. K.; Bulte, J. W. M.; Frank, J. A. Intracytoplasmic Tagging of Cells with Ferumoxides and Transfection Agent for Cellular Magnetic Resonance Imaging after Cell Transplantation: Methods and Techniques. *Transplantation* **2003,** 76, (7), 1123-1130.

22. Arruebo, M.; Fernández-Pacheco, R.; Ibarra, M. R.; Santamaría, J. Magnetic Nanoparticles for Drug Delivery. *Nano Today* **2007,** 2, (3), 22-32.

23. Okuhata, Y. Delivery of Diagnostic Agents for Magnetic Resonance Imaging. *Adv. Drug Delivery Rev.* **1999,** 37, (1-3), 121-137.

24. Weissleder, R.; Heautot, J. F.; Schaffer, B. K.; Nossiff, N.; Papisov, M. I.; Bogdanov, A., Jr.; Brady, T. J. MR Lymphography: Study of a High-Efficiency Lymphotrophic Agent. *Radiology* **1994,** 191, (1), 225-230.

25. Leuschner, C.; Kumar, C.; Hansel, W.; Soboyejo, W.; Zhou, J.; Hormes, J. LHRH-Conjugated Magnetic Iron Oxide Nanoparticles for Detection of Breast Cancer Metastases. *Breast Cancer Res. Treat.* **2006,** 99, (2), 163-176.

26. Kresse, M.; Wagner, S.; Pfefferer, D.; Lawaczeck, R.; Elste, V.; Semmler, W. Targeting of Ultrasmall Superparamagnetic Iron Oxide (USPIO) Particles to Tumor Cells in Vivo by Using Transferrin Receptor Pathways. *Magn. Reson. Med.* **1998,** 40, (2), 236-242.

27. Alexiou, C.; Arnold, W.; Klein, R. J.; Parak, F. G.; Hulin, P.; Bergemann, C.; Erhardt, W.; Wagenpfeil, S.; Lübbe, A. S. Locoregional Cancer Treatment with Magnetic Drug Targeting. *Cancer Res.* **2000,** 60, (23), 6641-6648.

28. Gallo, J. M.; Gupta, P. K.; Hung, C. T.; Perrier, D. G. Evaluation of Drug Delivery Following the Administration of Magnetic Albumin Microspheres Containing Adriamycin to the Rat. *J. Pharm. Sci.* **1989,** 78, (3), 190-194.

29. Goodwin, S. C.; Bittner, C. A.; Peterson, C. L.; Wong, G. Single-Dose Toxicity Study of Hepatic Intra-Arterial Infusion of Doxorubicin Coupled to a Novel Magnetically Targeted Drug Carrier. *Toxicol. Sci.* **2001,** 60, (1), 177-183.

30. Häfeli, U. O.; Sweeney, S. M.; Beresford, B. A.; Humm, J. L.; Macklis, R. M. Effective Targeting of Magnetic Radioactive 90Y-Microspheres to Tumor Cells by an Externally Applied Magnetic Field. Preliminary *in Vitro* and *in Vivo* Results. *Nucl. Med. Biol.* **1995,** 22, (2), 147-155.

31. Johnson, J.; Kent, T.; Koda, J.; Peterson, C.; Rudge, S.; Tapolsky, G. The MTC Technology: A Platform Technology for the Site-Specific Delivery of Pharmaceutical Agents. *Eur. Cell. Mater.* **2002,** 3, (Suppl. 2), 12-15.

32. Lübbe, A. S.; Bergemann, C.; Brock, J.; McClure, D. G. Physiological Aspects in Magnetic Drug-Targeting. *J. Magn. Magn. Mater.* **1999,** 194, (1-3), 149-155.

33. Lübbe, A. S.; Bergemann, C.; Huhnt, W.; Fricke, T.; Riess, H.; Brock, J. W.; Huhn, D. Preclinical Experiences with Magnetic Drug Targeting: Tolerance and Efficacy. *Cancer Res.* **1996,** 56, (20), 4694-4701.

34. Lübbe, A. S.; Bergemann, C.; Riess, H.; Schriever, F.; Reichardt, P.; Possinger, K.; Matthias, M.; Dorken, B.; Herrmann, F.; Gurtler, R.*, et al.* Clinical Experiences with Magnetic Drug Targeting: A Phase I Study with 4'-Epidoxorubicin in 14 Patients with Advanced Solid Tumors. *Cancer Res.* **1996,** 56, (20), 4686-4693.

35. Mah, C.; Fraites, T. J., Jr.; Zolotukhin, I.; Song, S.; Flotte, T. R.; Dobson, J.; Batich, C.; Byrne, B. J. Improved Method of Recombinant AAV2 Delivery for Systemic Targeted Gene Therapy. *Mol. Ther.* **2002,** 6, (1), 106-112.

36. Rudge, S.; Peterson, C.; Vessely, C.; Koda, J.; Stevens, S.; Catterall, L. Adsorption and Desorption of Chemotherapeutic Drugs from a Magnetically Targeted Carrier (MTC). *J. Controlled Release* **2001,** 74, (1-3), 335-340.

37. Widder, K. J.; Morris, R. M.; Poore, G. A.; Howard, D. P.; Senyei, A. E. Selective Targeting of Magnetic Albumin Microspheres Containing Low-Dose Doxorubicin: Total Remission in Yoshida Sarcoma-Bearing Rats. *Eur. J. Cancer Clin. Oncol.* **1983,** 19, (1), 135-139.

38. Metz, S.; Lohr, S.; Settles, M.; Beer, A.; Woertler, K.; Rummeny, E.; Daldrup–Link, H. Ferumoxtran-10-Enhanced MR Imaging of the Bone Marrow before

and after Conditioning Therapy in Patients with Non-Hodgkin Lymphomas. *Eur. Radiol.* **2006,** 16, (3), 598-607.

39. Daldrup-Link, H.; Rummeny, E.; Ihssen, B.; Kienast, J.; Link, T. Iron-Oxide-Enhanced MR Imaging of Bone Marrow in Patients with Non-Hodgkin's Lymphoma: Differentiation between Tumor Infiltration and Hypercellular Bone Marrow. *Eur. Radiol.* **2002,** 12, (6), 1557-1566.

40. Stark, D. D.; Weissleder, R.; Elizondo, G.; Hahn, P. F.; Saini, S.; Todd, L. E.; Wittenberg, J.; Ferrucci, J. T. Superparamagnetic Iron Oxide: Clinical Application as a Contrast Agent for MR Imaging of the Liver. *Radiology* **1988,** 168, (2), 297-301.

41. Elizondo, G.; Weissleder, R.; Stark, D. D.; Guerra, J.; Garza, J.; Fretz, C. J.; Todd, L. E.; Ferrucci, J. T. Hepatic Cirrhosis and Hepatitis: MR Imaging Enhanced with Superparamagnetic Iron Oxide. *Radiology* **1990,** 174, (3), 797-801.

42. Fujita, T.; Ito, K.; Honjo, K.; Okazaki, H.; Matsumoto, T.; Matsunaga, N. Detection of Hepatocellular Carcinoma: Comparison of T2-Weighted Breath-Hold Fast Spin-Echo Sequences and High-Resolution Dynamic MR Imaging with a Phased-Array Body Coil. *J. Magn. Reson. Imaging* **1999,** 9, (2), 274-279.

43. Reimer, P.; Balzer, T. Ferucarbotran (Resovist): A New Clinically Approved RES-Specific Contrast Agent for Contrast-Enhanced MRI of the Liver: Properties, Clinical Development, and Applications. *Eur. Radiol.* **2003,** 13, (6), 1266-1276.

44. Sharma, R.; Saini, S.; Ros, P. R.; Hahn, P. F.; Small, W. C.; de Lange, E. E.; Stillman, A. E.; Edelman, R. R.; Runge, V. M.; Outwater, E. K.*, et al.* Safety Profile of Ultrasmall Superparamagnetic Iron Oxide Ferumoxtran-10: Phase II Clinical Trial Data. *J. Magn. Reson. Imaging* **1999,** 9, (2), 291-294.

45. Harisinghani, M. G.; Barentsz, J.; Hahn, P. F.; Deserno, W. M.; Tabatabaei, S.; van de Kaa, C. H.; de la Rosette, J.; Weissleder, R. Noninvasive Detection of Clinically Occult Lymph-Node Metastases in Prostate Cancer. *N. Engl. J. Med.* **2003,** 348, (25), 2491-2499.

46. Nguyen, B. C.; Stanford, W.; Thompson, B. H.; Rossi, N. P.; Kernstine, K. H.; Kern, J. A.; Robinson, R. A.; Amorosa, J. K.; Mammone, J. F.; Outwater, E. K. Multicenter Clinical Trial of Ultrasmall Superparamagnetic Iron Oxide in the Evaluation of Mediastinal Lymph Nodes in Patients with Primary Lung Carcinoma. *J. Magn. Reson. Imaging* **1999,** 10, (3), 468-473.

47. Michel, S. C. A.; Keller, T. M.; Frohlich, J. M.; Fink, D.; Caduff, R.; Seifert, B.; Marincek, B.; Kubik-Huch, R. A. Preoperative Breast Cancer Staging: MR Imaging of the Axilla with Ultrasmall Superparamagnetic Iron Oxide Enhancement. *Radiology* **2002,** 225, (2), 527-536.

48. Bremer, C.; Allkemper, T.; Baermig, J.; Reimer, P. RES-Specific Imaging of the Liver and Spleen with Iron Oxide Particles Designed for Blood Pool MR-Angiography. *J. Magn. Reson. Imaging* **1999,** 10, (3), 461-467.

49. Simon, G. H.; Raatschen, H.-J.; Wendland, M. F.; von Vopelius-Feldt, J.; Fu, Y.; Chen, M.-H.; Daldrup-Link, H. E. Ultrasmall Superparamagnetic Iron-Oxide-Enhanced MR Imaging of Normal Bone Marrow in Rodents: Original Research. *Acad. Radiol.* **2005,** 12, (9), 1190-1197.

50. Bachmann, R.; Kreft, B.; Dombrowski, F.; Block, W.; Öksendal, A.; Schild, H. Enhanced Tumor Detection in the Presence of Liver Cirrhosis: Experimental Study on the Diagnostic Value of a Superparamagnetic Iron Oxide MR Imaging Contrast Agent (NSR 0430). *J. Magn. Reson. Imaging* **1999,** 9, (2), 251-256.

51. Saini, S.; Stark, D. D.; Hahn, P. F.; Wittenberg, J.; Brady, T. J.; Ferrucci, J. T., Jr. Ferrite Particles: A Superparamagnetic MR Contrast Agent for the Reticuloendothelial System. *Radiology* **1987,** 162, (1), 211-216.

52. Weissleder, R.; Elizondo, G.; Wittenberg, J.; Lee, A. S.; Josephson, L.; Brady, T. J. Ultrasmall Superparamagnetic Iron Oxide: An Intravenous Contrast Agent for Assessing Lymph Nodes with MR Imaging. *Radiology* **1990,** 175, (2), 494-498.

53. Weissleder, R.; Elizondo, G.; Wittenberg, J.; Rabito, C. A.; Bengele, H. H.; Josephson, L. Ultrasmall Superparamagnetic Iron Oxide: Characterization of a New Class of Contrast Agents for MR Imaging. *Radiology* **1990,** 175, (2), 489-493.

54. Bordat, C.; Sich, M.; Réty, F.; Bouet, O.; Cournot, G.; Cuénod, C. A.; Clément, O. Distribution of Iron Oxide Nanoparticles in Rat Lymph Nodes Studied Using Electron Energy Loss Spectroscopy (EELS) and Electron Spectroscopic Imaging (ESI). *J. Magn. Reson. Imaging* **2000,** 12, (3), 505-509.

55. Guimaraes, R.; Clément, O.; Bittoun, J.; Carnot, F.; Frija, G. MR Lymphography with Superparamagnetic Iron Nanoparticles in Rats: Pathologic Basis for Contrast Enhancement. *Am. J. Roentgenol.* **1994,** 162, (1), 201-207.

56. Dardzinski, B. J.; Schmithorst, V. J.; Holland, S. K.; Boivin, G. P.; Imagawa, T.; Watanabe, S.; Lewis, J. M.; Hirsch, R. MR Imaging of Murine Arthritis Using Ultrasmall Superparamagnetic Iron Oxide Particles. *Magn. Reson. Imaging* **2001,** 19, (9), 1209-1216.

57. Schmitz, S. A.; Coupland, S. E.; Gust, R.; Winterhalter, S.; Wagner, S.; Kresse, M.; Semmler, W.; Wolf, K. J. Superparamagnetic Iron Oxide-Enhanced MRI of Atherosclerotic Plaques in Watanabe Hereditable Hyperlipidemic Rabbits. *Invest. Radiol.* **2000,** 35, (8), 460-471.

58. Ruehm, S. G.; Corot, C.; Vogt, P.; Kolb, S.; Debatin, J. F. Magnetic Resonance Imaging of Atherosclerotic Plaque with Ultrasmall Superparamagnetic Particles of Iron Oxide in Hyperlipidemic Rabbits. *Circulation* **2001,** 103, (3), 415-422.

59. Dousset, V.; Delalande, C.; Ballarino, L.; Quesson, B.; Seilhan, D.; Coussemacq, M.; Thiaudiére, E.; Brochet, B.; Canioni, P.; Caillé, J. M. In Vivo Macrophage Activity Imaging in the Central Nervous System Detected by Magnetic Resonance. *Magn. Reson. Med.* **1999,** 41, (2), 329-333.

60. Beckmann, N.; Cannet, C.; Fringeli-Tanner, M.; Baumann, D.; Pally, C.; Bruns, C.; Zerwes, H.-G.; Andriambeloson, E.; Bigaud, M. Macrophage Labeling by SPIO as an Early Marker of Allograft Chronic Rejection in a Rat Model of Kidney Transplantation. *Magn. Reson. Med.* **2003,** 49, (3), 459-467.

61. Daldrup-Link, H. E.; Kaiser, A.; Helbich, T.; Werner, M.; Bjørnerud, A.; Link, T. M.; Rummeny, E. J. Macromolecular Contrast Medium (Feruglose) Versus Small Molecular Contrast Medium (Gadopentetate) Enhanced Magnetic Resonance Imaging: Differentiation of Benign and Malignant Breast Lesions. *Acad. Radiol.* **2003,** 10, (11), 1237-1246.

62. Troprès, I.; Grimault, S.; Vaeth, A.; Grillon, E.; Julien, C.; Payen, J.-F.; Lamalle, L.; Décorps, M. Vessel Size Imaging. *Magn. Reson. Med.* **2001,** 45, (3), 397-408.

63. Troprès, I.; Lamalle, L.; Péoc'h, M.; Farion, R.; Usson, Y.; Décorps, M.; Rémy, C. In Vivo Assessment of Tumoral Angiogenesis. *Magn. Reson. Med.* **2004,** 51, (3), 533-541.

64. Turetschek, K.; Roberts, T. P. L.; Floyd, E.; Preda, A.; Novikov, V.; Shames, D. M.; Carter, W. O.; Brasch, R. C. Tumor Microvascular Characterization Using Ultrasmall Superparamagnetic Iron Oxide Particles (USPIO) in an Experimental Breast Cancer Model. *J. Magn. Reson. Imaging* **2001,** 13, (6), 882-888.

65. Konda, S.; Aref, M.; Wang, S.; Brechbiel, M.; Wiener, E. Specific Targeting of Folate–Dendrimer MRI Contrast Agents to the High Affinity Folate Receptor Expressed in Ovarian Tumor Xenografts. *Magn. Reson. Mater. Phys., Biol. Med.* **2001,** 12, (2), 104-113.

66. Artemov, D.; Mori, N.; Okollie, B.; Bhujwalla, Z. M. MR Molecular Imaging of the Her-2/*neu* Receptor in Breast Cancer Cells Using Targeted Iron Oxide Nanoparticles. *Magn. Reson. Med.* **2003,** 49, (3), 403-408.

67. Shi, X.; Wang, S. H.; Swanson, S. D.; Ge, S.; Cao, Z.; Van Antwerp, M. E.; Landmark, K. J.; Baker, J. R., Jr. Dendrimer-Functionalized Shell-Crosslinked Iron Oxide Nanoparticles for *in-Vivo* Magnetic Resonance Imaging of Tumors. *Adv. Mater.* **2008,** 20, (9), 1671-1678.

68. Choi, H.; Choi, S. R.; Zhou, R.; Kung, H. F.; Chen, I.-W. Iron Oxide Nanoparticles as Magnetic Resonance Contrast Agent for Tumor Imaging Via Folate Receptor-Targeted Delivery. *Acad. Radiol.* **2004,** 11, (9), 996-1004.

69. Hu, F.; Wei, L.; Zhou, Z.; Ran, Y.; Li, Z.; Gao, M. Preparation of Biocompatible Magnetite Nanocrystals for in Vivo Magnetic Resonance Detection of Cancer. *Adv. Mater.* **2006,** 18, (19), 2553-2556.

70. Montet, X.; Weissleder, R.; Josephson, L. Imaging Pancreatic Cancer with a Peptide-Nanoparticle Conjugate Targeted to Normal Pancreas. *Bioconjugate Chem.* **2006,** 17, (4), 905-911.

71. Nasongkla, N.; Bey, E.; Ren, J.; Ai, H.; Khemtong, C.; Guthi, J. S.; Chin, S.-F.; Sherry, A. D.; Boothman, D. A.; Gao, J. Multifunctional Polymeric Micelles as Cancer-Targeted, MRI-Ultrasensitive Drug Delivery Systems. *Nano Lett.* **2006,** 6, (11), 2427-2430.

72. Kohler, N.; Sun, C.; Wang, J.; Zhang, M. Methotrexate-Modified Superparamagnetic Nanoparticles and Their Intracellular Uptake into Human Cancer Cells. *Langmuir* **2005,** 21, (19), 8858-8864.

73. Kohler, N.; Sun, C.; Fichtenholtz, A.; Gunn, J.; Fang, C.; Zhang, M. Methotrexate-Immobilized Poly(ethylene glycol) Magnetic Nanoparticles for MR Imaging and Drug Delivery. *Small* **2006,** 2, (6), 785-792.

74. Zhang, Y.; Kohler, N.; Zhang, M. Surface Modification of Superparamagnetic Magnetite Nanoparticles and Their Intracellular Uptake. *Biomaterials* **2002,** 23, (7), 1553-1561.

75. Zhang, Y.; Sun, C.; Kohler, N.; Zhang, M. Self-Assembled Coatings on Individual Monodisperse Magnetite Nanoparticles for Efficient Intracellular Uptake. *Biomed. Microdevices* **2004,** 6, (1), 33-40.

76. Sun, C.; Sze, R.; Zhang, M. Folic Acid-PEG Conjugated Superparamagnetic Nanoparticles for Targeted Cellular Uptake and Detection by MRI. *J. Biomed. Mater. Res., Part A* **2006,** 78A, (3), 550-557.

77. Landmark, K. J.; DiMaggio, S.; Ward, J.; Kelly, C.; Vogt, S.; Hong, S.; Kotlyar, A.; Myc, A.; Thomas, T. P.; Penner-Hahn, J. E.*, et al.* Synthesis, Characterization, and *in Vitro* Testing of Superparamagnetic Iron Oxide Nanoparticles Targeted Using Folic Acid-Conjugated Dendrimers. *ACS Nano* **2008,** 2, (4), 773-783.

78. Bulte, J. W. M.; Hoekstra, Y.; Kamman, R. L.; Magin, R. L.; Webb, A. G.; Briggs, R. W.; Go, K. G.; Hulstaert, C. E.; Miltenyi, S.; The, T. H.*, et al.* Specific MR Imaging of Human Lymphocytes by Monoclonal Antibody-Guided Dextran-Magnetite Particles. *Magn. Reson. Med.* **1992,** 25, (1), 148-157.

79. Cerdan, S.; Lötscher, H. R.; Künnecke, B.; Seelig, J. Monoclonal Antibody-Coated Magnetite Particles as Contrast Agents in Magnetic Resonance Imaging of Tumors. *Magn. Reson. Med.* **1989,** 12, (2), 151-163.

80. Funovics, M. A.; Kapeller, B.; Hoeller, C.; Su, H. S.; Kunstfeld, R.; Puig, S.; Macfelda, K. MR Imaging of the Her2/neu and 9.2.27 Tumor Antigens Using Immunospecific Contrast Agents. *Magn. Reson. Imaging* **2004,** 22, (6), 843-850.

81. Kang, H. W.; Josephson, L.; Petrovsky, A.; Weissleder, R.; Bogdanov, A. Magnetic Resonance Imaging of Inducible E-Selectin Expression in Human Endothelial Cell Culture. *Bioconjugate Chem.* **2002,** 13, (1), 122-127.

82. Pirko, I.; Johnson, A.; Ciric, B.; Gamez, J.; Macura, S. I.; Pease, L. R.; Rodriguez, M. In Vivo Magnetic Resonance Imaging of Immune Cells in the Central Nervous System with Superparamagnetic Antibodies. *FASEB J.* **2004,** 18, (1), 179-182.

83. Remsen, L. G.; McCormick, C. I.; Roman-Goldstein, S.; Nilaver, G.; Weissleder, R.; Bogdanov, A.; Hellström, K. E.; Hellström, I.; Kroll, R. A.; Neuwelt, E. A. MR of Carcinoma-Specific Monoclonal Antibody Conjugated to Monocrystalline Iron Oxide Nanoparticles: The Potential for Noninvasive Diagnosis. *Am. J. Neuroradiol.* **1996,** 17, (3), 411-418.

84. Tiefenauer, L. X.; Kuehne, G.; Andres, R. Y. Antibody-Magnetite Nanoparticles: *In Vitro* Characterization of a Potential Tumor-Specific Contrast Agent for Magnetic Resonance Imaging. *Bioconjugate Chem.* **1993,** 4, (5), 347-352.

85. Toma, A.; Otsuji, E.; Kuriu, Y.; Okamoto, K.; Ichikawa, D.; Hagiwara, A.; Ito, H.; Nishimura, T.; Yamagishi, H. Monoclonal Antibody A7-Superparamagnetic Iron Oxide as Contrast Agent of MR Imaging of Rectal Carcinoma. *Br. J. Cancer* **2005,** 93, (1), 131-136.

86. Tsourkas, A.; Shinde-Patil, V. R.; Kelly, K. A.; Patel, P.; Wolley, A.; Allport, J. R.; Weissleder, R. In Vivo Imaging of Activated Endothelium Using an Anti-VCAM-1 Magnetooptical Probe. *Bioconjugate Chem.* **2005,** 16, (3), 576-581.

87. Weissleder, R.; Lee, A. S.; Fischman, A. J.; Reimer, P.; Shen, T.; Wilkinson, R.; Callahan, R. J.; Brady, T. J. Polyclonal Human Immunoglobulin G Labeled with Polymeric Iron Oxide: Antibody MR Imaging. *Radiology* **1991,** 181, (1), 245-249.

88. Weissleder, R.; Lee, A. S.; Khaw, B. A.; Shen, T.; Brady, T. J. Antimyosin-Labeled Monocrystalline Iron Oxide Allows Detection of Myocardial Infarct: MR Antibody Imaging. *Radiology* **1992,** 182, (2), 381-385.

89. Sonvico, F.; Mornet, S.; Vasseur, S.; Dubernet, C.; Jaillard, D.; Degrouard, J.; Hoebeke, J.; Duguet, E.; Colombo, P.; Couvreur, P. Folate-Conjugated Iron Oxide Nanoparticles for Solid Tumor Targeting as Potential Specific Magnetic Hyperthermia Mediators: Synthesis, Physicochemical Characterization, and in Vitro Experiments. *Bioconjugate Chem.* **2005,** 16, (5), 1181-1188.

90. Wang, S. H.; Shi, X.; Van Antwerp, M.; Cao, Z.; Swanson, S. D.; Bi, X.; Baker, J. R., Jr. Dendrimer-Functionalized Iron Oxide Nanoparticles for Specific Targeting and Imaging of Cancer Cells. *Adv. Funct. Mater.* **2007,** 17, (16), 3043-3050.

91. Zhao, M.; Beauregard, D. A.; Loizou, L.; Davletov, B.; Brindle, K. M. Non-Invasive Detection of Apoptosis Using Magnetic Resonance Imaging and a Targeted Contrast Agent. *Nat. Med.* **2001,** 7, (11), 1241-1244.

92. Nahrendorf, M.; Jaffer, F. A.; Kelly, K. A.; Sosnovik, D. E.; Aikawa, E.; Libby, P.; Weissleder, R. Noninvasive Vascular Cell Adhesion Molecule-1 Imaging Identifies Inflammatory Activation of Cells in Atherosclerosis. *Circulation* **2006,** 114, (14), 1504-1511.

93. Sosnovik, D. E.; Schellenberger, E. A.; Nahrendorf, M.; Novikov, M. S.; Matsui, T.; Dai, G.; Reynolds, F.; Grazette, L.; Rosenzweig, A.; Weissleder, R.*, et al.* Magnetic Resonance Imaging of Cardiomyocyte Apoptosis with a Novel Magneto-Optical Nanoparticle. *Magn. Reson. Med.* **2005,** 54, (3), 718-724.

94. Kelly, K.; Nahrendorf, M.; Yu, A.; Reynolds, F.; Weissleder, R. In Vivo Phage Display Selection Yields Atherosclerotic Plaque Targeted Peptides for Imaging. *Mol. Imaging Biol.* **2006,** 8, (4), 201-207.

95. Moore, A.; Medarova, Z.; Potthast, A.; Dai, G. In Vivo Targeting of Underglycosylated MUC-1 Tumor Antigen Using a Multimodal Imaging Probe. *Cancer Res.* **2004,** 64, (5), 1821-1827.

96. Kelly, K. A.; Allport, J. R.; Tsourkas, A.; Shinde-Patil, V. R.; Josephson, L.; Weissleder, R. Detection of Vascular Adhesion Molecule-1 Expression Using a Novel Multimodal Nanoparticle. *Circ. Res.* **2005,** 96, (3), 327-336.

97. Weissleder, R.; Kelly, K.; Sun, E. Y.; Shtatland, T.; Josephson, L. Cell-Specific Targeting of Nanoparticles by Multivalent Attachment of Small Molecules. *Nat. Biotechnol.* **2005,** 23, (11), 1418-1423.

98. Reimer, P.; Weissleder, R.; Lee, A. S.; Wittenberg, J.; Brady, T. J. Receptor Imaging: Application to MR Imaging of Liver Cancer. *Radiology* **1990,** 177, (3), 729-734.

99. Weissleder, R.; Reimer, P.; Lee, A. S.; Wittenberg, J.; Brady, T. J. MR Receptor Imaging: Ultrasmall Iron Oxide Particles Targeted to Asialoglycoprotein Receptors. *Am. J. Roentgenol.* **1990,** 155, (6), 1161-1167.

100. Reimer, P.; Weissleder, R.; Wittenberg, J.; Brady, T. J. Receptor-Directed Contrast Agents for MR Imaging: Preclinical Evaluation with Affinity Assays. *Radiology* **1992,** 182, (2), 565-569.

101. Johansson, L. O.; Bjørnerud, A.; Ahlström, H. K.; Ladd, D. L.; Fujii, D. K. A Targeted Contrast Agent for Magnetic Resonance Imaging of Thrombus: Implications of Spatial Resolution. *J. Magn. Reson. Imaging* **2001,** 13, (4), 615-618.

102. Högemann, D.; Josephson, L.; Weissleder, R.; Basilion, J. P. Improvement of MRI Probes to Allow Efficient Detection of Gene Expression. *Bioconjugate Chem.* **2000,** 11, (6), 941-946.

103. Moore, A.; Basilion, J. P.; Chiocca, E. A.; Weissleder, R. Measuring Transferrin Receptor Gene Expression by NMR Imaging. *Biochim. Biophys. Acta* **1998,** 1402, (3), 239-249.

104. Moore, A.; Josephson, L.; Bhorade, R. M.; Basilion, J. P.; Weissleder, R. Human Transferrin Receptor Gene as a Marker Gene for MR Imaging. *Radiology* **2001,** 221, (1), 244-250.

105. Weissleder, R.; Moore, A.; Mahmood, U.; Bhorade, R.; Benveniste, H.; Chiocca, E. A.; Basilion, J. P. In Vivo Magnetic Resonance Imaging of Transgene Expression. *Nat. Med.* **2000,** 6, (3), 351-354.

106. Boutry, S.; Laurent, S.; Elst, L. V.; Muller, R. N. Specific E-Selectin Targeting with a Superparamagnetic MRI Contrast Agent. *Contrast Media Mol. Imaging* **2006,** 1, (1), 15-22.

107. Wadghiri, Y. Z.; Sigurdsson, E. M.; Sadowski, M.; Elliott, J. I.; Li, Y.; Scholtzova, H.; Tang, C. Y.; Aguinaldo, G.; Pappolla, M.; Duff, K.*, et al.* Detection of Alzheimer's Amyloid in Transgenic Mice Using Magnetic Resonance Microimaging. *Magn. Reson. Med.* **2003,** 50, (2), 293-302.

108. Brigger, I.; Dubernet, C.; Couvreur, P. Nanoparticles in Cancer Therapy and Diagnosis. *Adv. Drug Delivery Rev.* **2002,** 54, (5), 631-651.

109. Berry, C. C.; Curtis, A. S. G. Functionalisation of Magnetic Nanoparticles for Applications in Biomedicine. *J. Phys. D: Appl. Phys.* **2003,** 36, (13), R198-R206.

110. Jeong, U.; Teng, X.; Wang, Y.; Yang, H.; Xia, Y. Superparamagnetic Colloids: Controlled Synthesis and Niche Applications. *Adv. Mater.* **2007,** 19, (1), 33-60.

111. Gu, H.; Xu, K.; Xu, C.; Xu, B. Biofunctional Magnetic Nanoparticles for Protein Separation and Pathogen Detection. *Chem. Commun.* **2006**, (9), 941-949.

112. Ito, A.; Shinkai, M.; Honda, H.; Kobayashi, T. Medical Application of Functionalized Magnetic Nanoparticles. *J. Biosci. Bioeng.* **2005,** 100, (1), 1-11.

113. Baker, J. R., Jr.; Quintana, A.; Piehler, L.; Banaszak Holl, M.; Tomalia, D.; Raczka, E. The Synthesis and Testing of Anti-Cancer Therapeutic Nanodevices. *Biomed. Microdevices* **2001,** 3, (1), 61-69.

114. Hong, S.; Leroueil, P. R.; Majoros, I. J.; Orr, B. G.; Baker, J. R., Jr.; Banaszak Holl, M. M. The Binding Avidity of a Nanoparticle-Based Multivalent Targeted Drug Delivery Platform. *Chem. Biol.* **2007,** 14, (1), 107-115.

115. Kukowska-Latallo, J. F.; Candido, K. A.; Cao, Z.; Nigavekar, S. S.; Majoros, I. J.; Thomas, T. P.; Balogh, L. P.; Khan, M. K.; Baker, J. R., Jr. Nanoparticle Targeting of Anticancer Drug Improves Therapeutic Response in Animal Model of Human Epithelial Cancer. *Cancer Res.* **2005,** 65, (12), 5317-5324.

116. Majoros, I. J.; Myc, A.; Thomas, T.; Mehta, C. B.; Baker, J. R., Jr. PAMAM Dendrimer-Based Multifunctional Conjugate for Cancer Therapy: Synthesis, Characterization, and Functionality. *Biomacromolecules* **2006,** 7, (2), 572-579.

117. Majoros, I. J.; Thomas, T. P.; Mehta, C. B.; Baker, J. R., Jr. Poly(amidoamine) Dendrimer-Based Multifunctional Engineered Nanodevice for Cancer Therapy. *J. Med. Chem.* **2005,** 48, (19), 5892-5899.

118. Myc, A.; Majoros, I. J.; Thomas, T. P.; Baker, J. R., Jr. Dendrimer-Based Targeted Delivery of an Apoptotic Sensor in Cancer Cells. *Biomacromolecules* **2007,** 8, (1), 13-18.

119. Quintana, A.; Raczka, E.; Piehler, L.; Lee, I.; Myc, A.; Majoros, I.; Patri, A. K.; Thomas, T.; Mulé, J.; Baker, J. R., Jr. Design and Function of a Dendrimer-Based Therapeutic Nanodevice Targeted to Tumor Cells through the Folate Receptor. *Pharm. Res.* **2002,** 19, (9), 1310-1316.

120. Thomas, T. P.; Majoros, I. J.; Kotlyar, A.; Kukowska-Latallo, J. F.; Bielinska, A.; Myc, A.; Baker, J. R., Jr. Targeting and Inhibition of Cell Growth by an Engineered Dendritic Nanodevice. *J. Med. Chem.* **2005,** 48, (11), 3729-3735.

121. Thomas, T. P.; Myaing, M. T.; Ye, J. Y.; Candido, K.; Kotlyar, A.; Beals, J.; Cao, P.; Keszler, B.; Patri, A. K.; Norris, T. B.*, et al.* Detection and Analysis of Tumor Fluorescence Using a Two-Photon Optical Fiber Probe. *Biophys. J.* **2004,** 86, (6), 3959-3965.

122. Patri, A. K.; Myc, A.; Beals, J.; Thomas, T. P.; Bander, N. H.; Baker, J. R., Jr. Synthesis and in Vitro Testing of J591 Antibody-Dendrimer Conjugates for Targeted Prostate Cancer Therapy. *Bioconjugate Chem.* **2004,** 15, (6), 1174-1181.

123. Shukla, R.; Thomas, T. P.; Peters, J.; Kotlyar, A.; Myc, A.; Baker, J. R., Jr. Tumor Angiogenic Vasculature Targeting with PAMAM Dendrimer-RGD Conjugates. *Chem. Commun.* **2005**, (46), 5739-5741.

124. Stella, B.; Arpicco, S.; Peracchia, M. T.; Desmaële, D.; Hoebeke, J.; Renoir, M.; D'Angelo, J.; Cattel, L.; Couvreur, P. Design of Folic Acid-Conjugated Nanoparticles for Drug Targeting. *J. Pharm. Sci.* **2000,** 89, (11), 1452-1464.

125. Salazar, M.; Ratnam, M. The Folate Receptor: What Does It Promise in Tissue-Targeted Therapeutics? *Cancer Metastasis Rev.* **2007,** 26, (1), 141-152.

126. Woller, E. K.; Walter, E. D.; Morgan, J. R.; Singel, D. J.; Cloninger, M. J. Altering the Strength of Lectin Binding Interactions and Controlling the Amount of

Lectin Clustering Using Mannose/Hydroxyl-Functionalized Dendrimers. *J. Am. Chem. Soc.* **2003,** 125, (29), 8820-8826.

127. Lee, C. C.; MacKay, J. A.; Fréchet, J. M. J.; Szoka, F. C. Designing Dendrimers for Biological Applications. *Nat. Biotechnol.* **2005,** 23, (12), 1517-1526.

128. Hong, S.; Bielinska, A. U.; Mecke, A.; Keszler, B.; Beals, J. L.; Shi, X.; Balogh, L.; Orr, B. G.; Baker, J. R., Jr.; Banaszak Holl, M. M. Interaction of Poly(amidoamine) Dendrimers with Supported Lipid Bilayers and Cells: Hole Formation and the Relation to Transport. *Bioconjugate Chem.* **2004,** 15, (4), 774-782.

129. Leroueil, P. R.; Hong, S.; Mecke, A.; Baker, J. R., Jr.; Orr, B. G.; Banaszak Holl, M. M. Nanoparticle Interaction with Biological Membranes: Does Nanotechnology Present a Janus Face? *Acc. Chem. Res.* **2007,** 40, (5), 335-342.

130. Rockenberger, J.; Scher, E. C.; Alivisatos, A. P. A New Nonhydrolytic Single-Precursor Approach to Surfactant-Capped Nanocrystals of Transition Metal Oxides. *J. Am. Chem. Soc.* **1999,** 121, (49), 11595-11596.

131. Cushing, B. L.; Kolesnichenko, V. L.; O'Connor, C. J. Recent Advances in the Liquid-Phase Syntheses of Inorganic Nanoparticles. *Chem. Rev.* **2004,** 104, (9), 3893-3946.

132. Willis, A. L.; Turro, N. J.; O'Brien, S. Spectroscopic Characterization of the Surface of Iron Oxide Nanocrystals. *Chem. Mater.* **2005,** 17, (24), 5970-5975.

133. Corot, C.; Petry, K. G.; Trivedi, R.; Saleh, A.; Jonkmanns, C.; Le Bas, J. F.; Blezer, E.; Rausch, M.; Brochet, B.; Foster-Gareau, P*., et al.* Macrophage Imaging in Central Nervous System and in Carotid Atherosclerotic Plaque Using Ultrasmall Superparamagnetic Iron Oxide in Magnetic Resonance Imaging. *Invest. Radiol.* **2004,** 39, (10), 619-625.

134. Suwa, T.; Ozawa, S.; Ueda, M.; Ando, N.; Kitajima, M. Magnetic Resonance Imaging of Esophageal Squamous Cell Carcinoma Using Magnetite Particles Coated with Anti-Epidermal Growth Factor Receptor Antibody. *Int. J. Cancer* **1998,** 75, (4), 626-634.

135. Schaffer, B. K.; Linker, C.; Papisov, M.; Tsai, E.; Nossiff, N.; Shibata, T.; Bogdanov, A.; Brady, T. J.; Weissleder, R. MION-ASF: Biokinetics of an MR Receptor Agent. *Magn. Reson. Imaging* **1993,** 11, (3), 411-417.

136. Reimer, P.; Weissleder, R.; Shen, T.; Knoefel, W. T.; Brady, T. J. Pancreatic Receptors: Initial Feasibility Studies with a Targeted Contrast Agent for MR Imaging. *Radiology* **1994,** 193, (2), 527-531.